

bradscholars

Evaluation of Raman spectroscopy for application in analytical astrobiology. The application of Raman spectroscopy for characterisation of biological and geological materials of relevance to space exploration.

Item Type	Thesis
Authors	Page, Kristian
Rights	<p>
The University of Bradford theses are licenced under a Creative Commons Licence.</p>
Download date	2026-03-09 07:04:56
Link to Item	http://hdl.handle.net/10454/5716

Chapter 1

Introduction

1.1. Aims and objectives

The aim of this study is to evaluate Raman spectroscopy as an analytical tool for samples of potential significance in astrobiology and as an instrumental platform for interplanetary studies. Detection of life within extreme environments requires analytical equipment to be capable of producing a vast amount of information on samples while adhering to strict parameters regarding weight, power consumption and size of the instruments. Reproducibility and robustness of data acquired is required and therefore comparable data must be obtainable both on Earth and in an extraterrestrial environment. Raman spectroscopy is an analytical technique which will be used on board the ExoMars Rover developed by the European Space Agency and therefore this work aims to interrogate this technique within the context of this Martian mission.

To achieve this aim the following objectives were identified;

- Develop an analytical framework for comparison of instrument performance.
- Investigate instrumental performance of bench top instruments and a prototype instrument developed in conjunction with ESA for the ExoMars mission.
- Analysis of exemplar systems of organics of bio relevance, minerals of Mars relevance, biological materials and bio-minerals.

An analytical framework for instrument comparisons of performance is required to allow for reproducible data to be acquired between the ExoMars Raman instrument and

instruments on Earth. This involves the development of standards which can be used to test the limitations of instruments using clearly defined instrument validation parameters. These parameters will look at the sensitivity, range, limit of detection, limit of quantification, robustness, selectivity, linearity, accuracy and precision of an instrument. Standards produced to fulfill these parameters must also be astrobiological relevant and suitable for Raman analysis.

To investigate instrumental performance of bench top instruments and the ExoMars rover a comparative sample analysis must be performed. To do this a prototype instrument will be developed to match the specifications of the spectrometer that will be used in the ExoMars mission. The prototype instrument will then produce spectra comparable to that which will be obtained on the Martian surface. By optimizing data acquisition between bench top instruments and the prototype instrument these methods can be applied directly to the ExoMars mission. To investigate the instrumental performance between the spectrometers suitable astrobiological samples can be used and instrument validation parameters applied to the samples.

When comparative data can be obtained between different spectrometers for astrobiological standards, investigation of exemplar systems can be interrogated. This will involve the analysis of samples of complex organics which are not simple single sample compounds. Analysis of these samples will allow for comparative data on similar systems which may be found on the surface of Mars. Processing such as the grinding and mixing of geological inclusions will be analysed and the impact this has upon a known organic inclusion within the sample will be interrogated.

1.2. Theory of Raman spectroscopy

1.2.1. The physical basis of Raman scattering

For a molecule to be Raman active a change in polarizability (α) is required to take place during a molecular vibration^[1-6]. The equation for such an event is defined as;

$$\left(\frac{\partial\alpha}{\partial Q}\right) \neq 0$$

In this equation the co-ordinator of vibration is defined as Q ^[1-6]. The ability for a molecule to be polarized can be defined by;

$$\mu = \alpha E$$

Here the polarizability of the molecule is related to an induced dipole moment^[1-6], μ . E relates to the electric field strength, which at a given time, t , can be given by;

$$E = E_o \cos 2\pi\nu t$$

The frequency of the laser is defined by ν and E_o is the electric field amplitude^[1-6]. The following equation allow us to obtain define the frequency of the laser;

$$\nu = \frac{c}{\lambda}$$

This reveals that the wavelength λ is proportional to the frequency of the laser ν . The rate of this proportionality is defined by a constant, c , which in this case relates to the speed of light^[1-6]. The speed of light can be numerically defined as $3 \times 10^8 \text{ m s}^{-1}$ S.I. With the introduction of wavenumbers, $\tilde{\nu}$, the equation can be manipulated such that;

$$\tilde{\nu} = \frac{\nu}{c} = \frac{1}{\lambda} (\text{cm}^{-1})$$

When two molecules interact there is a transfer of energy. Using this energy transfer from the electric field of the molecules a new equation is obtained;

$$\Delta E = h\nu = h\frac{c}{\lambda} = hc\tilde{\nu}$$

This equation is expressed in terms of energy difference, ΔE . The magnitude of ΔE relates to the vibrational transition, between 3×10^3 and 10^2 cm^{-1} . $6.626 \times 10^{-34} \text{ J s}$ (Planck's constant) can be used as the value of h and gives the proportionality of the equation^[1-6].

Scattering of monochromatic light from a laser is used in Raman spectroscopy and occurs in the visible, near infrared or near ultraviolet range. Based on inelastic scattering of a photon, this scattering is often referred to as Raman scattering^[1-6]. Energy of the laser photons can be shifted either up or down as the laser interacts with phonons in the system. Information about the phonon modes in the system can then be derived from this shift.

Rayleigh scattering (Figure 1.1.1) can occur in the detection of molecules which could potentially give false information regarding a molecule^[1-6]. This scattering arises when particles smaller than the wavelength of light cause the light to be scattered.

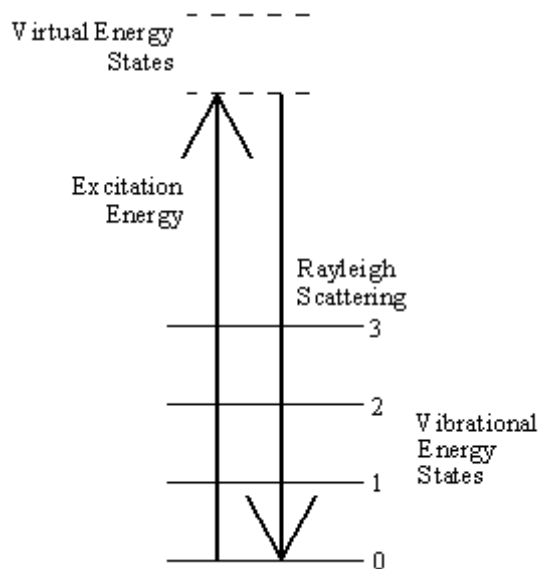


Figure 1.1.1. Diagram to show Rayleigh Scattering

When light interacts with the electron cloud of a molecule, the Raman Effect occurs^[1-6]. As the laser photons bounce off the molecule energy is lost and the molecules vibrate. While this is happening the electrons become excited and enter into a virtual state. The molecule begins at a ground state, is excited into a virtual energy state and then relaxes into a vibrational excited state. This process results in the scattered photon having less energy and the light has a frequency shift^[1-6]. This generates Stokes Raman scattering (Figure 1.1.2).

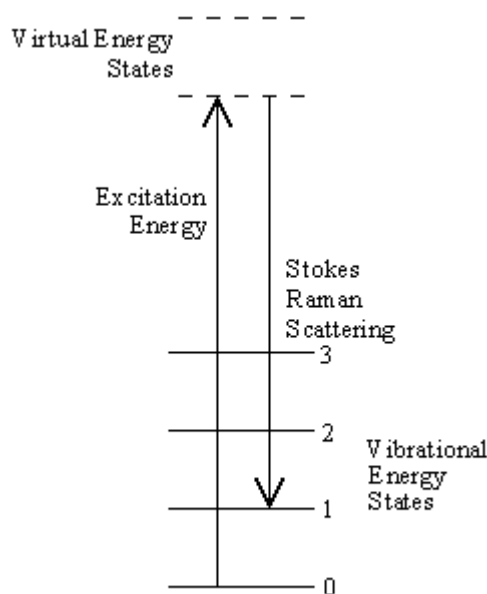


Figure 1.1.2. Diagram of Stokes Raman scattering.

If the molecule was already in an elevated vibrational energy state then the excitation energy causes the molecule to enter the virtual energy state, however when it relaxes once again it returns to a rested vibrational energy state (Figure 1.1.3). This scattering is Anti-Stokes Raman scattering^[7]. Based on these shifts associated with the different molecular vibrations a spectrum can be produced. Raman shift, in wavenumbers (cm^{-1}), can be calculated by the energy difference between two different vibrational levels;

$$\bar{\nu} = \frac{1}{\lambda_{\text{incident}}} - \frac{1}{\lambda_{\text{scattered}}}$$

Whereby $\lambda_{\text{scattered}}$ is the wavelength of the scattered photons and $\lambda_{\text{incident}}$ is the wavelength of the incident^[1-6].

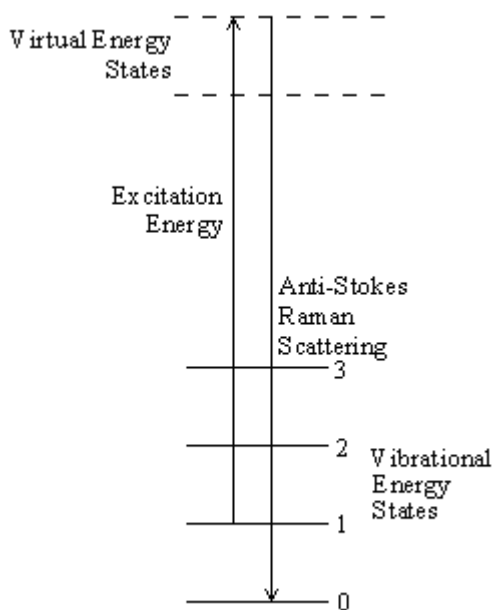


Figure 1.1.3. Diagram of Anti-Stokes Raman scattering.

For Raman scattering to occur it is always crucial for different vibrational states to occur and these interactions occur virtually simultaneously. The non-resonance Raman Effect is not dependent on wavelengths of an excitation laser due to the state changes being between virtual states. However while the actual spectrum does not depend on the

laser excitation, when the excitation is close to the energy requirement for a transition between states then resonance Raman or fluorescence can occur. The nature of these intermediate states can vary along with the time scales of the processes. A fluorescence process usually takes more than 10^{-9} s, whereas a Raman transition can be completed in less than one picosecond^[1-6]. Relaxed fluorescence (Figure 1.1.4) occurs when the excitation energy excites the molecule into an increased excitation state, then drops down between excited energy states and then returns to its original vibrational energy state^[1].

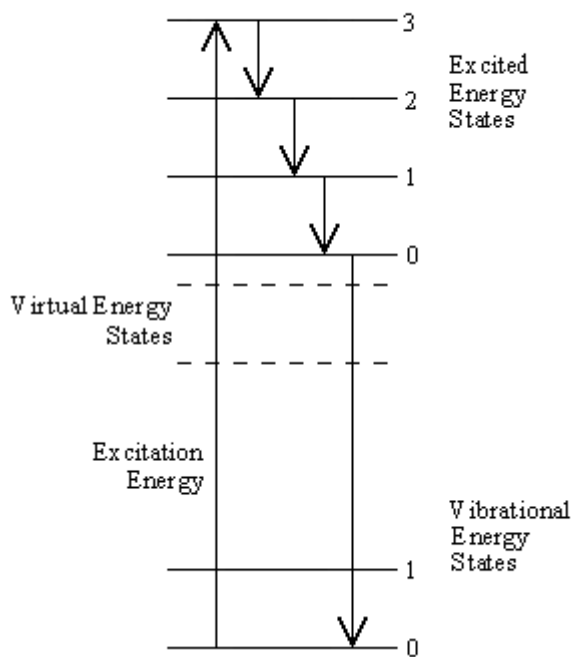


Figure 1.1.4. Diagram of Relaxed fluorescence.

The presence of fluorescence within a spectrum will normally mask the majority of Raman features as it is far more intense than Raman scattering^[1-6]. The presence of any Raman or fluorescence resonance effects is directly related to the laser excitation wavelength. The presence of fluorescence can only occur when sufficient energy has been provided by the excitation photons for the molecule to reach an excited energy

state. Therefore one way to avoid fluorescence emissions is to select a laser excitation wavelength which will not produce fluorescence in the region of interest. Due to the inadequate energy to initiate fluorescence, near-infrared laser wavelengths often avoid emissions^[1]. Additionally while UV laser wavelengths do cause fluorescence the energy is distinct from the Raman signal and so a spectrum can be obtained without this fluorescence. In instances where the fluorescence is derived from impurities or a surrounding material a Raman microscope can be used to avoid such areas and limit the fluorescence^[7].

1.2.2. Chemical application of Raman spectroscopy

Raman spectroscopy is a spectroscopic technique used to study both vibration and rotational changes within a molecule^[8]. Any Raman spectrum produced has different features due to each vibration being very specific to the individual chemical bonds within the molecule. In organic molecules this region occurs between 500-2000 cm^{-1} and is commonly referred to as the fingerprint region, due to its unique identifiable features.

If a molecule can be rotated, reflected, inverted or have a similar change occur without changing its appearance then the object displays symmetry. The process of doing these changes is known as a symmetry operation^[1-6]. The line through which the reflection or rotation occurs can be defined as the symmetry element. Mirror planes are labelled as σ_h , σ_v and σ_d whereby the letters used indicate the orientation of plane with respect to any rotation axes that are present. For the rotation axis C_n is the label used where the n indicated the angle, $360/n$, through which the rotation occurs. Where a reflection and rotation both occur S_n is used. Inversion center is defined as i and E , Identity, is a

symmetry element where doing nothing to the object leaves it looking the same as it originally did^[9].

Group theory can be used to predict how many vibrational modes will be present in a Raman spectrum of the molecule where the molecule contains symmetry^[1-6]. However not all modes are Raman active and instead are IR active. The number of different Raman active bands is derived from the different molecular symmetries of a sample. Therefore this can be useful in identifying materials such as isomers where each molecule will have different symmetries and therefore different vibrational modes.

If a molecule has a change in polarizability in relation to the vibrational coordinate, then that molecule will produce the Raman Effect^[1-6]. This effect arises from a deformation within the electron cloud around the bonds within the molecule. If there is symmetry within the molecule then the Raman shift can be observed. This shift is equal to the vibrational level involved and the intensity is derived from the degree of polarizability change^[1-6].

1.2.3. Instrumentation

All Raman spectrometers have a similar design; they all have a laser and a detector. All systems contain mirrors to redirect the laser beams and filters to alter the laser power.

Details of the components are shown in figure 1.1.5.

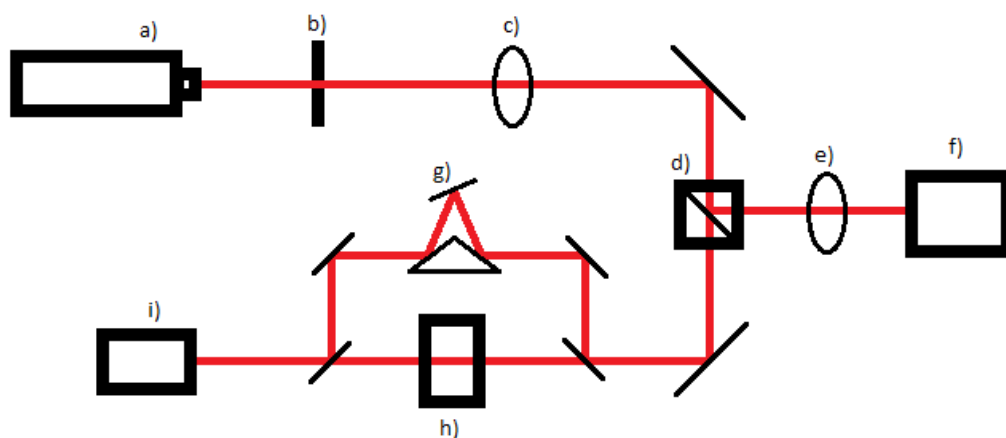


Figure 1.1.5. Schematic of the major components of Raman spectrometers a) Laser, b) pinhole, c) filters, d) Beam splitter and notch filters, e) optics/lens, f) sample, g) grating, h) interferogram and i) detector

In all Raman spectrometers a laser beam is produced at a source and the wavelength of this laser can vary depending on the instrument used and its purpose. Once the laser is activated it first enters a pinhole aperture which rejects residual scattered rays originating from the laser and prevents them from entering the system. It will then be subjected to a filter which can be used to reduce the laser power and prevent damage to the sample. The beam then enters a beam splitter which directs the beam towards a sample and is focused onto the sample using a lens or microscope optics. The laser beam hits the sample which will be focused a preset distance away from the optics and lens.

Rayleigh scattering produces wavelengths close to the laser line and therefore such scattering must be removed by filtering out these wavelengths. Wavelengths are therefore only dispersed onto the detector if they are a certain distance away from the laser line. Due to the strong intensity of Rayleigh scattering compared to the weak natural Raman scattering, separation is difficult. For this reason a holographic diffraction grating is used along with several dispersion stages. This allows for a far greater amount of laser rejection. In FT Raman systems an interferogram can be used.

The interferogram records all the monitored wavelengths and therefore can detect signal spikes.

The final component of a Raman spectrometer is the detector. The detector allows the signal to be identified and plotted on a computer. Originally photomultiplier tubes (PMTs) were commonly used in Raman spectrometers; these detectors however require long acquisition times and are often relatively large. Therefore detectors which have far faster acquisition times and a much smaller size have become more common. These charge-coupled devices (CCD) detectors have thus allowed instruments to be portable and the spectrometers are no longer required to be constantly in a static position.

1.3. Context of Study

Life is defined as the condition that distinguishes animals, plants, fungi and viruses from inorganic matter, including the capacity for growth, reproduction, functional activity, and continual change preceding death^[10]. For many years mankind has searched for life on other planets and as time has passed our ability to detect life on these extraterrestrial bodies has advanced. The most likely candidates in searching for life within our solar system are currently believed to be: Mars, Europa and Titan. Being the closest planet to Earth, Mars has always been looked at as having the greatest potential for life. Even back in 19th century the theory of life on Mars was speculated^[11]. However at that time the ideas of life on Mars were very different to those hypothesised today. Whereas once it was believed that Mars had features such as canals^[11] and an atmosphere much like Earths, once probes and more powerful telescopes were developed it became clear that such life could not possibly exist there^[12].

1.3.1. Martian mineralogy

In its early life Mars is believed to have had tectonic activity, volcanism and large bodies of water similar to Earth today. Mars today however is very different, due to its lack of a substantial atmosphere. Like Earth, Mars has mountains, volcanoes, valleys, deserts and ice caps in its polar regions. It features the largest mountain, Olympus Mons, and the largest canyon, Valles Marineris, currently known in our Solar System. The Martian core, like that of the Earth, is proposed to be partially fluid and consists mainly of iron and sulphur. The mantle consists of mainly silicates and while the planet now has no magnetic field, its partially magnetised crust indicates it may have done in the past. The composition of the Martian surface is a very important factor when considering interplanetary space missions.

The most common material found on Earth-like planets are silicates^[13] and orbital spacecraft^[14,15] have indicated that this is the same for Mars, with the silicates being of basaltic composition. This is further supported by the studies of Martian meteorites^[16] and spacecraft sent to the surface of Mars^[17,18]. The main silicates identified on Mars are; olivine, pyroxene and plagioclase. These have been observed and mapped by several Mars orbiting spacecraft^[19-22]. Silicates have been detected within the soil in at least two Martian landing sites; Gusev Crater and Meridiani Planum^[23]. It has also been demonstrated that during weathering of both olivine and pyroxene, pure silica can be produced^[24]. A clay silicate; montmorillonite, has also been identified as a potential mineral on the surface of Mars^[25]. Silicates become important in the search for life due to their ability to indicate water; a required component for life. Hydrated silicates, e.g. zeolites, would indicate water on the Martian surface^[26-28] however these are yet to be detected.

Carbonates are another material expected to be found readily on the Martian surface. This hypothesis is derived from the early Martian atmosphere being similar to that of Earth's; with both carbon dioxide and water being abundantly present and thus the formation of carbonates possible^[29-31]. In addition to atmospheric water, liquid water is also likely to have existed on the surface due to volcanic activity. These volcanoes would have produced large quantities of gasses ejected into the atmosphere producing a greenhouse effect^[29,32]. The carbonate siderite is believed to be present on the Martian surface due to the readily available carbon dioxide predicted to be present in the early Martian atmosphere and the extensive sources of iron in subsurface rocks^[33-38]. Additionally without the presence of oxygen, siderite remains stable and therefore these samples are likely to be present today on the surface^[39,40]. However previous missions have only detected very few carbonates within the Martian regolith^[41,42]. These low concentrations may be explained by volcanic dissolution of carbonates^[34,43], masking from other crystals such as sulphates and halites^[33] or the lack of atmospheric water meaning the carbonates only form a thin film^[39].

Mars obtains its red colouration from the ferric compounds; iron oxides and oxyhydroxides which make up a large amount of the Martian regolith^[44-48]. Mössbauer Spectrometry has been used specifically for the identification of these iron compounds^[49-52] and they are primarily found in the form of haematite^[53-55]. Haematite detected on Mars is likely to be derived from meteoric weathering^[56-58], hydrothermal processes^[59,60] or alteration of volcanic ash^[54,61]. Additionally, it is possible for haematite to be derived as the end product of several chemical pathways relevant to Mars^[62,63]. Haematite is the only iron oxide which can remain stable in present day conditions^[40]. The second most commonly detected material on the Martian surface is

goethite^[48,64,65]. However, unlike haematite, goethite is less stable in the current Martian environment^[40,66]. The compound is therefore likely to only form in the earlier environment where both water and carbon dioxide were more readily available^[67,68].

Another compound important in the mineralogy of Mars is sulphur in the form of sulphates. These compounds have been detected on the Martian surface in a greater concentration than that of Earth^[44,45,69-73]. The distribution of sulphates on Mars appears to be spread equally across all regions of the surface^[74,75]. The source of these compounds is proposed to be from alteration of volcanic rock due to oxidation^[76,77]. The sulphates are mainly found in the form of gypsum^[78], jarosite^[79] and magnesium sulphates^[73,80,81].

1.3.2. Life on Mars

On Mars the presence of magnesium, sodium, potassium and chloride are all elements important for the growth of living organisms. However while Mars may once have had an atmosphere, it has been swept away in solar winds^[12,82] and the surface is exposed to extreme temperatures^[12,83]. The surface conditions on Mars are thought to be too harsh for Earth-like organisms to exist, however organisms called extremophiles still could potentially survive in such environments^[84-86]. Extremophiles are organisms that survive in, and may even require, environments outside the normal parameters for life on Earth which would be detrimental to most other forms of life^[85,87-89].

Mars was not always believed to be such a harsh environment^[12,87] and if Mars once had a climate similar to Earth's then it is possible that life evolved there in the same way it did here. This is enhanced by speculation that meteorites from Mars could have seeded

life on Earth^[87]. It is still possible to detect life based on the nature of the compounds needed to make up a living organism. This involves detection of compounds referred to as biomarkers^[86,90-94] compounds which are indicative of life. Biomarkers are biological markers which are complex molecular fossils derived from biochemicals in living organisms^[95].

The biomarkers of relevance to the detection of life on Mars have previously been defined by Parnell *et al*^[96]. There are two types of biomarkers extant; living or recently dead and extinct; long dead or fossilized. While these biomarkers are indicative of life, it is important to consider inorganic origins, therefore proof of life would require detection of multiple biomarkers within a sample.

In the search for extant biomarkers it is expected that informational macromolecules, energy-rich storage compounds and lipid-rich membranes would all be observed as these are the main components within any living organism. The energy-rich storage compounds are constantly being broken down and resynthesized within living cells and they do not exist outside of cells due to their high-energy bonds. Therefore the presence of these compounds is only possible where life is present. This means that compounds such as adenosine triphosphate (ATP), phosphoenolpyruvate and acetyl phosphate become important biomarker to indicate life^[96]. Additionally this also makes ATP synthase, a compound which produces ATP^[97], an important biomarker.

Deoxyribonucleic acid (DNA), like ATP, is highly unlikely to occur outside of biological systems as it would also degrade rapidly outside cells. Therefore detection of DNA or pyrimidines and purines would be a direct confirmation of extant life.

Polypeptides within cells exist predominantly as molecular chaperones^[98] and therefore the chaperones would likely be the most prominent polypeptide biomarker. From the cell membrane lipid-based molecules can be derived and these have been observed to persist in the fossil record^[99,100] making them good targets as biomarkers.

Cyanobacteria, which get their distinct colour from the presence of the light harvesting pigment phycocyanin, is an organism which has been detected in extreme environments on Earth thus making it a potential candidate for life on Mars^[101,102]. The carotenoid structures, which occur in pigments, have also been found in sediments without apparent degradation^[103]. Beta-carotene is a carotenoid that is produced by many microorganisms and has been implicated as a possible Martian biomarker^[104]. Trehalose and ectoine are two other potential extant biomarkers used by bacteria they are found in extreme hypersaline conditions^[105].

Extinct biomarkers are compounds of biological origin which remain stable for prolonged periods after the organism has died. Proteins and amino acids are broken down readily on Earth, however on Mars they may remain preserved due to the lack of microbes to break them down^[106]. Long chain fatty acids, from cell membranes^[107], are another potential biomarker that are very stable^[106].

Most extinct biomarkers are derived from degraded materials produced from the breakdown of organisms. When chlorophyll is degraded it can produce phytol^[108]. The phytol is then broken down to form pristane and phytane. These two compounds remain stable even in high temperatures^[109] and have been detected in ancient sedimentary deposits^[110] making them excellent extinct biomarkers. Carotenoids have previously been discussed with relation to extremeophiles, however outside living cells they

contain many highly reactive conjugated bonds and therefore do not remain stable for prolonged periods. As the compounds degrade much more stable molecules are produced such as alkyl trimethylbenzenes and alkyl trimethylcyclohexane^[111,112].

Hopanoids are very predominant in living organisms^[113] and hopanes are common in fossilized organic materials^[114,115]. These hopanes are very stable and often derived from other hopanoids, diploptene or diplopterol. Similar to hopanes, steranes and diasteranes are geologically stable with diasteranes being the more stable of the two. They are derived from sterols along with many other degradant products^[116]. However unlike the hopanoids they do require oxygen for formation. These considerations indicate that a rich organic chemistry may persist in protected or sheltered Martian environments. Hence, the deployment of Raman spectroscopy instrumentation, with their capacity to identify and discriminate between such species is highly desirable.

1.3.3. Mars Missions

There have been many missions to Mars beginning in the 1960s including flyby probes, orbiters, landers and rovers. One of the first missions to Mars was the Soviet Mars 1M programs launched in 1960, however this mission was not successful like many of the other early missions to Mars^[117]. The first successful flyby of Mars was the Mariner 4 in 1965 and this was then followed by two further flybys in 1969 by Mariner 6 and 7^[118]. These orbiters produced data on the possibility of carbonates containing water on the Martian surface^[119]. In 1971 Mariner 9 was the first successful spacecraft to achieve orbit around Mars^[118]. This was then followed up in 1976 by Viking 1 and 2 which both were orbiters. These orbiters were among the first to detect possible indications of streams on the Martian surface^[120]. Viking 1 became the first spacecraft to successfully

land on Mars and perform detailed analysis of the landing site^[17,121]. The next spacecraft to arrive at Mars was in 1997 with the Mars Global Surveyor, which had a thermal emission spectrometer onboard^[19,122] and the data for this mission has been made publically available^[123]. Also in 1997 the Mars Pathfinder arrived and landed on the Martian surface, this spacecraft was also one of the first to successfully deploy a rover onto Mars, allowing a greater analysis of geological samples on the surface^[18,45]. The Mars Exploration Rovers; MER-A Spirit and MER-B Opportunity successfully deployed in 2004, these rovers were however believed to of been contaminated with *Bacillus safensis* and therefore introduced the issue of sample contamination when looking for life on Mars^[124]. The Mars Reconnaissance Obiter arrived in Martian orbit in 2006 and in 2008 one of the most recent spacecraft to travel to Mars; Phoenix, landed on the Martian surface^[125].

In 2018, ESA and NASA plan to launch the ExoMars mission to Mars which will involve a rover deployed on the Martian surface to carry out both exobiology and geochemistry research^[126]. The primary objective for this mission will be to search for signs of life past or present. It will also investigate water and geochemical distribution in the shallow subsurface, study the surface environment and investigate the planet's subsurface^[127]. The rover will carry with it the "Pasteur payload" which will contain a panoramic imaging system, contact instruments and an analytical laboratory^[128-130].

The panoramic instruments will be used to characterise the Martian surface and subsurface environment. To visually characterise the environment and identify important targets a panoramic camera system including two wide angle cameras and a high resolution camera^[131,132]. An infrared spectrometer will be used for remote

identification of water based compounds and a ground penetrating radar will establish subsurface stratigraphy.

The contact instruments will comprise of a close-up imager, a Mössbauer Spectrometer and the rover's drill. The imager will work in close proximity of the surface rocks to examine them and the Mössbauer Spectrometer will study the iron content of rocks and soil^[49-52]. For subsurface samples, up to 2 meters, the drill will be deployed to produce a core sample and deliver it for analysis^[133].

After visual inspection of a sample, under the microscope, if it is deemed interesting it will be ground up and transferred into the analytical laboratory. In this analytical laboratory detailed analysis will be carried out on the sample using multiple instruments. An X-Ray diffractometer will be used to determine the mineral composition and crystalline phases of the sample^[134]. The Mars Organics Detector will search for amino acids, nucleobases and polyaromatic hydrocarbons using a very highly sensitive detector. A measurement of the oxidation and degradation reactivity of the Martian soil and atmosphere will be performed via the Mars Oxidant Sensor. A Gas Chromatograph Mass Spectrometer will be used to search for the organic molecules over a broad range and also perform atmospheric analysis. An antibody based instrument, the Life Marker Chip, will be used to detect biomarkers. Finally the Raman/LIBS spectrometer will be used to determine mineralogical and geochemistry within the sample and also to identify mineral phases from water based processes^[135,136]. Extensive work has been carried out to demonstrate the application of using Raman spectroscopy on the Martian surface^[90,94,137-140].

1.3.4. Remote Raman Spectroscopy

The Raman spectrometer on board the European Space Agency ExoMars rover was originally intended for use in geological identification of inorganic materials. However the role of this spectrometer has been expanded due to the Raman ability to also detect organic components. Raman is ideal for this type of role as it is both non-invasive and non-destructive, allowing it to retain samples of significance without destroying them. In the search for life this is crucial, to find life and destroy the sample at the same time would defeat the original purpose of such an experiment. Related to this is its ability to analyse samples *in situ* without the need for preparation of the sample. Due to the CCD detector being used the analysis time of a sample is rapid thus this allows many samples to be looked at with minutes. Unlike some other techniques, such as mass spectrometry, no vacuum is required^[141,142]. There are however also disadvantages in using Raman spectroscopy, the main one being that thermal decomposition of samples can occur if laser excitation power is too high. There are also issues which can be attributed to equipment costs, fluorescence of samples and the low sensitivity compared to other techniques^[141,142].

In its original design, the Raman spectrometer on board the ExoMars rover was to be coupled with a laser-induced breakdown spectrometer (LIBS)^[143]. While the LIBS instrument is destructive, as it requires ablation of atoms, the Raman instrument uses scattering and other effects to analyse molecular bonds, therefore it is non-destructive. The instrument was to contain both a 532 nm Raman continuous laser and a 1064 nm LIBS pulse laser. Images from the samples would be produced on a 2048x2048 pixel charge coupled device (CCD) detector. Spectra would be obtainable within the 240-840 nm range with a resolution of 8 cm^{-1} for Raman and 0.2 nm for LIBS. Laser output at

the sample will be 50 Mw from the 500 Mw at the source^[128]. However, the LIBS capability has been de-scoped in the latest instrument configuration.

Such an instrument can have great importance within the detection of life, however to optimize the instrument for this type of detection it is required to test it with known samples under a controlled environment. Therefore the custom built prototype mirror optical bench (MOB) Raman spectrometer was developed. This instrument is designed to be identical to that of the instrument on board the ExoMars rover and therefore allows comparative research to be carried out.

For the Raman spectrometer to be useful in the identification of organic materials of importance it is required to be able to rapidly and accurately identify samples of relevance. For this to be possible the instruments spectra must be comparable to that of the standard commercially available instruments. Two things are required for such comparability and optimization of the instruments to be possible; understanding of the samples and the effect of different conditions on reproducibility of data.

By performing a limits of detection study on known samples it is possible to identify the minimum amount of material required to be present for a positive identification of an organic component. Using samples comparable to those potentially found on the surface of Mars the potential for identification can be established. After obtaining reproducible data using known samples it is then possible to alter individual conditions or altering the way features are calculated within the systems. By observing the effects of these changes it is possible to become aware of how to optimize conditions for data acquisition and thus obtain results with far greater clarity and accuracy. This optimized protocol can then be applied to the rover instrument to obtain comparable data.

Using the custom built prototype system based on the specifications of the rover it is possible to simulate the data potentially obtained on Mars. The prototype instrument can be optimized to produce identical samples to commercially available instruments and thus comparable data between the two types of instruments can be produced. For comparability between different instruments the analysis of the samples will need to take place on exactly the same samples at exactly the same position for identical spectra to be obtained. Once comparable spectra can be obtained with simple standards then the instruments can be used for more complex real world samples which will be comprised of many different materials.

Chapter 2

Experimental

2.1. Instrumentation

In this work Raman spectra were obtained using several different instruments. Two bench-top instruments were used: a Bruker IFS66/FRA 106 FT-Raman spectrometer and a Renishaw InVia Reflex Spectrometer. The European Space agency (ESA) mission to Mars will use a Raman elegant bread-board (EBB) system^[143] which was designed specifically for the mission. To allow for a comparable study of data an instrument was produced using the same specifications and used for additional analysis of samples. This instrument was identified as the mirror optical bench (MOB) prototype instrument. The specifications for each instrument can be seen in table 2.1.1.

Model	InVia	IFS66/FRA 106	N/A
Wavelength (nm)	785/633	1064	532
Type	Benchtop	Benchtop	Benchtop
Instrument	Renishaw	Bruker	MOB
Software	WiRE	OPUS	Custom
Laser Power	50 mW	100 mW	30 mW
Spectral Range	150-3200 cm^{-1}	200-3000 cm^{-1}	175-4350 cm^{-1}
Resolution	2 cm^{-1}	4 cm^{-1}	5 cm^{-1}
Detector	CCD	Ge detector	CCD

Table 2.1.1. Specifications of different instruments used

2.1.1. Renishaw InVia Raman Instrument

The Renishaw InVia is equipped with a thermoelectrically cooled charged coupled device (CCD) detector and diode lasers emitting at 633 nm or 785 nm. It is coupled to a

Leica DMLM microscope with 5X, 20X and 50X objective lenses were utilized. The maximal output power of the diode laser at 50mW at the source. Daily calibration of the wavenumber axis is required and is achieved by recording the Raman spectrum of silicon (1 accumulation, 10 seconds) for static modes. If necessary, an offset correction is performed to ensure that the position of the silicon band is $520.50 \pm 0.10 \text{ cm}^{-1}$. Spectra were recorded with the accumulation of 1 scan, at 100% laser power and with a 10 s exposure unless otherwise stated.

2.1.2. Bruker IFS66/FRA 106 FT-Raman Instrument

The Bruker IFS66/FRA 106 FT-Raman instrument is equipped with an Nd^{3+} /YAG laser emitting at 1064 nm emitting at 100 mW at the source. All spectra were recorded with a 4 cm^{-1} spectral resolution and using 500 spectral scans, unless otherwise stated. The spectrometer was controlled by a PC with OPUS software. The instrument was calibrated against the peak positions present in the spectrum of sulphur. Once a spectrum was obtained an appropriate offset correction was applied within the OPUS software.

2.1.3. MOB instrument

The MOB spectrometer was assembled from several commercial components to provide a flexible optical bench for CCD evaluation and sample performance. The instrument was designed to match the Raman LIBS instrument proposed for the ESA ExoMars mission as closely as possible. The instrument setup can be seen in figure 2.1.1.

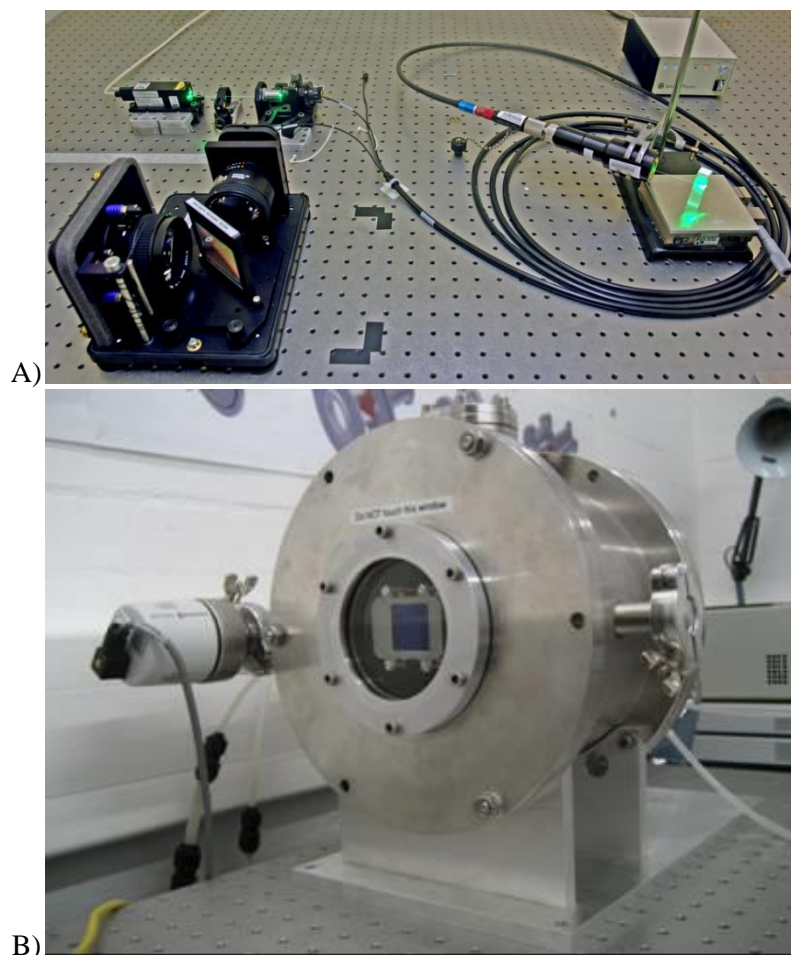


Figure 2.1.1. Photographs of the MOB instrument. The image A) shows the laser source, probe and spectrograph. Image B) shows the CCD and an early prototype housing

In figure 2.1.1 the different components of a Raman spectrometer can be seen. In image A the laser source is situated to the top left, the laser beam then travels through fibre optic cable to the probe and sample to the right, the signal then travels back into more fibre optic cables to the spectrograph at the bottom left. From the spectrograph the laser is then displayed on to the CCD which can be seen in image B.

The laser source for the MOB instrument was an Elforlight G4-30 laser which had a laser wavelength of 532 nm. The output of the laser was fixed at 30 mW, this was altered using notch filters. The laser travelled through 5m of fibre optic cable to a Kaiser MR probe head. The probe was specifically designed for the 532 nm wavelength

produced by the laser and it allowed for the spectral range of $175 - 4350 \text{ cm}^{-1}$. It was a non-contact sampling optic and had a working focal distance of 50mm. Once exposed to the sample the laser was sent to a Kaiser Holospec *f*/1.8 Holographic Imaging Spectrograph through a 50 micron slit 8mm high. The spectrograph used a HoloPlex™ Grating for the 532 nm wavelength covering the spectral range of 100 to 4350 cm^{-1} . The spectral resolution of the spectrograph was 5 cm^{-1} . A standard camera adaptor was present for imaging. The CCD was housed in an Andor CCD housing and on the CCD two orders were dispersed over 26 mm. The spectrometer was controlled by a laptop with custom built software, which obtained data directly from the CCD image, and this data was then converted to XY data. The parameters for the instrument were designed to match the specifications of the Raman/LIBS EBB spectrometer as closely as possible.

2.1.4. Data Analysis

After acquisition of spectra using the Raman instruments the spectra were subjected to the process detailed in figure 2.1.2. All instruments were calibrated, as detailed above, prior to data collection. Once a spectrum had been collected it was converted into a file format that could be opened in the GRAMS AI software. Both the MOB and Delta Nu Inspector Raman instruments produced data files which could be opened in the GRAMS AI software without the need for any type of file conversion. The Delta Nu Inspector Raman instrument produced data files which were in the proprietary GRAMS format as .SPCs. The MOB instrument exported data as an ASCII XY file and these file types, like .spc files, can be opened within the GRAMS AI software without the need for conversion. The two Renishaw Raman instruments produced spectra as .wxd files and these were converted in the instrumental WiRE 3 software into the Galactic .spc file types. The Bruker IFS66 created files in propriety OPUS format, a GRAMS AI

converter was used to convert these files into the required .spc files. After opening the data in the GRAMS AI software the data analysis performed can be seen schematically in figure 2.1.2.

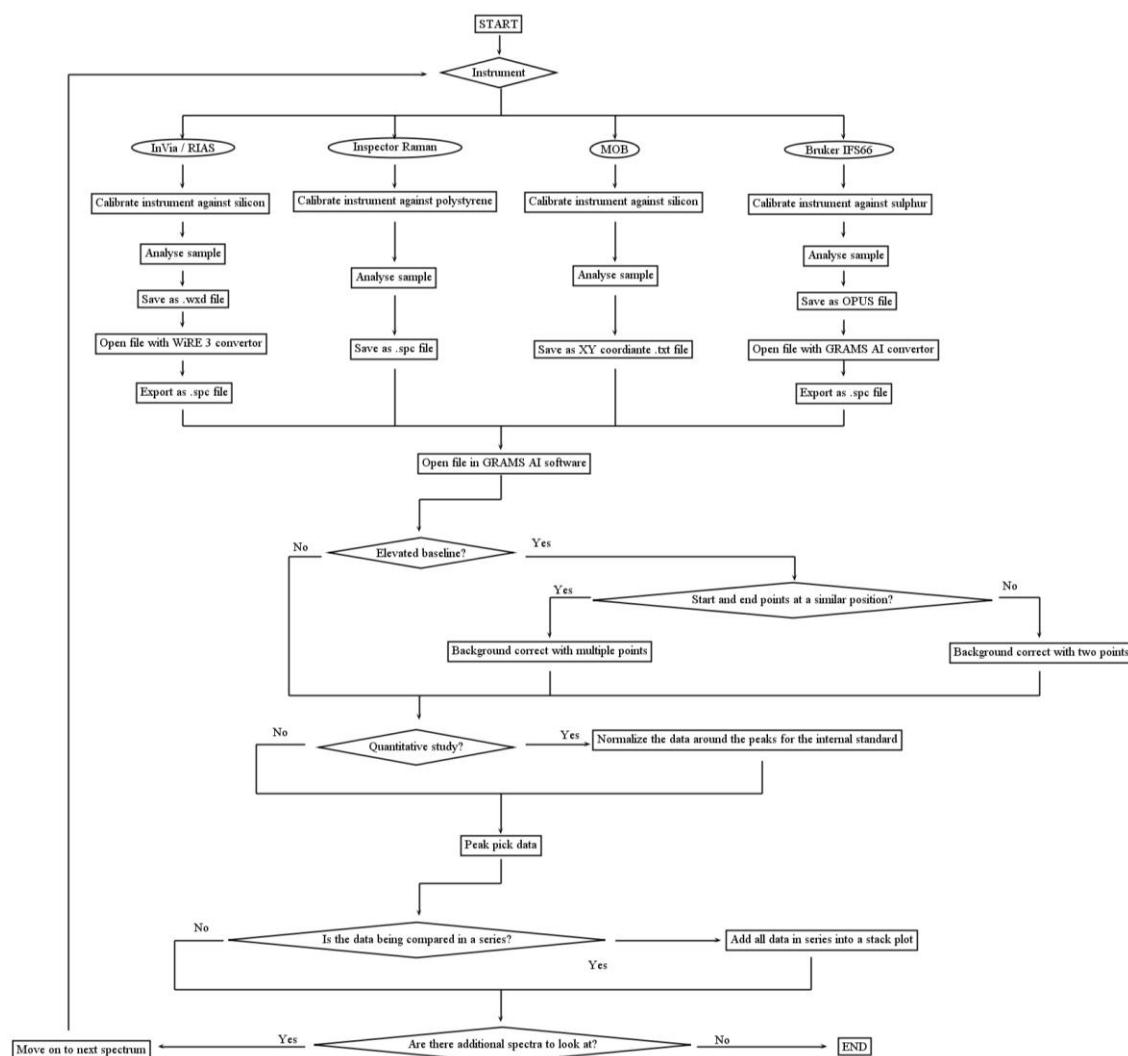


Figure 2.1.2 Diagram showing systematically how spectra are processed after collection.

Samples with an elevated baseline required a baseline correction. The samples which contained an elevated baseline were identified as spectra which featured regions with a broad increase in intensity greater than 20% of the maximum peak intensity. Examples of elevated baselines observed can be seen in figure 2.1.3.

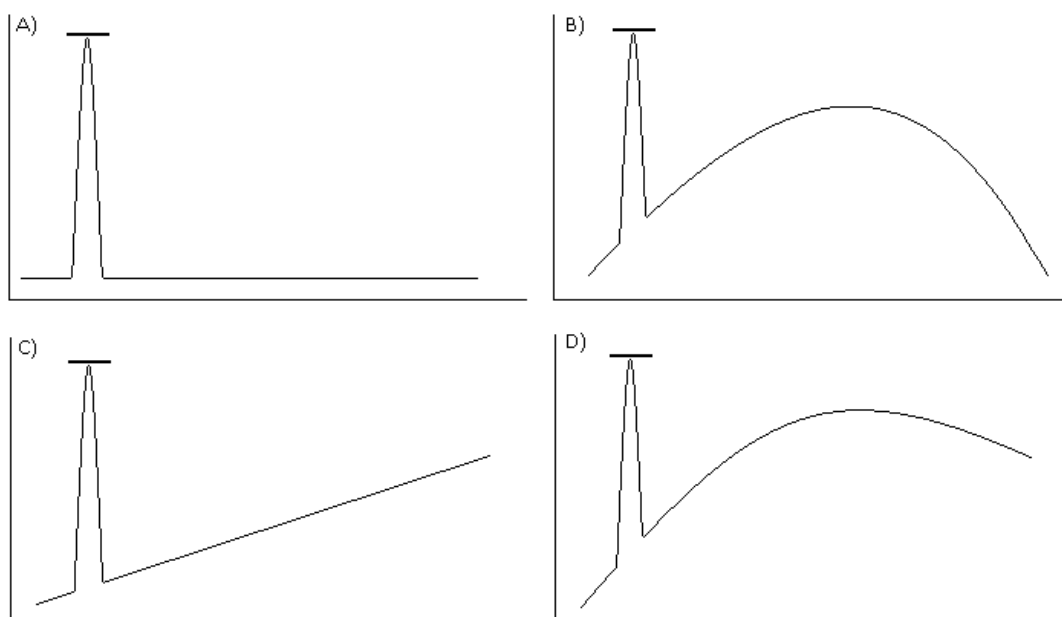


Figure 2.1.3. Examples of spectra and baseline correction methods used. A) No baseline correction needed, B) Baseline correction over multiple points, C) Baseline correction over two points and D) Baseline correction over multiple points.

In figure 2.1.3 the different types of backgrounds which occur in the spectra can be seen. In A, no background occurs and the first and last points are at equal intensities. For the spectrum B, a background is present, however the first and last points are at similar positions and therefore a simple two point correction would not resolve this baseline. For this spectrum, and spectrum D, multiple points are needed to correct this baseline. To correct with multiple points a curve was produced by plotting the baseline every 250 cm^{-1} and connecting up all these points. For spectrum C the first and last points were used to produce a straight line which was used as a baseline.

For quantitative studies an internal standard was used where an inert reagent was included with the samples. This normally took the form of a solvent which produced distinct Raman bands. When such samples were present all spectra within the series were normalised to this band, by taking the intensity of the largest peak within the spectrum and then dividing the whole spectrum by this value. The resultant spectra all

had a maximum intensity of 1 and therefore the relative intensities could be easily measured.

After the spectral processing had been performed all spectra had their peaks identified and recorded into a peak table for later reference. Within the GRAMS AI software this involved the use of the peak picking function. Using this function allowed the peaks to be automatically picked within predefined thresholds. If peaks of relevance were not identified with this automated procedure then either the thresholds were altered. Once all relevant peaks were identified the save peak table was used to export the information into an easily readable text document. In the table positions, areas and intensities for the all peaks were recorded.

For datasets where spectra were compared, such as limits of detection studies, all the spectra of relevance were opened, ordered and placed into a stack-plot. The spectra within the stack-plot were then labelled using the add text function and the image was copied and saved into a word document. Where only a single sample was relevant the image was spectrum was copied and saved into a word document without opening other files or stacking data.

2.2. Sample preparation

For all synthetic samples produced the same standards were used. Table 2.2.1 details all the standards used in this work, their source and purity.

Name	Source	Grade / Purity
Gypsum	Sigma-Aldrich	≥99%
Calcite	Sigma-Aldrich	≥99%
Naphthalene	Aldrich	99%
Anthracene	Sigma	≥99%
Sodium carbonate	Sigma-Aldrich	≥99%
Sodium sulphate	Sigma-Aldrich	≥99%
Calcium chloride	Sigma-Aldrich	≥93%
Beta-carotene	Fluka	≥97%
Phenanthracene	Aldrich	98%
Phenylalanine	Sigma Aldrich	≥98%
Aragonite	Alfa Aesar	≥99%
Jarosite	Alfa Aesar	≥99%
Trehalose	Sigma-Aldrich	≥99%
Montmorillonite	Sigma-Aldrich	≥99%
Goethite	Sigma-Aldrich	≥99%

Table 2.2.1 Standards used, details of source and purity

2.2.1. Establishing a Protocol for Analysis of Inorganic and Organic Mixtures

2.2.1.1. Analysis of prepared Organic and Inorganic Mixtures

For this section of work several samples of organic and inorganic mixtures were supplied for analysis with Raman spectroscopy prepared by a project student (Jacquie Courdy). Standards of gypsum (JC111) and calcite (JC112) were compared against synthetically produced calcium sulphate dihydrate (JC113) and calcium carbonate (JC114). Mixtures of inorganic and organic samples were then compared and details of these samples can be seen in Table 2.2.2.

Calcite-Naphthalene samples				
Percentage	Mass of naphthalene /g	Mass of Calcium chloride /g	Mass of Sodium carbonate /g	Code
25	1.00	1.50	1.50	JC143
15	0.60	1.70	1.70	JC144
10	0.40	1.80	1.80	JC145
5	0.20	1.90	1.90	JC146
2	0.08	1.96	1.96	JC147
1	0.04	1.98	1.98	JC148
0.5	0.02	1.99	1.99	JC149
Gypsum-Naphthalene samples				
Percentage	Mass of naphthalene /g	Mass of Calcium chloride /g	Mass of Sodium sulphate /g	Code
25	1.00	1.50	1.50	JC150
15	0.60	1.70	1.70	JC151
10	0.40	1.80	1.80	JC152
5	0.20	1.90	1.90	JC153
2	0.08	1.96	1.96	JC154
1	0.04	1.98	1.98	JC155
0.5	0.02	1.99	1.99	JC156

Table 2.2.2. Mass of compounds used to form gypsum-naphthalene and calcite naphthalene mixtures

The samples coded JC111 to JC114 and JC152 to JC156 were analysed using Raman spectroscopy. The samples were magnified using the x50 objective for both one accumulation and then again for 5 accumulations. Following this, spectra of samples JC143 to JC156 were recorded for 5 accumulations using the x5, x20 and then x50 objectives.

Map Number	Number of points	Distance between points(μm)	Objective
1	9	2	X20
2	121	2	X20
3	121	2	X20
4	25	5	X5

Table 2.2.3. Map parameters used in analysis

Raman spectroscopy maps were collected for the JC144 sample, which contained 15% naphthalene in calcite. 5 maps were produced using different parameters. All maps were

obtained from 1 accumulation for 1 second at 100% laser power; the varying parameters for each map are shown in Table. 2.2.3.

2.2.1.2. Preparation of Inorganic and Organic Mixture

All samples prepared of inorganic and organic mixtures follow a similar method, where they are mixed as two solids, a solid and solution or two solutions. The inorganic components used in the mixtures were all prepared by the same method. Samples within this section were verified using powder X-ray diffraction and comparing the resultant with the ICDD and PD4 databases. For calcite the samples were prepared by mixing a solution of calcium chloride dihydrate and sodium carbonate. The solvents were then removed using either rotary evaporation or filtration. Gypsum was prepared by the same method using sodium sulphate in the place of the sodium carbonate. Figure 2.2.1 shows the equations and amounts used in each sample synthesis.

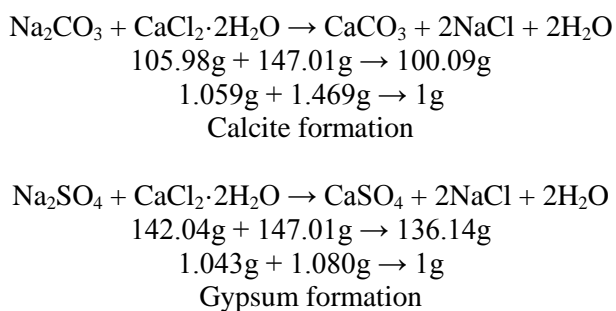


Figure 2.2.1. Equations for formulation of inorganic components and amounts needed to produce 1 g.

For preparation of these inorganic compounds several different solvents were used.

Table 2.2.4 shows details of the samples produced, solvents used and the method of solvent removal.

Code	Calcium chloride		Sodium sulphate/carbonate		Solvent removal	Product
	Solvent	Volume	Solvent	Volume		
KP111	Water	10 cm ³	Water	10 cm ³	Rotary evaporation	Calcite
KP112	Acetone	10 cm ³	Water	10 cm ³	Rotary evaporation	Calcite
KP113	Water	1 cm ³	Water	6 cm ³	Filtration	Calcite
KP114	Water	1 cm ³	Water	6 cm ³	Rotary evaporation	Calcite
KP132	Water	40 cm ³	Water	6 cm ³	Rotary evaporation	Gypsum

Table 2.2.4. Table showing different pure inorganic products produced for analysis

To produce mixtures of two solutions the same method was used for all samples. The organic component was dissolved in acetone and this solution was added to the inorganic solvent. Due to the insolubility of the resultant inorganic components, the precursors were instead used in water solutions. The three solutions (organic and two inorganic precursors) were simultaneously combined. Once combined the samples were then reduced using rotary evaporation. All samples produced used acetone to form the organic solution except for sample KP121, which used methanol in its place. Details of the all the samples can be found in table 2.2.5.

Code	Inorganic phase	Calcium chloride		Sodium carbonate / sulphate		Organic phase	Mass of organic (g)	Volume of solvent (cm ³)
		Mass (g)	Volume of water (cm ³)	Mass (g)	Volume of water (cm ³)			
KP120	Calcite	0.5	10	0.5	10	Naphthalene	0.5	10
KP121	Calcite	0.5	10	0.5	10	Naphthalene	0.5	10
KP127	Calcite	0.16	2	0.22	1	Naphthalene	0.05	2
KP128	Calcite	0.11	2	0.15	1	Naphthalene	0.05	2
KP129	Calcite	0.05	2	0.7	1	Naphthalene	0.05	2
KP130	Calcite	0.05	2	0.7	1	Naphthalene	0.1	2
KP131	Calcite	0.05	2	0.7	1	Naphthalene	0.15	2
KP133	Gypsum	0.16	2	0.16	1	Naphthalene	0.05	2
KP134	Gypsum	0.11	2	0.10	1	Naphthalene	0.05	2
KP135	Gypsum	0.05	2	0.05	1	Naphthalene	0.05	2
KP136	Gypsum	0.05	2	0.05	1	Naphthalene	0.1	2
KP137	Gypsum	0.05	2	0.05	1	Naphthalene	0.15	2

Table 2.2.5. Table showing different mixtures produced using solution-solution mixing methods.

Mixtures produced from a solid and solution all followed the same generic formula. For these samples the organic solutions were added to solid standards of the inorganic compounds. As in the solution-solution mixing methods, the organic compound was dissolved in acetone and then, when added to the inorganic solid, reduced using rotary evaporation. Table 2.2.6 details all the samples produced using this method.

Code	Inorganic phase	Amount of inorganic	Organic phase	Amount of organic	Acetone volume
KP115	Calcite	0.15 g	Naphthalene	0.05 g	10 ml
KP116	Calcite	0.10 g	Naphthalene	0.05 g	10ml
KP117	Calcite	0.05 g	Naphthalene	0.05 g	10 ml
KP118	Calcite	0.05 g	Naphthalene	0.10 g	20 ml
KP119	Calcite	0.05 g	Naphthalene	0.15 g	30 ml
KP138	Gypsum	0.15 g	Naphthalene	0.05 g	10 ml
KP139	Gypsum	0.10 g	Naphthalene	0.05 g	10ml
KP140	Gypsum	0.05 g	Naphthalene	0.05 g	10 ml
KP141	Gypsum	0.05 g	Naphthalene	0.10 g	20 ml
KP142	Gypsum	0.05 g	Naphthalene	0.15 g	30 ml
KP145	Calcite	0.15 g	Anthracene	0.05 g	10 ml
KP146	Calcite	0.10 g	Anthracene	0.05 g	10ml
KP147	Calcite	0.05 g	Anthracene	0.05 g	10 ml
KP148	Calcite	0.05 g	Anthracene	0.10 g	20 ml
KP149	Calcite	0.05 g	Anthracene	0.15 g	30 ml
KP150	Gypsum	0.15 g	Anthracene	0.05 g	10 ml
KP151	Gypsum	0.10 g	Anthracene	0.05 g	10ml
KP152	Gypsum	0.05 g	Anthracene	0.05 g	10 ml
KP153	Gypsum	0.05 g	Anthracene	0.10 g	20 ml
KP154	Gypsum	0.05 g	Anthracene	0.15 g	30 ml

Table 2.2.6. Table showing different mixtures produced using solid-solution mixing methods.

2.2.1.3. Goethite samples and Martian soil simulant samples

Three sets of samples were prepared with mixtures of a Martian soil simulant (MRS07) and beta-carotene, goethite and beta-carotene and goethite and anthracene. The organic components were added to the solid inorganic components to form a solid-solid

mixture. For each sample set, 5 different sample concentrations were prepared to produce 1, 2, 5, 10 and 25 % w/w samples.

2.2.2. Development of Criteria for Instrument Performance Comparison

In this section three mixtures were used: naphthalene in toluene, naphthalene in acetone and calcite in trehalose. For the naphthalene in toluene mixtures; naphthalene was dissolved in different quantities of toluene to produce of 1, 5, 10, 25, 50, and 100 % w/v solutions. This process was then repeated using acetone as a solvent. For the trehalose and calcite mixtures the previously used solid-solid method was used to produce mixtures of 5, 10 and 25 % w/w mixtures.

For the systematic identification of compounds work in this chapter, standards of several organic and inorganic compounds were analysed using Raman spectroscopy. Anthracene, beta-carotene, naphthalene, phenanthracene and phenylalanine were all organic compounds interrogated. Aragonite, calcite, gypsum and jarosite were all analysed as inorganic compounds. Details of these standards can be found in the table 2.2.2.

2.2.3. Instrument performance comparators

This section of work investigated the comparability of two different Raman instruments: the InVia and MOB instrument. All samples analysed in this section were investigated previously. Therefore their spectra was already established and interpreted. The experimental work within this section involved optimization of the spectra through alterations to the instrumental parameters. The calcite and trehalose mixtures

interrogated in chapter 4 were used as standards in the development of a reproducible method of obtaining reproducible spectra between the two instruments.

The prototype instrument's probe was mounted at the 90 degree angle so that the laser pointed downwards towards a flat sample. A stage was prepared where nanometre movements could be performed on the slide in X, Y and Z planes. The stage and probe were then housed within an enclosure to minimize light at the sample. Two slides were prepared on top of one another; the upper slide had a hole in the middle to house the sample. The midpoint in the X and Y directions were measured and marked on the slide. These markings allowed for lining the laser up into the middle of the sample on both instruments, on the InVia using the microscope and on the prototype instrument using the stage.

To compensate for differences within homogeneity of the sample multiple points were looked at. Each point was a set known distance from the centre of the slide. This distance was consistently used to travel in all directions around the midpoint of the slide to produce a 3 by 3 grid of points. Spectra were recorded at all these points on each instrument and then compared.

After establishing the issues with reproducibility within this setup on the micron scale a hole was drilled in a thin copper slide to produce a mask. Samples were analysed using Raman spectroscopy through the mask. To test the effect the slide had on spectra of the sample; silicon and the previously used calcite trehalose mixtures were analysed through the mask.

Inorganic phase	Organic phase	Concentration % w/w	Code
Gypsum	Glycine	25%	GG04
Gypsum	Glycine	1%	GG01
Gypsum	Trehalose	1%	GT01
Calcite	Naphthalene	10%	CN03
Calcite	Naphthalene	1%	CN01
Calcite	Phenylalanine	25%	CP04

Table 2.2.7 Table of samples analysed

Using the instrument validation parameters developed in chapter 4 several samples were produced which contained desirable spectral features (Table 2.2.7). These samples were analysed using the slide and mask on both the Renishaw InVia and prototype MOB Raman spectrometers.

Data from the Rover instrument was converted into XY data files, therefore for comparison within GRAMS these files were first converted into .SPC files. Due to differences within the spectral ranges analysed with both instruments any regions below 220 cm^{-1} or above 2200 cm^{-1} were removed. This allowed easy comparison of finger print regions produced by both instruments. To remove background from the samples all sets of spectra were baseline corrected using multiple points with the baselines set to zero.

2.2.4. Exemplar systems

Three geological standards were analysed using Raman spectroscopy; trona, sodium bicarbonate and thermaonatrite. The spectra for these standards were then compared to the unknown sample believed to be trona.

The samples; 5 α -cholestane, 5 α -ergostane-3 β ,11 β -diol, ergosterol, 17 α -(H),21 β -(H)-hopane in solution and hop-21(22)-ene in solution were sourced through Sigma Aldrich. Table 2.2.8 shows the structure of each sample. Each of these samples was from distinct biomarker groups which allowed for the identification of peaks indicative of the sample group and additionally of individual peaks enabling differentiation to be accomplished between the individual compounds.

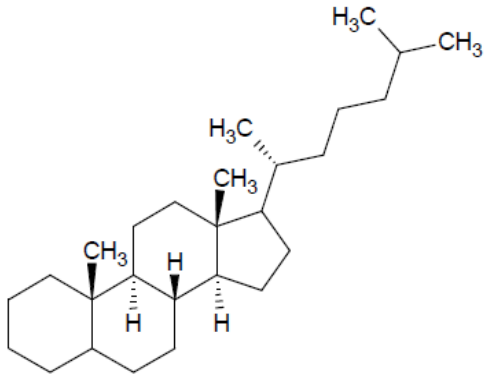
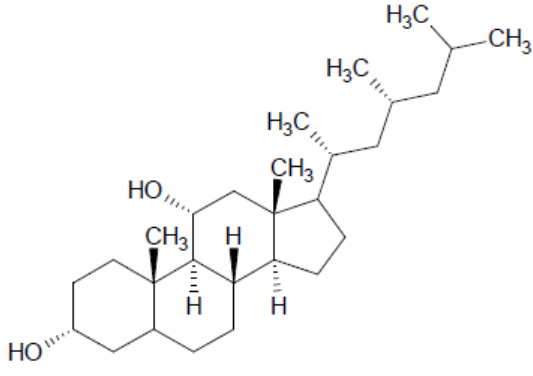
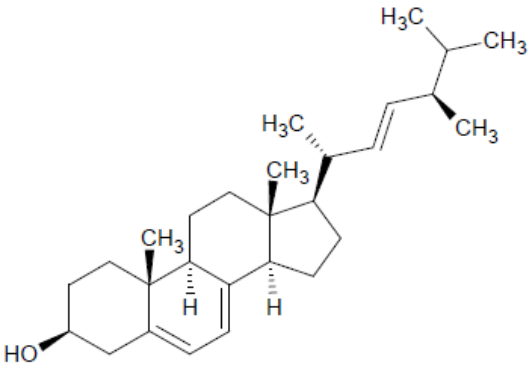
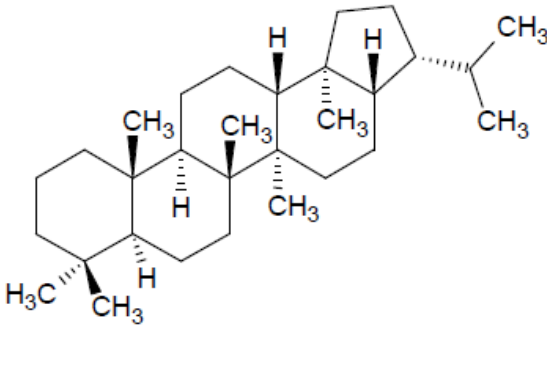
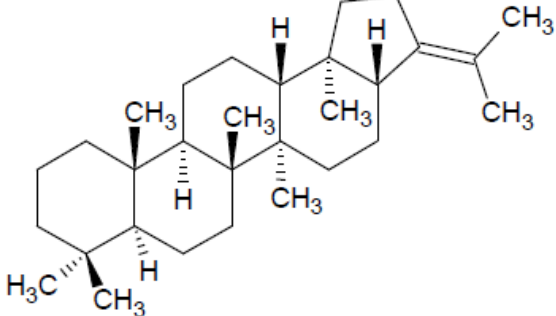
<p style="text-align: center;">5α-cholestane</p> 	<p style="text-align: center;">5α-ergostane-3β,11β-diol</p> 
<p style="text-align: center;">Ergosterol</p> 	<p style="text-align: center;">17α-(H),21β-(H)-hopane</p> 
Hop-21(22)-ene	
	

Table 2.2.8. The chemical structure of each biomarker

Following analysis of the individual compounds the samples ergosterol and cholestane were used to produce a variety of mixed powder samples. These samples were prepared for analysis by Raman spectroscopy to establish if detection and differentiation between the two compounds was possible. The mixtures were created using the % w/w mixtures shown in table 2.2.9.

Sample No.	Cholestane (mg)	% Composition	Ergosterol (mg)	% Composition
1	0.0	0	40.0	100
2	0.4	1	39.6	99
3	0.8	2	39.2	98
4	2.0	5	38.0	95
5	4.0	10	36.0	90
6	10.0	25	30.0	75
7	20.0	50	20.0	50
8	30.0	75	10.0	25
9	36.0	90	4.0	10
10	38.0	95	2.0	5
11	39.2	98	0.8	2
12	39.6	99	0.4	1
13	40.0	100	0.0	0

Table 2.2.9 Composition of cholestane and ergosterol mixed powder samples

Thirteen w/w mixed samples were prepared in total and subjected to analysis using the 50x objective lens, the 20x objective and the 5x objective lens using the 785nm laser for 1 spectral acquisition at 50% laser power and a 10 second exposure time. The spectra were then subjected to baseline correction and normalisation using GRAMS AI software.

To prevent loss of sample, the hopanoid samples were analysed in the glass bottles in which they were supplied. For the hopanoid sample analysis was carried out using a 15x objective lens, at the 785 nm laser line, 100% power for 1 spectral acquisition and a 10 second exposure time.

To supplement the work on the solid mixtures of compounds, samples of known concentrations of ergosterol in solution were prepared. A 0.1 M standard solution was prepared by dissolving 1.00 g of ergosterol in dichloromethane in a 25 cm³ volumetric flask. A 10 cm³ portion of the sample was transferred to a 10 cm³ volumetric flask from which a 2 cm³ sample was removed. The solution was made up to 10 cm³ by addition of dichloromethane. Again a 2 cm³ sample was removed and the remaining solution made up to the 10 cm³ by addition of dichloromethane. This process was repeated until ten sample solutions were obtained of known concentration.

The samples were analysed in a mirrored cuvette cell using the 15x objective lens and the 785nm laser at 100% power for 1 spectral acquisition with a 10 second exposure time. The spectrum for each liquid sample was again baseline corrected and subject to normalisation.

Raman spectra were obtained from a sample of halite rock from the Yungay region of the Atacama Desert. Sites of possible inclusions on and within the samples had been identified and therefore spectra were obtained from various different locations on each sample. A section of the inclusion and rock was then broken off, ground using a mortar and pestle and then mixed in a ball mill. The resultant mixture was then analysed using a 3 by 3 grid system with the Renishaw InVia Raman spectrometer.

Nine samples of different bacteria were supplied from University College London. Both freeze dried and liquid cultures of the samples were supplied and are shown in table 2.2.10.

Bacterial strain	Label	Cell density in liquid culture	Mass of lyophilized powder
E.coli	EC	9×10^9 cells/ml	0.138 g
Deinococcus radiodurans	DR	3×10^7 cells/ml	0.102 g
Brevundimonas sp. MV.7	MV.7	3×10^8 cells/ml	0.053 g
Rhodococcus sp. MV.10	MV.10	9×10^6 cells/ml	--
Synechocystis sp. PCC6803 (cyanobacterium)	cyano	2×10^7 cells/ml	0.045 g

Table 2.2.10. Bacterial samples analysed using Raman Spectroscopy

Samples were all analysed using both 1064 nm (Bruker IFS66/FRA 106 FT-Raman instrument) and 633 nm (InVia instrument). The bacteria were then irradiated with an 80 kGy gamma ray dose and analysed again. A sample of *Deinococcus radiodurans* was placed onto a slide, analysed using Raman spectroscopy. The sample was then photon irradiated and analysed a second time

2.3. Storage and systematic naming of samples

Upon collection of several datasets with multiple parameters for various concentrations a method of easy cataloguing is required. Due to the high volume of data collected, a method of having easy access to a certain file would require a large amount of time to locate. Therefore an easy way of identifying each sample was needed, however due to the large number of variables in each sample a simple systematic naming convention would give no information.

Prior to any work on making the data easily identifiable the data first had to be collated into a single location for easy access. The simplest way to do this was to create a database and enter each sample into it. Therefore the 260 different samples were entered into a database. Information was entered into the database under the headings shown in Table 2.3.1:

Name	Description
Date of entry	Date at which the sample data was placed into the database
Unicode	A unique identifying code which gave details about all the parameters of each sample. (See below)
working code	The identifying code on the samples after preparation
originator	The initials of the person who prepared the sample
lab book ref	The identifying code of the sample in the corresponding lab book
Solvent	Solvent used to prepare the solution
Mixing type	Method of how the samples were prepared e.g. Solid-solid, Solid-solution or Solution-solution
inorg phase	Inorganic phase within the sample
organic phase	Organic phase within the sample
ratio w/w	Ratio of organic to inorganic or percentage weight by weight
DB ref original	Filename of the sample
R-1064	Hyperlink to Raman 1064nm spectrum
R-785	Hyperlink to Raman 785nm spectrum
R-633	Hyperlink to Raman 633nm spectrum
R-514.5	Hyperlink to Raman 514.5nm spectrum
XRD	Hyperlink to X-ray defraction pattern
FTIR	Hyperlink to FTIR spectrum
preparation notes	Additional notes relating to the sample

Table 2.3.1 Details of the different sections within the database and their description

For the Unicode value a unique identifying name was needed for each sample. However to make identifying each sample easier it was desired that this code also was able to identify what a sample was simply from its name. To keep this naming a code was used within the database (Appendix 1): Using the devised code the files are named based on the following information:

EX08 - Refers to the ExoMars Project (the EX part) data collected in 2008 (the 08 part)

Cal, Gyp, Goe, Mon or MRS - Referring to the inorganic material being Calcite, Gypsum, Goethite, Montmorillonite or MRS07

Nap, Ant, Pan, Tre, Cel, Pal, Gly, β -C or Glu - Referring to the organic material being Naphthalene, Anthracene, Phenanthracene, Trehalose, Cellulose, Phenylalanine, Glycine, β -Carotene Glucose

rX_X or p100_X - Refer to the ratio of the mixture, either r meaning ratio or p meaning based of a percentage.

EXXX - Refers to the sample number

XX - Initials of the person who prepared the sample.

All 260 entries were then entered into the database and names were generated. To link up spectra, hyperlinks were made linking each spectrum obtained to the sample.

Chapter 3

Establishing a Protocol for Analysis of Inorganic and Organic Mixtures

The aim of this section is to investigate methodology for reproducible analysis of inorganic and organic mixtures. This includes deducing the ability for Raman spectroscopy to obtain accurate and precise limit of detection values and an optimal analysis protocol is produced. Different mixing methods are interrogated and their resultant sample homogeneity investigated and the optimal sample preparation method is devised. Using these protocols, the ability for Raman spectroscopy to detect an organic in exemplar Mars relevant materials is established.

3.1. Raman Analysis of an Organic Compound within an Inorganic Matrix.

The search for life on Mars requires looking for an organic material within an inorganic matrix. Organic materials are often indicative of life and as such several organic compounds have been identified as signs of life^[94,96,144-146]. The organic compound in most instances would occupy niche areas within the inorganic soil or rocks^[94,145]. This has been observed in Antarctic lacustrine sediments^[147], endoliths from Antarctic cold deserts^[86] and organic materials within Martian meteorites^[148]. Therefore when simplified into a laboratory environment this means the process involves looking for an organic within an inorganic. To find an indication of extant or extinct life within a Martian environment a technique for detecting these types of samples is required. To facilitate this, evaluation specimens of known concentrations were prepared for analysis by Raman spectroscopy. Prior to looking at real samples within a controlled

environment it must be established if the instrument can actually detect organic compounds within an inorganic one, and therefore simple mixtures are used.

For samples to be comparable to that which would be found on the surface of Mars, careful selection of suitable organic and inorganic materials must be chosen. For the purposes of this work the inorganic materials of gypsum and calcite were chosen and the organic material naphthalene was used. Inorganic materials often found on the surface of Mars include sulphates such as gypsum^[78] and carbonates such as calcite^[145]. Naphthalene was used as polycyclic aromatic hydrocarbons have been previously identified in meteorite samples and the presence of such compounds could indicate the presence of microbes^[149-151].

In this section of work mixtures were produced of the organics and inorganics at different concentrations. From these mixtures of different concentrations, limits of detection for the Raman instrument can be calculated. To use limits of detection accurately; homogenous mixtures are required. This requires an organic material to be “included” within the inorganic sample. There are 3 different ways in which samples can be prepared in inclusions; “physical” inclusions, physisorption and chemisorption^[152]. In a “physical” inclusion the organic molecules are surrounded by the inorganic particles and thus become trapped as the sample comes out of solution^[153]. In physisorption the different compounds become attracted to each other via hydrogen bonding or weak van der Waal’s forces^[153]. Chemisorption occurs when either covalent or ionic bonds form between the inorganic and organic molecules^[153].

Mixtures of organic and inorganic compounds can be created using several different states: solid-solid, solid-solution, and solution-solution. In solid-solid mixing the two

compounds are simply ground or mixed together in the solid form. In solid-solution mixing one component is dissolved into solution and this solution is then mixed with the other compound in solid form. Solution-solution mixing occurs when both compounds are mixed together while dissolved in a suitable solvent. Upon mixing of samples the solvent was removed from the mixture using rotary evaporation and the remaining material contained only the organic and inorganic components.

Twelve different samples were produced; six of calcite with naphthalene mixtures, produced by mixing naphthalene in solution with sodium carbonate and calcium chloride. Another six were produced with gypsum mixtures using sodium sulphate and calcium chloride with the naphthalene in solution. Raman spectra were obtained of each of the samples, of the original formed compounds prior to mixture and also of the pure compounds.

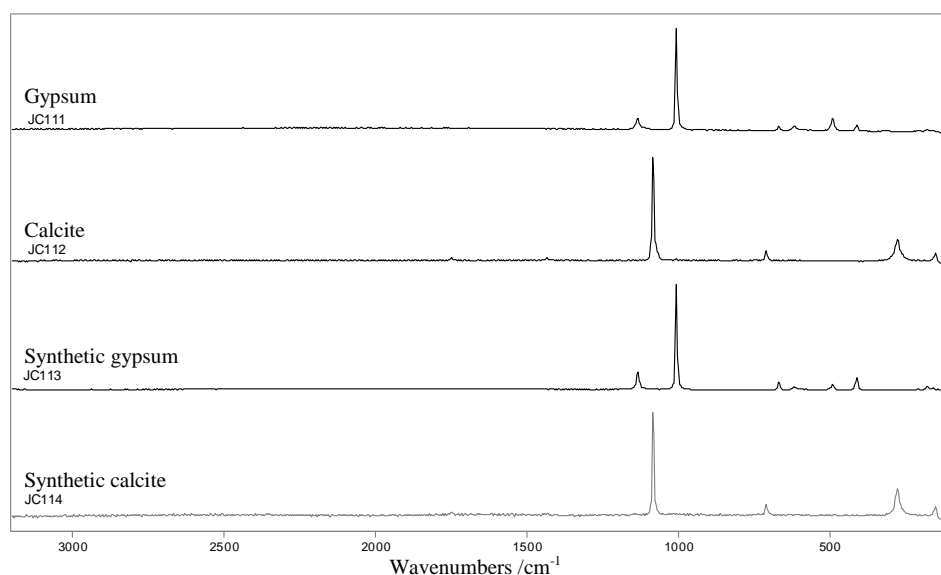


Figure 3.1.1. Raman spectrum of gypsum and calcite standard samples and the synthetic samples (JC111 to JC114)

Spectra were obtained of the inorganic material produced and of the standards of each inorganic compound (Figure 3.1.1). For the gypsum standard (JC111) and the synthetic

gypsum (JC113) all the major peaks were consistent. In table 3.1.1 all the peaks in the naphthalene spectrum are identified and assigned.

Wavenumbers /cm ⁻¹	Assignment ^[154,155]
1141	v ₃ antisymmetric stretch vibration modes
1007	v ₁ symmetric stretch vibration modes of SO ₄
620	v ₄ antisymmetric bending vibration modes
493	v ₂ symmetric bending of SO ₄
409	v ₂ symmetric bending of SO ₄

Table 3.1.1. Peak assignments for gypsum standard

In the synthetic sample of gypsum peaks were present at 1139 cm⁻¹, 1005 cm⁻¹, 621 cm⁻¹, 491 cm⁻¹ and 409 cm⁻¹ and these peaks are all similar to those present in the standard spectrum^[154,155]. This indicates a strong match between the two samples; JC111 and JC113. Minor shifts present within the synthetic peaks can be attributed to the broadening of the peaks due to instrument resolution. Instrument resolution affects the accuracy to which peaks can be resolved and therefore at low resolutions, peaks will appear broader. The peak attributed to the symmetric stretch vibration mode of SO₄^[154,155] at 1005 cm⁻¹ is the most intense peak within both spectra of the samples and has a similar signal to noise ratio. Some differences do occur; the intensity ratios between the peaks at 491 cm⁻¹ and 409 cm⁻¹, relating to the symmetric bending of SO₄^[154,155]. This is can be attributed to the samples position whereby the samples are orientated differently. Disorientating gypsum has previously been established to effect the relative intensities of peaks within the spectrum, whereby the orientation of the gypsum can alter the relative band intensities within the spectrum and even, at some orientations, remove bands entirely^[156]. Similar observations have also been made about calcite crystals^[157].

Wavenumbers /cm ⁻¹	Assignment ^[158]
1087	ν_1 -Symmetric CO ₃ stretching
713	ν_4 -Symmetric CO ₃ deformation
282	T(Ca, CO ₃)
155	T(Ca, CO ₃)

Table 3.1.2. Peak assignments and structure of calcite (T, translational lattice mode.)

The same result occurs when comparing the spectrum of calcite (JC112) and that of synthetic calcite (JC114) produced from mixing calcium chloride and sodium carbonate in solution. Peaks are present in both spectra at 1086 cm⁻¹, 708 cm⁻¹, 278 cm⁻¹ and 156 cm⁻¹ (Table 3.1.2). In this instance the peak at 1084 cm⁻¹, associated with CO₃²⁻ stretching, produces the strongest intensities in both spectra and has a similar signal-to-noise ratio observed. Therefore its presence, when seen in a mixture, would be indicative of this compound. Similar relative intensity shifts and peak position shifts can be seen as observed that were seen in the gypsum samples.

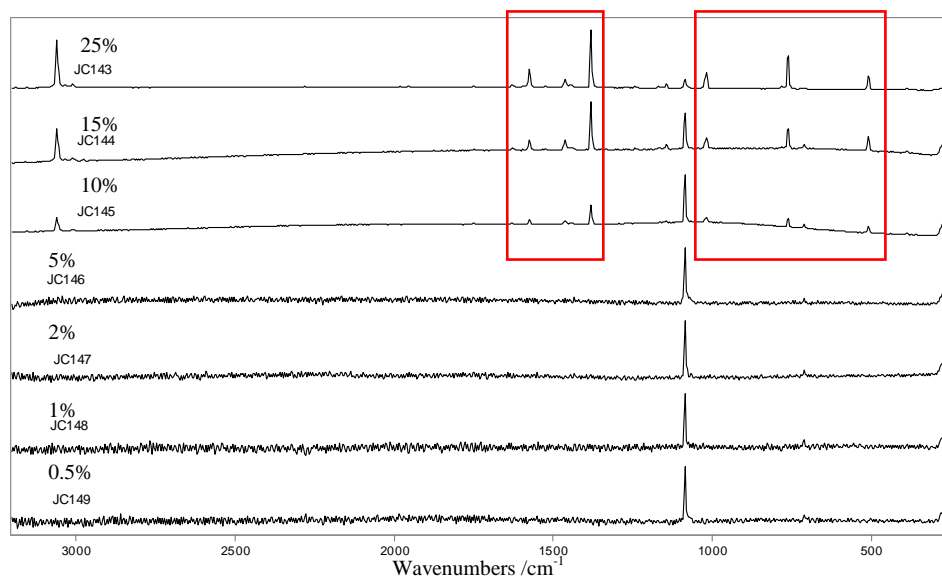


Figure 3.1.2 Raman spectrum of calcite-naphthalene mixtures at different concentrations from 25% (JC143) to 0.5% (JC149)

Spectra were obtained of the samples of calcite and naphthalene mixtures JC143 to JC149 produced using solution-solution mixing (Figure 3.1.2). The samples are ordered and displayed from highest naphthalene concentration of 25 %, JC143, to lowest

concentration of 0.5 %, JC149. The organic component only remains visible at higher concentrations; samples 25% (JC143) to 10% (JC145).

Wavenumbers /cm ⁻¹	Assignment ^[159]
3057	CH stretching
1629	CC stretching
1578	CC stretching
1380	CH in-plane bending
1169	CH in-plane bending
1147	Ring symmetric deformation, ring trigonal deformation
1021	CH out-of-plane bending
764	Ring antisymmetric deformation, bending CH

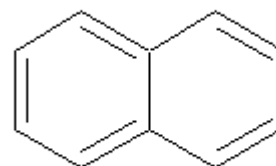


Table 3.1.3. Peak assignments and structure of naphthalene

Table 3.1.3 shows all the bands associated with naphthalene and the bands at 3055 cm⁻¹, 1576 cm⁻¹, 1461 cm⁻¹, 1380 cm⁻¹, 1017 cm⁻¹, 765 cm⁻¹ and 508 cm⁻¹ are present within these spectra. The major peaks at 1380 cm⁻¹, relating CH bending, and 3055 cm⁻¹, relating to the CH stretching, both remain present in the spectra where the naphthalene concentration is at or above 10%. From this it can therefore be assumed that for concentrations above 10% the organic component would be visible.

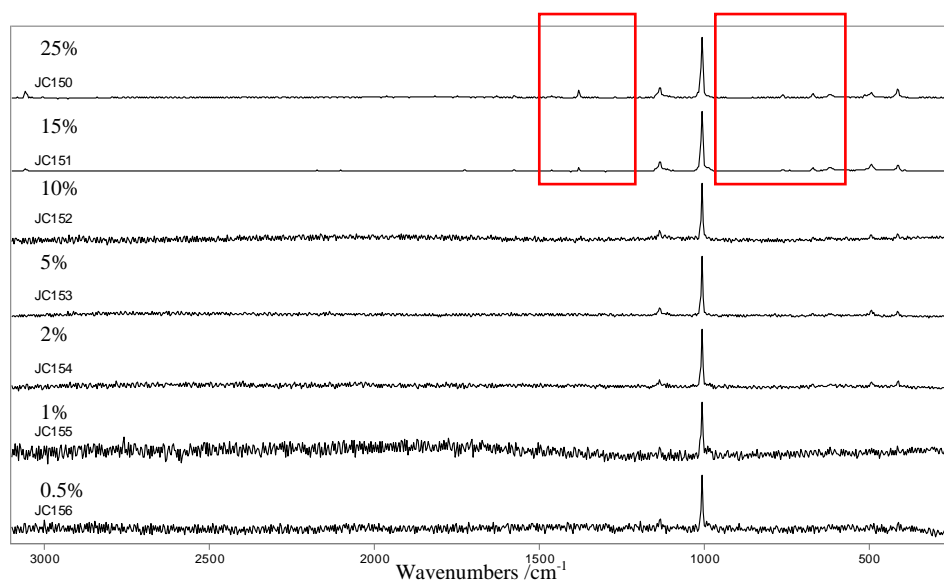


Figure 3.1.3 Raman spectrum of gypsum-naphthalene mixtures from 25% (JC150) to 0.5% (JC156)

Spectra were obtained of the samples containing naphthalene and gypsum, JC150 to JC156, where the concentration of naphthalene within the mixture was reduced between each sample (Figure 3.1.3). Organic present within the spectra only occurs in samples JC150 and JC151. The bands at 3055 cm^{-1} , 1380 cm^{-1} and 765 cm^{-1} are present within these spectra. The major peaks at 1380 cm^{-1} , relating to CC and CH bonds and 3055 cm^{-1} , relating to the CH bonding, both remain present in the spectra where the naphthalene concentration is at or above 15%. Therefore theoretically any presence of organic above 15% would be visible.

For these samples the relative intensities all follow a similar trend where the Raman peak intensities are proportional to the concentration. One of the potential issues of the mixing method used here was that the sample may not be homogenous, which would result in spectra where components appear to have a higher or low concentration than they should have. Therefore to investigate whether these results are reliable, investigation of the concentrations within the samples and the homogeneity of the

samples is required. To do this several maps were produced of the same sample over different locations.

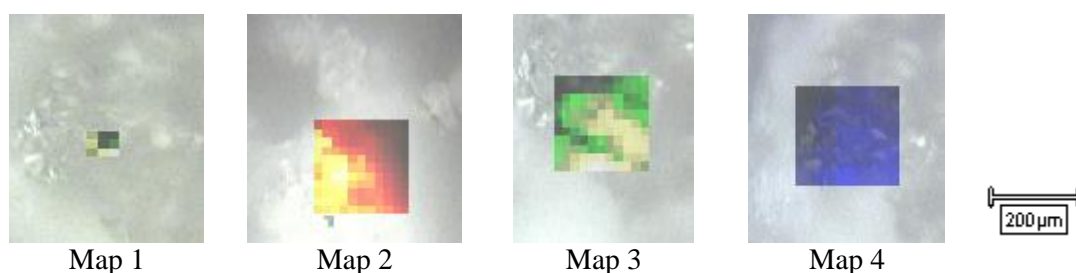


Figure 3.1.4 Maps of sample 15 % naphthalene in calcite JC144

Five Raman maps were performed on the sample of 15 % naphthalene in calcite; JC144. This sample was used due to it consistently showing both calcite and naphthalene components within the Raman spectra obtained. The maps produced show there is not always an even distribution of organic materials within the samples. Map 1. Looked at the variation within 9 points over 2 μm . In this map several differences between the points can be observed, however the small area used makes the map unrepresentative of the whole sample. Therefore Map 2 was produced at a second location using 121 points of a 2 μm size. In this map a large amount of inorganic material is found to the southwestern region. This distribution difference may have been derived due to defocusing of the laser and therefore a second region was investigated using the same parameters; Map 3. In this map two very distinct regions of organic compounds can be seen and these do not appear to be derived from a defocusing of the sample. Therefore this map is a clear indication that homogeneity is an issue for the samples. To show the effect of homogeneity over a much larger area Map 4 was produced using the x5 objective rather than the x20 used in all previous samples. In the map it can be seen that where spectra are obtained from multiple locations over a much larger area, the spectral differences average out to have a more even distribution.

These maps show that while detection of naphthalene within an inorganic mixture is possible the samples are not homogenous. From these maps it can clearly be seen that all the samples have variation and unless every point of the sample was mapped it would be difficult to obtain a truly representative spectrum of the sample. Therefore it must be assumed that there will be variation within the spectrum. By using multiple different points within the spectrum this allows some of the extremes of these differences to be seen. Taking the average of these points the data then becomes a more accurate spectrum of the sample. For limits of detection studies to be carried out it must be reproducible and thus further work must be carried out to look into why the samples are not homogeneous. To do this the methods of sample preparation and ways to optimize the mixing of the two materials must be investigated.

3.2. Preparation of Inorganic and Organic Mixtures

Having established the issues with homogeneity in the previous section, this section looks at attempting to increase the homogeneity observed. This is carried out through preparation of the samples using different inorganic and organic mixing methods. Different mixing techniques are used in an attempt to obtain samples with optimal homogeneity, and therefore the least variation across the sample. There are several different methods to produce such mixing; simple preparation of mixing the two solids, dissolving one solid and then depositing the solution onto this solid or to combine the compounds while they are both in solution.

The methods for formation of calcite and gypsum from solutions of calcium chloride and sodium sulphate or sodium carbonate have been well established in the literature^[160-162]. During the formulation process the precursor materials are required to be in solution. At this stage the addition of an organic component is possible and this organic compound can either be added as a solid, solid-solution mixing, or as a solution, solution-solution mixing. This work will concentrate on the mixing using solid-solution techniques and solution-solution techniques. For the majority of cases the organic compounds are relatively easy to dissolve using common solvents. The inorganic compounds however were relatively insoluble and therefore their more soluble precursors were dissolved and added to the organic. This in turn added an additional area of investigation, due to the possibility of interactions between the precursors and the solvents or the precursors and the organic materials.

Based on the method of the preparation of inorganic compounds carried out previously, a sample of gypsum was prepared using minimum quantities of water as a solvent. This

sample of gypsum was used to prepare all the solid-solution mixtures of varying concentrations containing naphthalene and anthracene as organic phases. Samples were also prepared using calcite for comparison between solution-solution and solid-solution mixing. 30 samples were produced in total with 3:1, 2:1, 1:1, 1:2 and 1:3 ratios of organic to inorganic using solution-solution and solid solution mixing techniques. Samples KP127-131 were produced using solution-solution mixing of calcite with naphthalene and KP133-137 used the same mixing technique for gypsum with naphthalene. For solid-solution mixing; KP115-119 were produced of calcite and naphthalene, KP138-142 gypsum and naphthalene, KP145-149 calcite and anthracene and KP150-154 gypsum and anthracene. These samples were then analysed using Raman spectroscopy at 6 different locations. For more details of these samples see Tables 2.6 and 2.7 in Chapter 2.

All the samples produced a white precipitate which visually was indistinguishable between each sample. Samples of calcite and naphthalene mixtures were also prepared using different solvents and different concentrations. In these samples it was again impossible to distinguish between the different samples visually. All samples were analysed using Raman spectroscopy and a spectral map was performed on the 1:1 naphthalene in calcite sample, KP117, to identify how homogenous the mixture was.

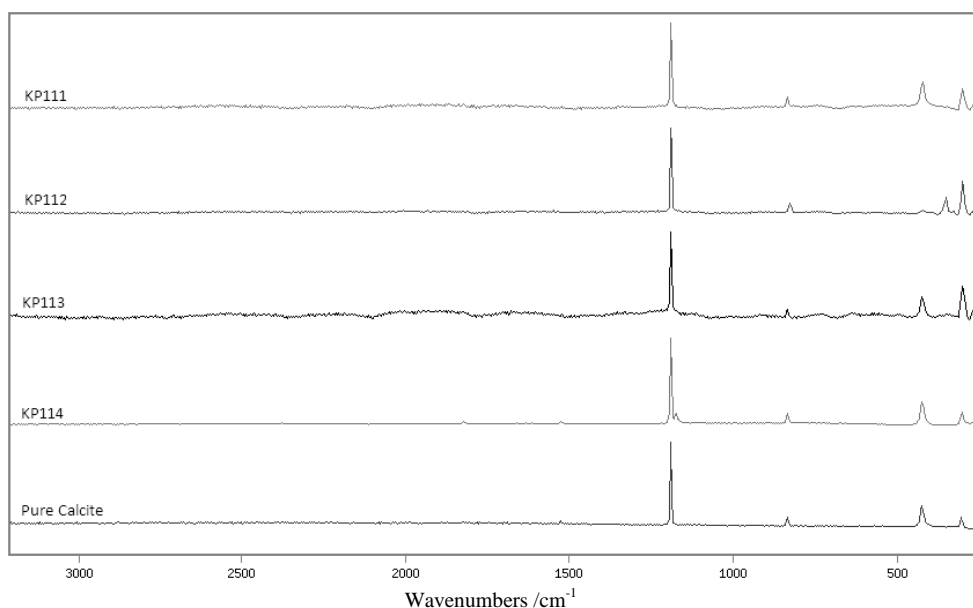


Figure 3.2.1. Raman spectrum of calcite samples produced from solvents using excess water (KP111), excess water and acetone (KP112), minimum water quantities and filtration (KP113) and minimum water quantities (KP114).

Figure 3.2.1 shows the pure calcite standard against that of the different samples of calcite produced using different solvents. Each of the calcite samples were prepared using slightly different conditions. KP111 was produced from using water as the only solvent in excess. For KP112, in acetone the sodium carbonate component was completely insoluble and therefore the sample was prepared using acetone in excess as a solvent for the calcium chloride and water in excess for the sodium carbonate. In KP113 the calcite was produced from using a minimum amount of water as the only solvent and filtering the product to remove the excess solvent. KP114 also used a minimum amount of water as the only solvent but used rotator evaporation to remove the excess solvent. While the major peaks remain present in the spectrum, KP112 features peaks much weaker than in the other samples at 275 cm^{-1} , this band relates to the translational lattice mode of Ca and CO_3^{158} . A new band occurs at 201 cm^{-1} which indicates that aragonite was also formed. This was confirmed from the powder x-ray diffraction and compared against database standards.

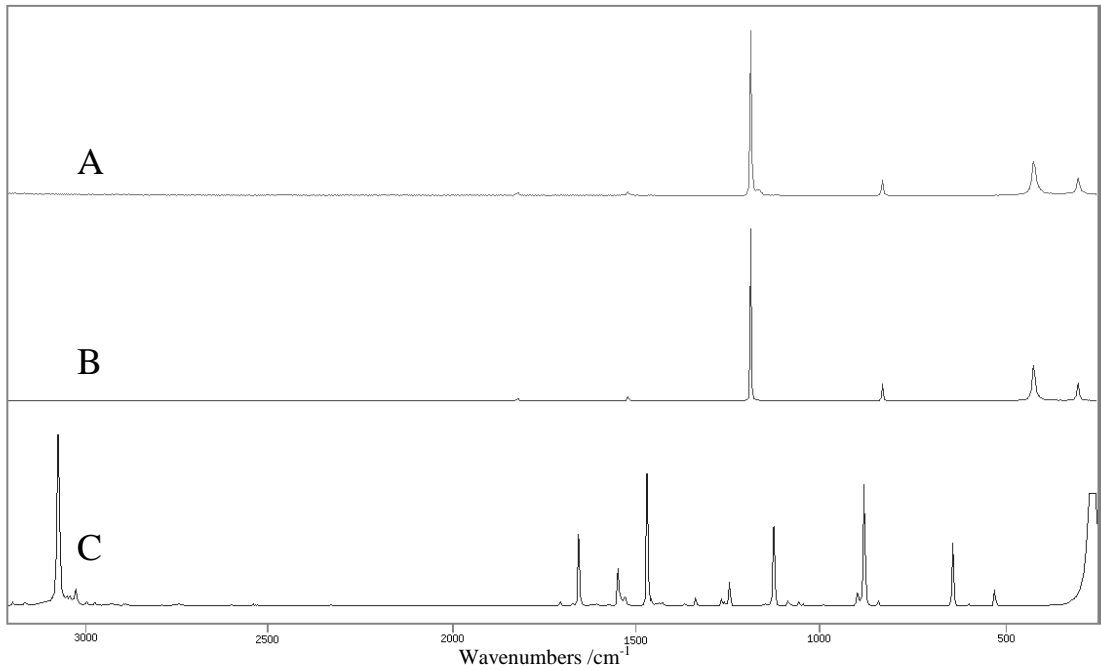


Figure 3.2.2. Raman spectra of A) KP120- Solution-solution mixture of calcite and naphthalene using the solvents water and acetone, B) Calcite and C) Naphthalene.

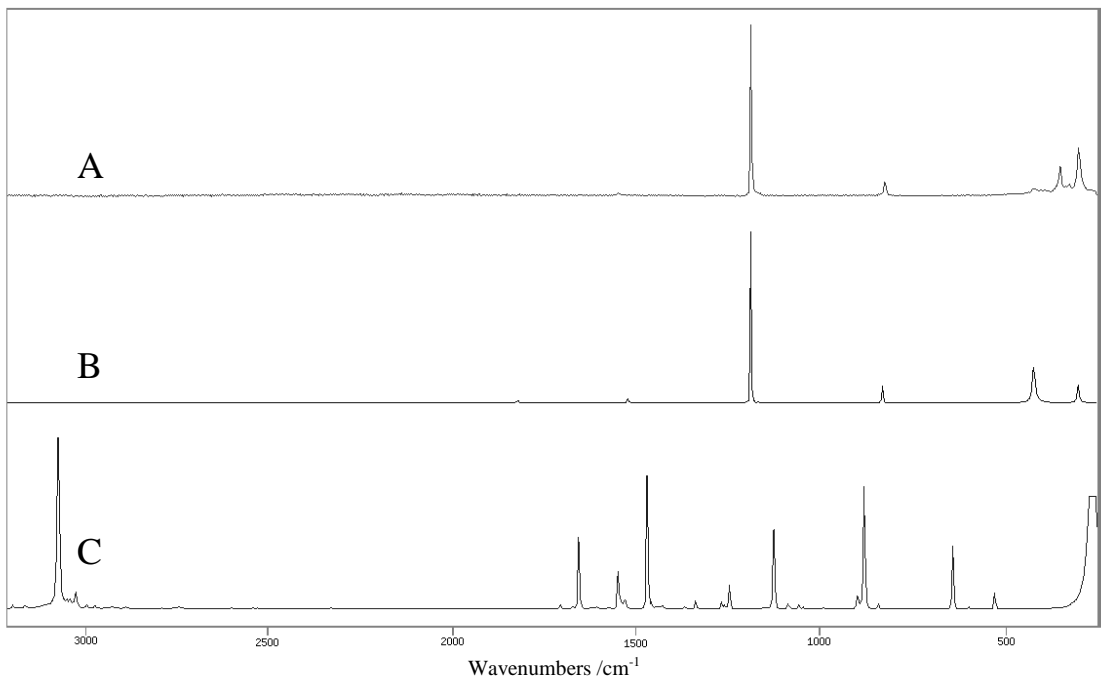


Figure 3.2.3. Raman spectra of A) KP121- Solution-solution mixture of calcite and naphthalene using the solvents water and methanol, B) Calcite and C) Naphthalene.

Figure 3.2.2 shows the spectrum of solution-solution mixed calcite and naphthalene KP120 and spectra of pure components. The presence of the naphthalene is not detectable due to its low concentration within this sample. In this spectrum a band at

275 cm^{-1} is present in this solvent and there is no peak at 201 cm^{-1} therefore the spectrum produced matches the pure calcite. However in figure 3.2.3 the band at 275 cm^{-1} does not appear and instead an aragonite peak at 201 cm^{-1} occurs. The only difference between samples KP120 and KP121 is the solvent used. In KP120 acetone was used to dissolve the naphthalene, whereas in KP121 methanol was. Therefore this indicates the methanol solvent having an interaction with the formation of the calcite. This difference was also observed in the previous spectrum of sample KP112; whereby the different bands occurred. However the presence of acetone within the KP112 sample appeared to be the cause of the interaction. To prevent the issue observed in sample KP112, the KP120 sample had been prepared where the organic and inorganic solutions were dissolved in separate containers before adding them together. Therefore the difference seen in KP112 must arise from acetone directly being the solvent for sodium carbonate rather than it simply being present. From this it can be deduced that the use of water for the inorganic components and the use of acetone for the organic component is desirable.

Issues with homogeneity of the solid state mixtures have been clearly identified as a problem in Raman spectroscopy. By looking at individual signals for the organic and inorganic component it is possible to identify how extreme the variation within the intensities can be. To do this the spectra of calcite and naphthalene mixtures were investigated over nine different locations. The peak intensities at each of these locations were recorded and plotted against the concentration of the sample. From the graph plotted it would then be possible to see how the homogeneity can vary depending on location.

The spectra from nine different points were collected for samples of 5%, 10% and 25% naphthalene in calcite. The spectra were then baseline corrected with the baseline set to zero. All spectra were normalized using the calcite peak at 1085 cm^{-1} . The intensity was then recorded for the peak at 1381 cm^{-1} .

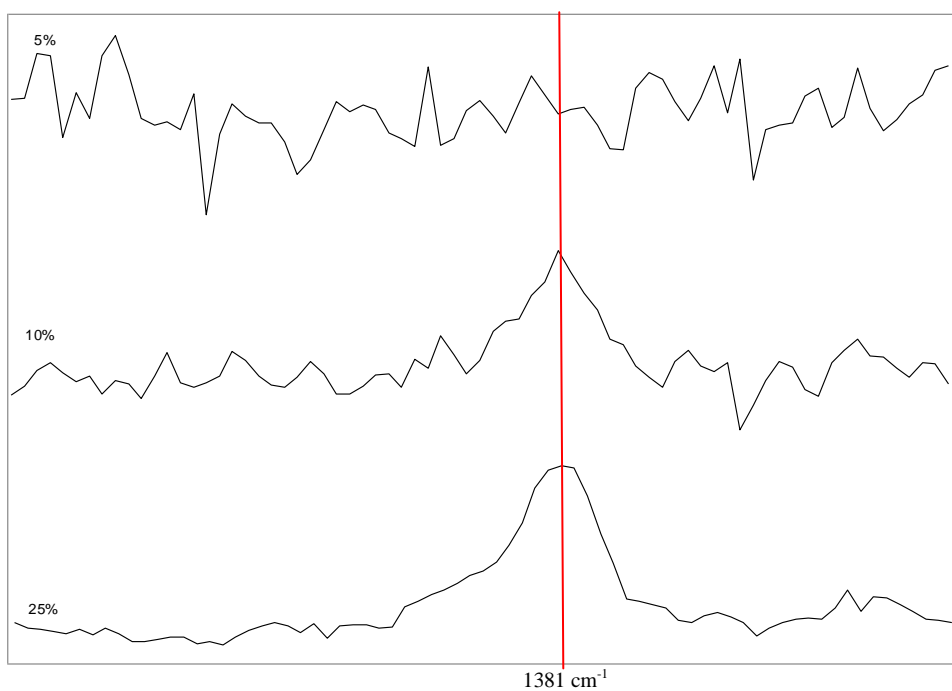


Figure 3.2.4 Raman spectrum of a single peak at 1381 cm^{-1} within the spectrum of naphthalene in calcite at different concentrations

Figure 3.2.4 shows the Raman spectra of the peaks at 1381 cm^{-1} for one location at each concentration. From the spectra it can clearly be seen that signal for the peak is indistinguishable from the noise at the 5% concentration. Therefore the values obtained at this point will be at the noise floor for the spectrum. The peaks present in the 10% and 25% samples both show an increasing signal-to-noise ratio as expected with the increase in concentration.

Percentage	25%	10%	5%
Region 1	2.2177	1.2787	0.2402
Region 2	4.5420	2.4848	0.0379
Region 3	3.3468	2.1714	0.4588
Region 4	3.7974	1.7419	0.0755
Region 5	3.1846	0.5795	0.2460
Region 6	1.7881	0.7088	0.2209
Region 7	3.2099	0.9491	0.2674
Region 8	3.7682	1.0083	0.0648
Region 9	3.1483	1.0784	0.4158

Table 3.2.1 Table showing different intensities ($\times 10^2$) of the peak at 1381 cm^{-1} within mixtures of naphthalene and calcite.

Table 3.2.1 shows the intensities for the peak at each individual location. From this it can be seen that as intensity increases as the concentration increases. However it is also clear that there is variation within the intensities relating to the different locations.

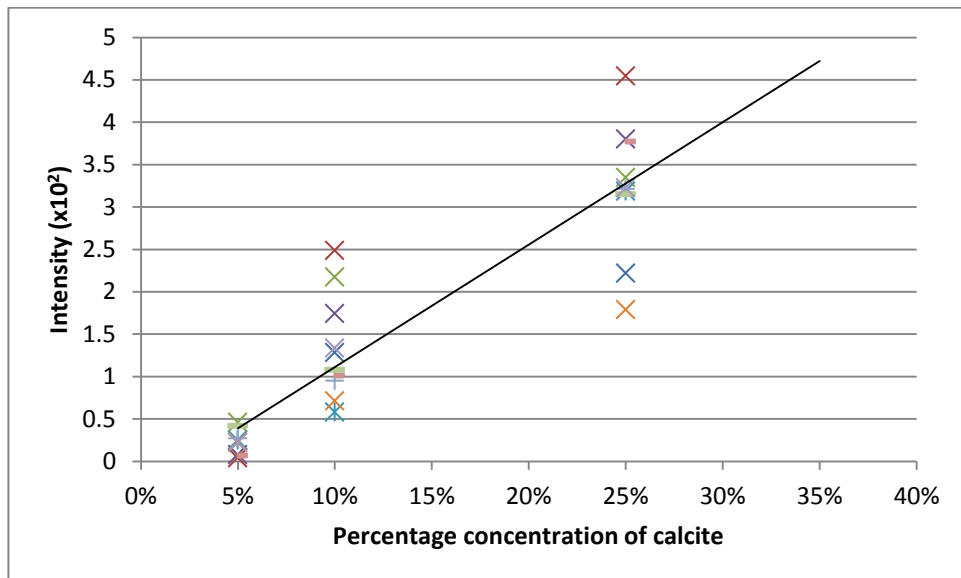


Figure 3.2.5 Scatter plot showing varying values for percentage concentration vs. intensity

Figure 3.2.5 shows the different locations with concentration plotted against intensity. From this it can be seen that using a line of best fit the concentration is directly proportional to the Raman intensity. As mentioned previously the variation of the intensities is very broad. Several of the intensities for the concentration at 25% are lower than the intensities at 10%. It is also clear from the graph that some intensities for

the 10% concentration are very similar to the intensities of the 5% concentration. This means that some 10% intensities may be partially or completely noise, as the signal intensity is below the instrumental limit of detection. Therefore these types of mixtures could not reliably be used to predict limit of detection values. However by looking at the averages across all points the results obtained, points which are more representative of the whole sample can be used.

3.2.1. Naphthalene systems

3.2.1.1. Solution-Solution mixing

Solution-solution mixing and solid solution mixing was carried. These methods were used to detect differences between them and allow for optimal mixing of the samples. While solution-solution mixing has the potential to produce the most homogenous mixing of the samples it requires complete dissolution of the solute. Additionally, in the previous section the presence of acetone as a solvent for the sodium carbonate molecules alters the final inorganic compound produced. While acetone is not used as the solvent for the inorganic precursors, when combined with the acetone used as the solvent for the organic, there is the potential for interactions.

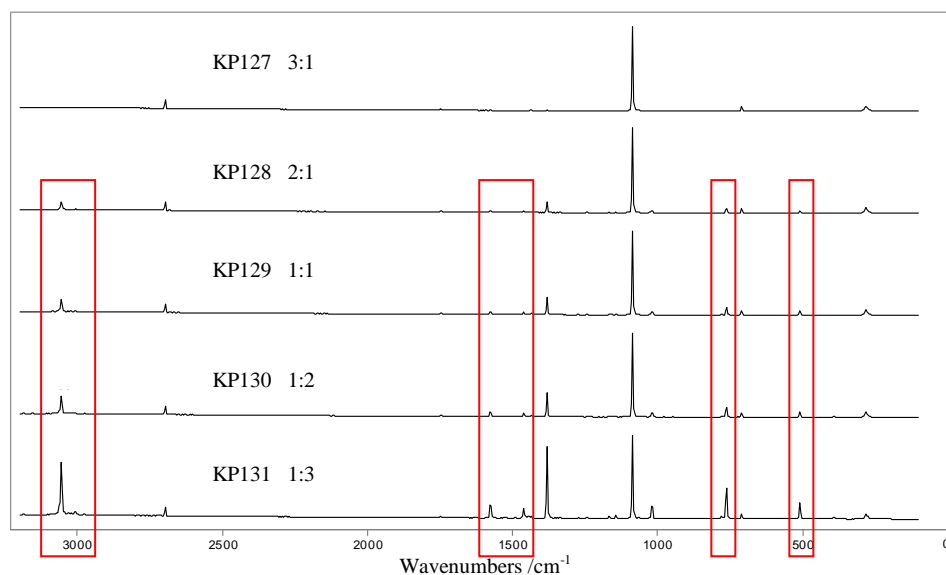


Figure 3.2.6 Raman spectrum of solution-solution mixed calcite and naphthalene samples KP127-31

The samples of calcite naphthalene solution-solution mixtures (KP127-KP131) were analysed using Raman spectroscopy (Figure 3.2.6). The spectra obtained clearly show the presence of naphthalene within the calcite in all the samples except where the organic concentration was lowest and the ratio of inorganic to organic was 3:1 (KP127). In all the samples where the concentration was higher than this, the naphthalene peaks at 3057 cm^{-1} , CH stretching, and 1380 cm^{-1} , CH in-plane bending, were present. As the concentration of the organic component increases it can clearly be seen that the peaks corresponding to naphthalene also increase. In the spectrum of 1:3 calcite to naphthalene the most intense peak of naphthalene and the most intense peak of calcite have a ratio of relative intensities of almost 1:1. In this sample the presence of a background was limited due to the strong intensities of the Raman signals within the spectrum.

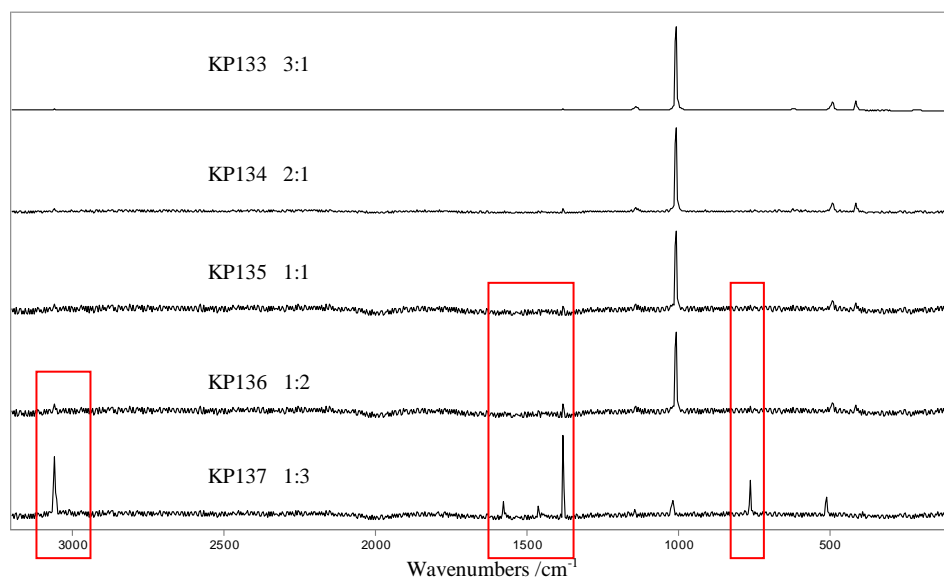


Figure 3.2.7 Raman spectrum of solution-solution mixed gypsum and naphthalene samples KP133-37

Using Raman spectroscopy the samples of solution-solution mixed gypsum and naphthalene (KP133-KP137) were analysed (Figure 3.2.7). The background present within the samples obtained masked the majority of the Raman signals obtained. Only the final spectrum (KP137) shows the presence of naphthalene. However it seems unlikely that the increase between the ratios of 1:2 gypsum to naphthalene and 1:3 gypsum to naphthalene would cause such a change. Peak intensities should be proportionally to concentration, however the relative intensities go from being 0:1 in KP136 to approximately 6:1 in KP137. Such an increase is very unlikely and therefore the explanation for such an increase is likely to be attributed to the sampling and a location of high naphthalene presence being analysed. Due to the intensity of the noise derived from the background it is not possible to detect naphthalene within any of the samples KP133 to KP136. While there appears to be a peak in the sample KP136 at 1380 cm^{-1} , which would indicate the presence of naphthalene, the signal-to-noise ratio is too weak to state with certainty that a signal is present.

3.2.1.2. Solid-Solution mixing

This section looks at the differences between the samples produced through the solid-solution technique. This technique involved the addition of the organic component in solution to the inorganic component as a solid. The systems analysed look at the effects of the calcite and gypsum as inorganics with the organic naphthalene components as investigated in the previous section. Additionally spectra were obtained with anthracene as the organic component.

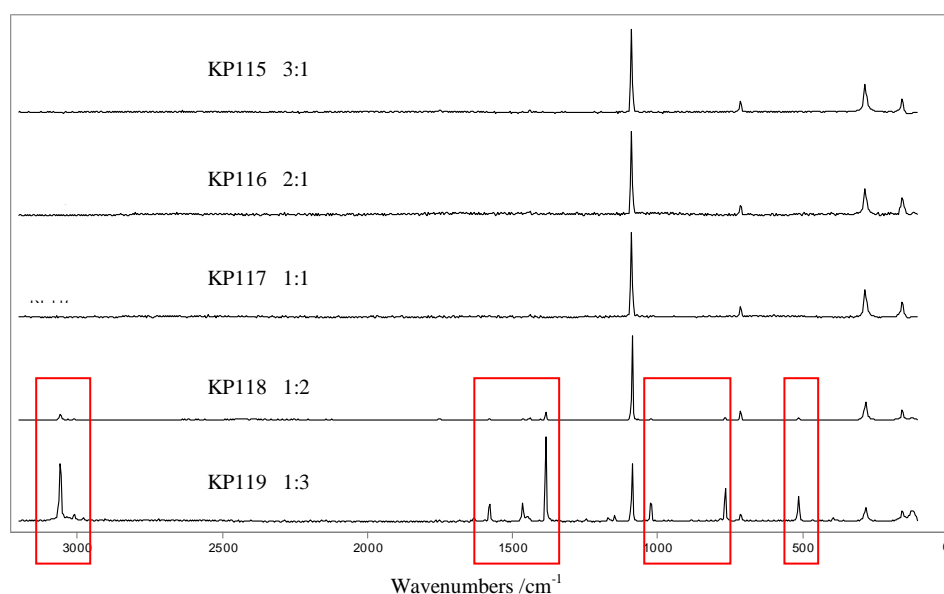


Figure 3.2.8. Raman spectrum of solid-solution mixed calcite-naphthalene samples KP115-19

Figure 3.2.8 shows the Raman spectra obtained from the calcite-naphthalene samples, KP115 to KP119. As with the samples produced through solution-solution mixing, there is only a minor background and the signal-to-noise ratio of samples is strong enough to clearly identify peaks. However, as in the sample KP137, the sampling method used produces spectra from a non-homogenous area in sample KP119. The relative intensities of calcite to naphthalene are too strong for the differences to be based on the concentration increases alone. The most intense naphthalene peaks at 3057 cm⁻¹ and

1380 cm^{-1} are present within the KP118 sample and therefore indicate the presence of naphthalene in the mixture.

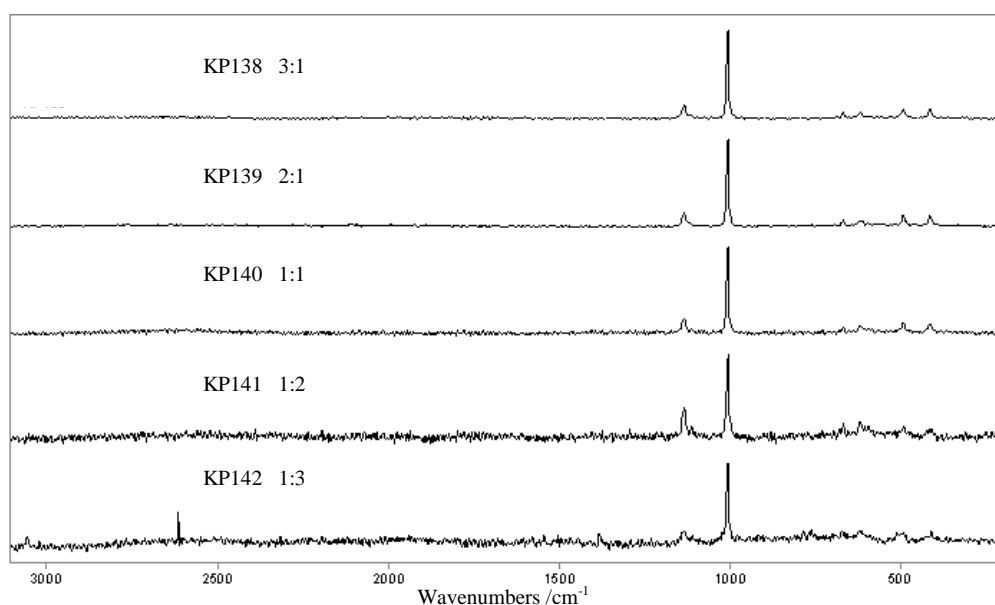


Figure 3.2.9. Raman spectrum of solid-solution mixed gypsum-naphthalene samples KP138-42

The Raman spectra obtained for samples KP138 to KP142 do not show the presence of naphthalene (Figure 3.2.9). The presence of a background in the spectra of samples KP138 to KP140 is minimal and does not degrade the signal of the gypsum peaks. However in samples KP141 and KP142 only the peaks at 1141 cm^{-1} and 1007 cm^{-1} remain distinguishable from the background and due to the weak scattering abilities of the naphthalene compared to the gypsum it would be unlikely to see any of the organic. The signal present at approximately 2600 cm^{-1} can be attributed to a cosmic ray hitting the CCD detector and therefore produces a false signal.

3.2.2. Anthracene systems

Anthracene, like naphthalene, is polycyclic aromatic hydrocarbon and can be used as a biomarker in the detection of life^[96]. Structurally it is similar to that of naphthalene with

an additional ring. Due to their similar structure the Raman spectrum of anthracene and naphthalene are similar. Table 3.2.2 shows the peak positions and assignments of the main Raman signals.

Wavenumbers /cm ⁻¹	Assignment
3056	CH stretching
3029	CH stretching
1633	CC stretching
1558	CC stretching
1398	CC stretching
1260	CH in-plane bending
1187	CH in-plane bending
1164	Ring symmetric deformation, ring trigonal deformation
1008	CH out-of-plane bending
753	Ring antisymmetric deformation, bending CH

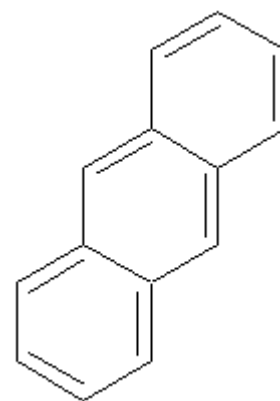


Table 3.2.2 Peak assignments and structure of anthracene

Several samples were prepared of inorganic-anthracene mixtures, KP145 to KP149 which used calcite as the inorganic and KP150 to KP154 which used gypsum as the inorganic. All of these samples were prepared using solid-solution mixing and analysed using Raman spectroscopy.

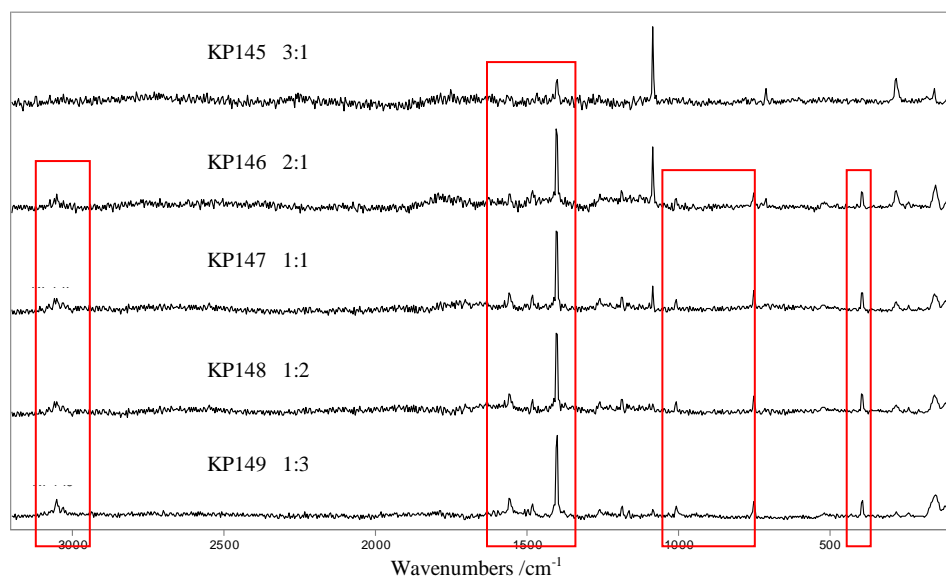


Figure 3.2.10 Raman spectrum of solid-solution mixed calcite and anthracene samples KP145-49

The Raman spectra obtained for the solid-solution mixed calcite and anthracene samples KP145 to KP149 contained a large background which was removed (Figure 3.2.10).

While the background produced more noise in the spectra, this noise did not mask the most intense signals associated with calcite nor anthracene. The most intense peak of anthracene at 1398 cm^{-1} , associated with CC stretching, can clearly be seen in all spectra. In the spectra obtained the presence of the calcite is only detectible in the samples KP145-KP147.

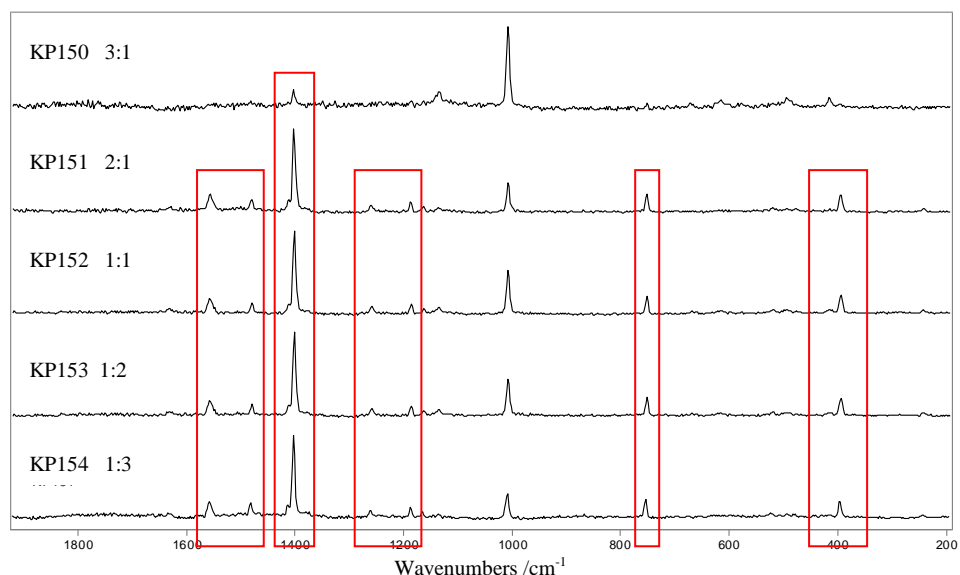


Figure 3.2.11 Raman spectrum of solid-solution mixed gypsum and anthracene samples KP150-54

The spectra obtained from solid-solution mixed gypsum and anthracene samples KP150 to KP154 (Figure 3.2.11) show a similar presence of anthracene in all the spectra as can be seen in figure 3.2.9. The spectra of these samples produced a far stronger signal-to-noise ratio but still retained a background. KP151 to KP154 show unexpected ratios of organic to inorganic component peak intensities. In these 4 spectra the intensities appear to vary very little. This is due to the sampling positions, whereby the samples were not homogenous and the spectra obtained were from regions of large concentrations of anthracene.

From the spectra obtained it is clear that homogeneity remains present within the sample regardless of preparation technique. Therefore solid-solid mixing of samples is the most desirable method of preparation of organic and inorganic mixtures due to the simplicity of the mixing technique and that it is the only method which does not introduce additional compounds to the samples. By applying the 9 point grid systems the homogeneity of the samples becomes a less significant factor in the analysis of the samples.

3.3. Spectra from Goethite and Martian soil simulate samples

The previous sections within this chapter have looked at different mixing techniques and the issues of homogeneity when looking at solid mixtures. The samples previously analysed all produce distinct Raman signals within the spectrum due to being pure samples. On Mars however these inorganics are not the most common geological materials and any inorganic mixture is also likely to contain multiple inorganic compounds. This section of work looks at the detection of an organic component when it is in a mixture with goethite and a Martian soil simulate.

Goethite is an iron oxyhydroxide and has the chemical formula $\text{FeO}(\text{OH})$. It's presence on Mars was detected in Gusev, a Martian crater, by NASA's Spirit rover. The presence of goethite on Mars is very important in the detection of life on Mars as it is an indication of liquid water in that the formation of goethite often requires liquid water. This standard was obtained from Sigma-Aldrich.

Compound	Concentration (%)	Compound	Concentration (%)
Na – Montmorillonite	47.7	Al_2O_3	14.10
Kaolinite	9.9	SiO_2	34.60
Haematite (+ SiO_2)	21.3	SO_3	5.10
(19.17% Fe_2O_3 , 1.3% SiO_2)	13.0	Cl	0.20
Anhydrite	7.1	K_2O	0.17
Magnesium Sulphate	1.0	CaO	6.09
Na_2O	2.52	TiO	0.10
MgO	3.43	FeO	18.56

Table 3.3.1 Components of MRS07

The final inorganic component investigated in this chapter was that of a Martian soil simulate identified as MRS07. This sample was supplied by the German Space Agency and was produced to have comparable constituents to that of the soil on Mars (Table

3.3.1). Using this as an inorganic component is crucial in establishing the ability to detect organic components as it represents the spectrum obtained from a real sample.

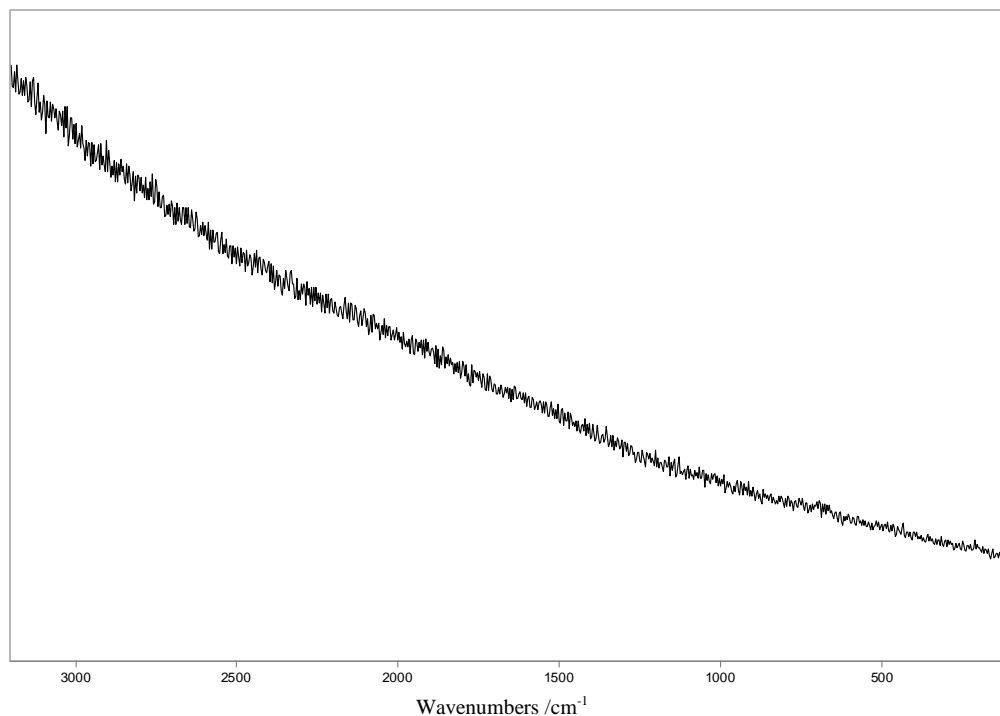


Figure 3.3.1. Spectrum of Martian soil simulant MRS07 exposed for 10 seconds over 1 accumulation at 100% laser power

The spectra of several components within the MRS07 samples individually produce broad background features therefore a background was expected to be produced in these samples (Figure 3.3.1.). The Raman spectrum of MRS07 shows no spectral features and thus will not produce signal that may mask any signals. However the background produced by the compound may potentially mask the Raman signal of organic components. The MRS07 was prepared to be like the soil found on Mars, for this reason there are lots of components of this mixture which all produce several different bands and backgrounds, thus detection of signal in such a mixture becomes much harder. Therefore for these samples, in addition to preparing mixtures with anthracene, samples were produced using beta-carotene as the organic component. Beta-carotene is a very

strong Raman scatter and has a much greater signal-to-noise ratio than those of the organic components used in the previous sections. It is additionally a biomarker indicative of life^[96].

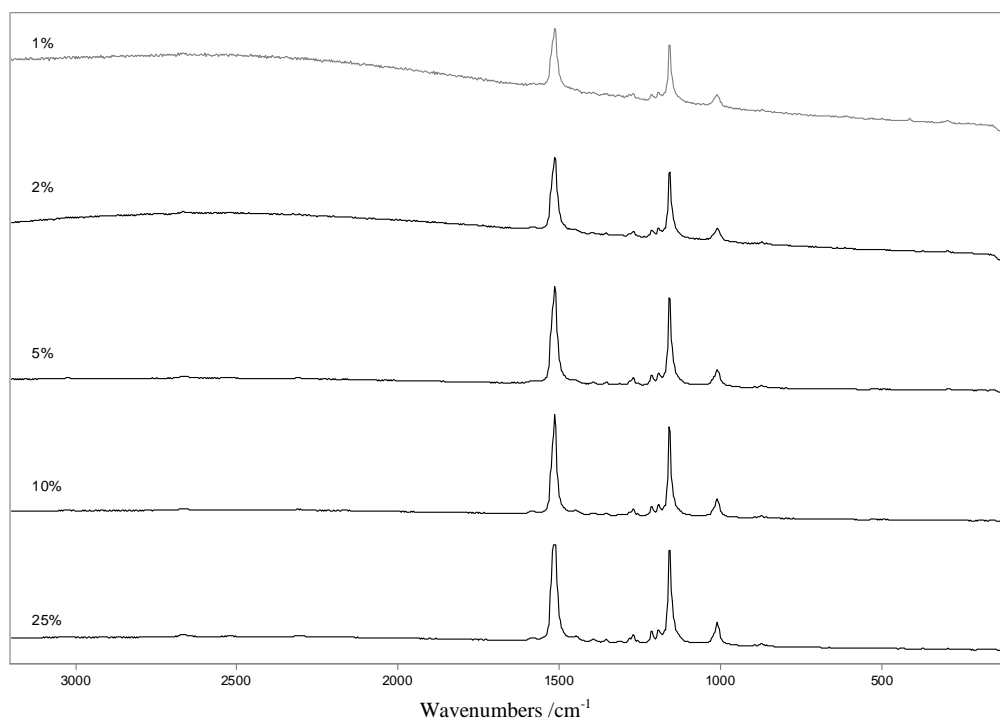


Figure 3.3.2. Raman spectra of MRS07 and Beta-Carotene mixtures

The spectra produced of MRS07 and beta-carotene mixtures (Figure 3.3.2.) clearly show the beta-carotene detectable. At lower concentrations, of 1% and 2% the background masks several minor signals above 2000 cm^{-1} . However even at these low concentrations the majority of the Raman bands derived from the beta-carotene are still identifiable. Therefore detection of such compounds on the surface of Mars could be possible.

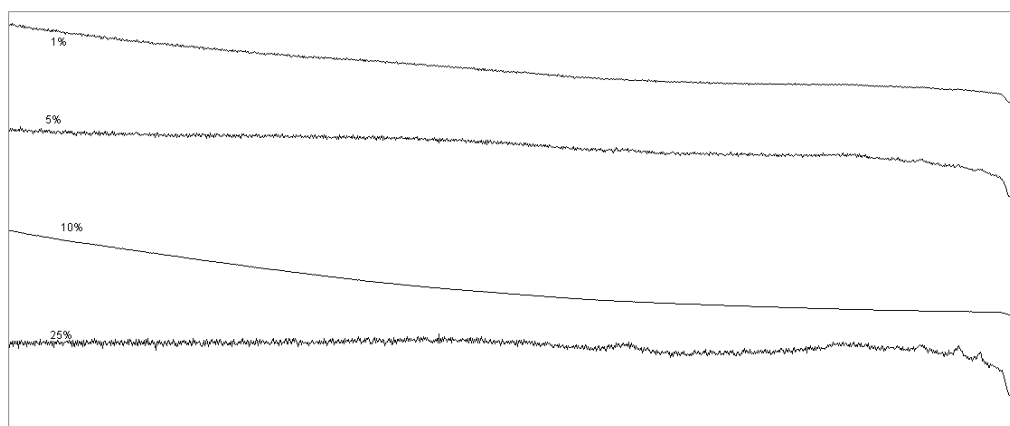


Figure 3.3.3. Raman spectra of goethite anthracene mixtures

From the spectra of goethite anthracene mixtures (Figure 3.3.3) the presence of anthracene within the mixture cannot be seen. This is due to the weak Raman bands produced by the anthracene being masked by the background signal produced by the goethite. Therefore the organic component detectable within goethite is required to be a stronger Raman scatterer. For this reason the spectrum of goethite and beta-carotene mixtures were investigated (Figure 3.3.4).

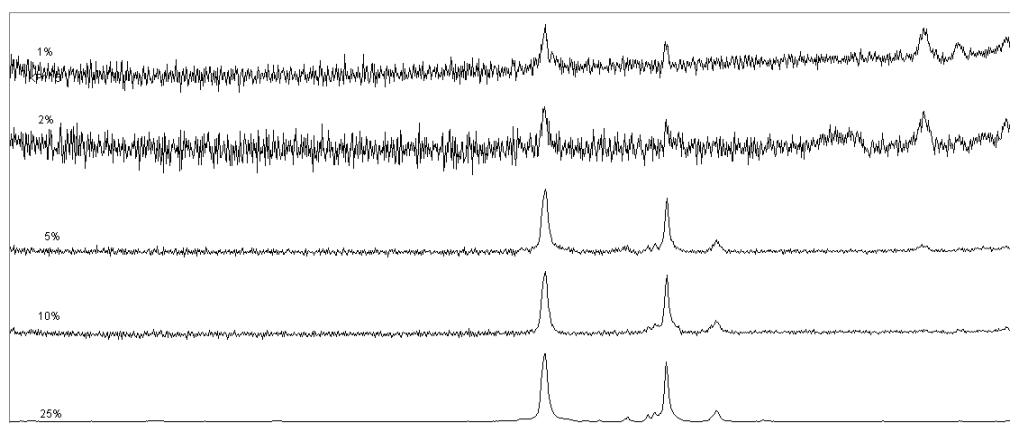


Figure 3.3.4. Raman spectra of goethite and beta-carotene mixtures

Beta-carotene is a much stronger Raman scatterer and it is easily distinguishable from the goethite at all concentrations. The signal-to-noise ratio improves greatly as the concentration of Beta-carotene increases and so the identification of minor peaks becomes possible above 5%.

From the results obtained an organic compound can be seen within the Mars relevant samples. The spectra produced also show a linear increase in intensities proportional to the concentration increases. This indicates that the by averaging 9 points of analysis the spectra are representative of the sample. Thus these samples could be used to produce a calibration curve from which limit of detection values could be obtained.

3.4. Conclusions

In this chapter investigation of organic and inorganic mixtures was performed using Raman spectroscopy. From mixtures of two solid materials it was clearly established that homogeneity becomes a primary issue with location and identifying the organic component. To minimize these homogeneity issues multiple different samples were prepared under different conditions to produce the most homogenous sample. A method of using nine different points was devised to produce representative data of the whole samples. These methods were then applied to simulate samples consisting of similar properties of Martian soil. Using the devised protocols detection of an organic was possible in these samples.

Chapter 4

Development of Criteria for Instrument Performance Comparison

The aim of this section is to develop a set of objective criteria for performance comparison between the laboratory instruments and the prototype instrument. This will be achieved using standard instrument validation methods relating to: sensitivity, range, limit of detection, limit of quantification, robustness, selectivity, linearity, accuracy and precision^[6,163]. The effects of noise upon the spectrum will be investigated and a suitable method of calculation determined. Using calibration curves validation parameters will be identified for potential control standards. The effect of laser power will also be investigated to determine the suitability of the standards and their stability. Using all this information the peaks of several standards will be assigned and these values will be used in developing an automated systematic identification of spectra.

4.1. Signal-to-noise ratio effects on instrument performance

To identify signal within a spectrum a way to distinguish between what can be defined as noise and what can be defined as signal must first be established. This is an important feature to identify when potentially looking at instrumental validation parameters as error obtained from noise directly impacts calculations relating to limits of detection and quantification. In astrobiology this information is vital as any organic matter could potentially be in a mixture at low concentration and knowing the matrix response could allow for the detection of life that would otherwise be missed.

The primary difference between noise and signal in a Raman spectrum is that from signal useful information can be derived whereas from noise no useful information can be obtained. There are three types of noise: random, non-random and determinate^[4]. Random noise decreases very slowly with more spectral accumulations and therefore having more accumulations improves a signal-to-noise ratio. This relationship however is not linear and as more time is taken for additional accumulations the improvement in signal-to-noise ratio decreases. Non-random noise does not constantly occur and can be observed as drift within the spectrum. The cause of this can be from effects such as change within temperature during analysis. The final type of noise is determinate noise which occurs the same every time a spectrum is collected. Therefore signal-to-noise ratios do not change with more accumulations as the increase is linear. As additional spectra are added together this becomes the main source of noise.

Commonly observed forms of noise include shot noise, background light and instrument noise. Shot noise is derived from the statistical nature of light itself^[4]. This form of noise occurs mainly in sub-1000 nm laser wavelengths. Another form of noise can be derived from the environment in the form of light sources, such as fluorescent lights. Due to Raman bands having a weak intensity background light can also be a substantial problem. Noise can also be derived from the sample itself due to fluorescence and blackbody radiation. Fluorescence is a broad feature seen as a slow changing baseline in the spectrum, only some samples absorb light strongly and convert the photons to fluorescence photons. Blackbody radiation occurs in all samples due to their temperature being greater than absolute zero and this becomes more predominant when heating samples. The final cause of noise relates to the instrument itself and is a constant effect related to the design of the instrument itself.

There are multiple ways to calculate the noise present in the spectrum and these values have a direct impact on the limit of detection value obtained. Therefore the impact of differences in noise calculation techniques must be investigated prior to deciding upon an optimal method of obtaining transferable limit of detection methods. For six naphthalene in toluene solutions, root mean squared (RMS) values and noise peak heights were used to compare different noise calculation techniques.

In the previous chapters the importance of naphthalene as a potential Martian biomarker has been identified. Naphthalene additionally can be a very useful control sample due to it containing multiple strong Raman band intensities. This allows for information to be obtained about the range, selectivity, accuracy and precision of an instrument. The range is observed by indentifying the spectral range over which bands can be detected. The selectivity of the instrument can be determined by looking at the resolution of the peaks and identifying any spectral overlap between them. The accuracy and precision of the instrument can be obtained using the peak positions from multiple acquisitions.

The naphthalene was dissolved in a suitable solvent; toluene. The solvent was used to prevent issues with homogeneity being observed and problems with sample focus. Additionally the toluene was used as an internal standard for the samples whereby all spectra could be normalised around the toluene peaks.

Conc.	Sigma (5 points)	Sigma (10 points)	Sigma (20 points)	Sigma (30 points)	Sigma (50 points)
1%	0.004341	0.005702	0.00502	0.004918	0.005138
5%	0.004965	0.004508	0.004770	0.004881	0.00462
10%	0.002886	0.003063	0.005095	0.005098	0.004974
25%	0.004748	0.006543	0.005402	0.005314	0.004934
50%	0.005596	0.005454	0.005578	0.005432	0.005698
100%	0.00312	0.002902	0.003983	0.004275	0.004329
Average	0.00427	0.004696	0.004976	0.004986	0.004950
Standard deviation	0.001067	0.001477	0.000563	0.000409	0.000465

Conc.	Sigma (100 points)	Sigma (200 points)	Sigma (300 points)	Sigma (500 points)
1%	0.004821	0.005146	0.005480	0.005591
5%	0.004445	0.004508	0.004583	0.005134
10%	0.004529	0.004925	0.005134	0.005524
25%	0.004981	0.004926	0.005077	0.005124
50%	0.005236	0.005000	0.005382	0.005385
100%	0.004649	0.004536	0.005108	0.005590
Average	0.004777	0.004840	0.005127	0.005391
Standard deviation	0.000297	0.000259	0.000312	0.000216

Table 4.1.1 Table showing the average noise intensities over several points and their standard deviations

Within the spectra obtained, the region between $\sim 1700\text{ cm}^{-1}$ and 2300 cm^{-1} appeared to show no Raman signals and remained flat with only noise present. This region was used to identify the impact of using the peak heights of the noise to calculate a noise average (Table 4.1.1). To understand the importance of sampling size on the average background noise 5, 10, 20, 30, 50, 100, 200, 300, 500 points were used to work out each noise average. For each of these ranges the individual noise averages were calculated and their standard deviation. Based on the standard deviations obtained it was clear that the more points that were used in the sample the less the variation from the mean. For this reason calculations for noise from this method were based off of the mean values for 500 points.

Conc.	771-966 range	1764-2448 range	Whole spectral range
1%	0.00388	0.00486	0.07709
5%	0.00337	0.00446	0.07707
10%	0.00302	0.0043	0.07637
25%	0.00299	0.00462	0.07866
50%	0.00328	0.00477	0.08087
100%	0.00385	0.00467	0.08375
Average	0.00339	0.00461	0.07896
Standard deviation	0.00039	0.00020	0.00284

Table 4.1.2 Table showing the RMS values obtained for different regions using one peak

To allow for a comparison of noise values in relation to the method for which they were obtained, RMS values were also obtained using the GRAMS/AI software (Table 4.1.2).

The RMS noise was calculated from the noise variation compared to the spectral baseline. Three regions were used; 771 cm^{-1} to 966 cm^{-1} , 1764 cm^{-1} to 2448 cm^{-1} and finally the whole spectrum. Each region used had an increasingly larger amount of noise points. These values were averaged and standard deviation obtained. The impact of taking the whole spectrum clearly showed a lot of variation within the noise values due to changes in background and minor peaks. For this reason the RMS noise values for the 1764 cm^{-1} to 2448 cm^{-1} region were used.

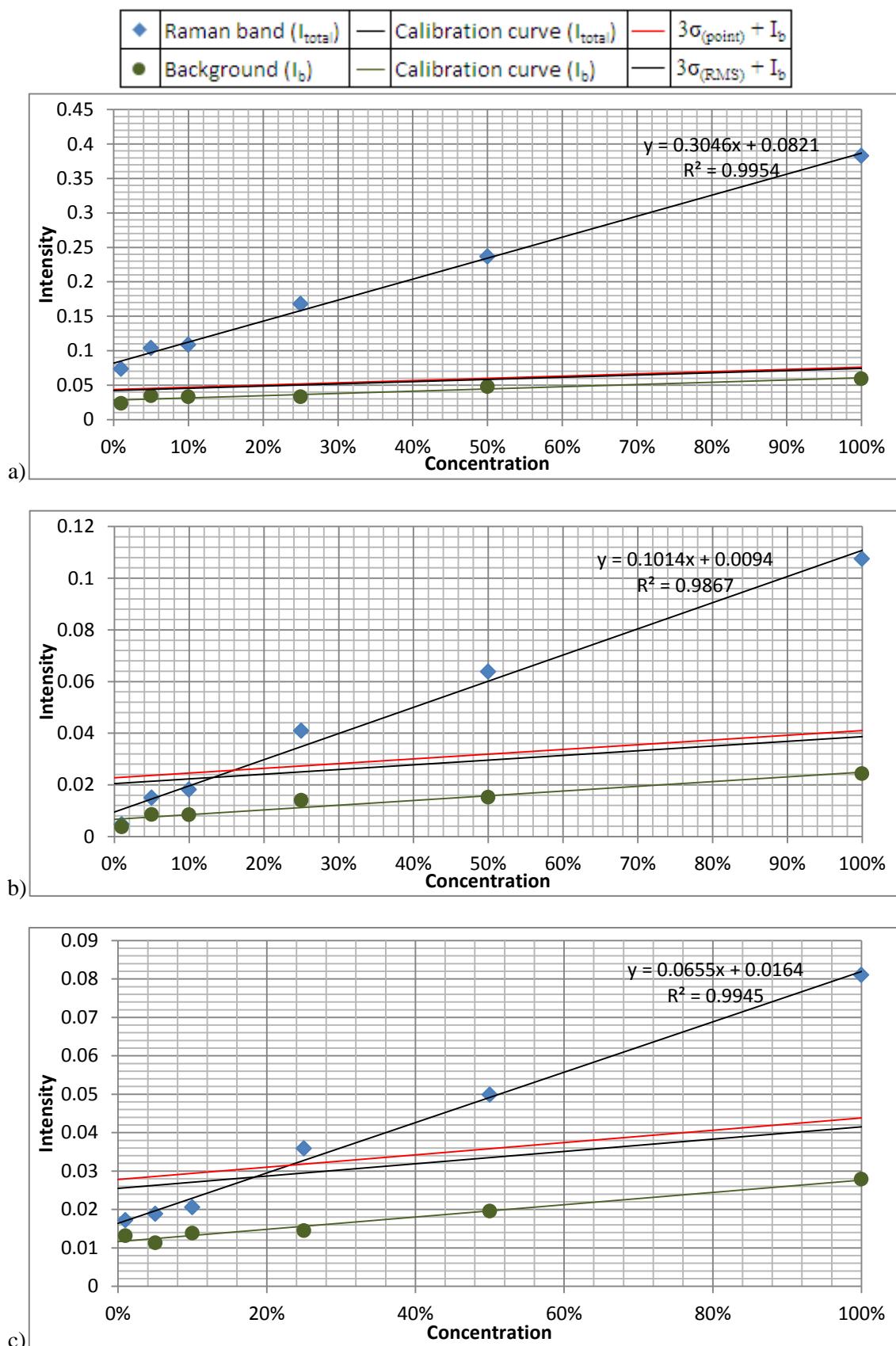


Figure 4.1.1. Concentration vs. intensity plot for naphthalene in toluene solutions with limit of detection values calculated using RMS and point noise calculations at peaks a) 1378 cm⁻¹ b) 759 cm⁻¹ and c) 1461 cm⁻¹

Peak	759 cm ⁻¹		1378 cm ⁻¹		1461 cm ⁻¹	
Noise Type	Point	RMS	Point	RMS	Point	RMS
Noise Value (σ)	.0054	0.0046	0.0054	0.0046	0.0054	.0046
LOD (I_{Total})	0.0258	0.0228	0.0401	0.0375	0.0315	0.0284
LOD (%)	16.1	13.	-13.8	-14.6	23.0	18.4

Table 4.1.3. Limit of detection values obtained when calculating noise using 500 points and RMS over the range 1724-2448 cm⁻¹

Using both the multiple point and RMS noise calculations limits of detection were produced (Table 4.1.3 and Figure 4.1.1). The differences observed between the different peaks and the spurious result for the 1378 cm⁻¹ peak will be discussed and investigated in section 4.2. From the results observed, the RMS calculations appear to be the more desirable method of obtaining noise, due to the lower standard deviation within the data sets obtained. However the RMS values always work over a defined range within the GRAMS/AI software. This presents a problem where a defined noise region contains peaks. This was observed when looking at the whole spectrum. An example of the type of issue that could occur in this calculation technique can be seen in calculating RMS for naphthalene in acetone solutions.

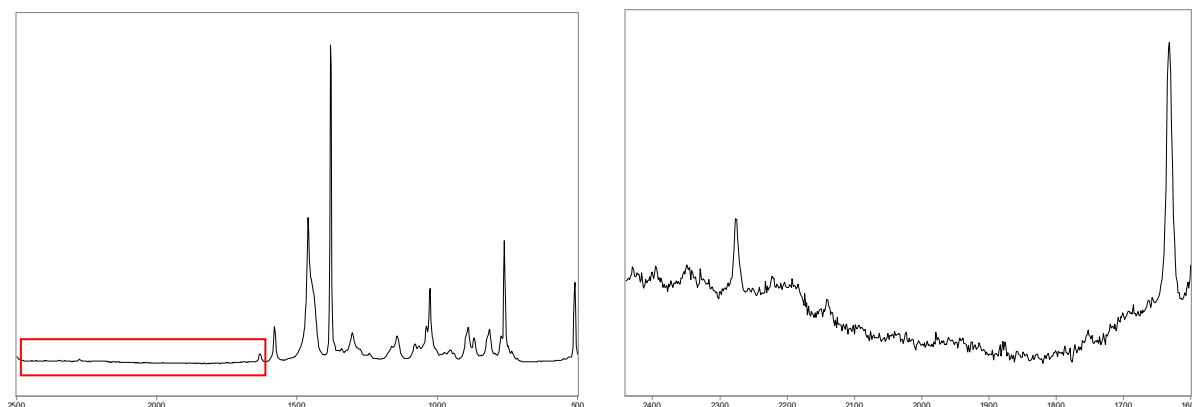


Figure 4.1.2. Spectra of the naphthalene in acetone (left) with 2440 cm⁻¹ and 1600 cm⁻¹ region enhanced (right)

When calculating the RMS noise within the naphthalene in acetone solutions the calculation used would occur over the 2440 cm⁻¹ and 1600 cm⁻¹ region. However while

this region appears to be purely noise, when the whole spectrum is observed, upon magnification it becomes clear that this region also contains numerous bands distinct from the noise (Figure 4.1.2). Therefore in this instance the minor bands in this region would be assigned as noise and thus increase the noise threshold for the spectrum. Using the single point calculations these bands would be identified as outliers and so not included in the noise calculation. Due to the ability to remove bands within the noise the single point calculations is the optimal method for noise calculations in this work.

4.2. Instrument validation

In the previous section the optimal method for calculating noise within a spectrum was identified. Using this it is possible to perform instrument validation using calibration curves to derive; linearity, accuracy, precision sensitivity, limits of detection and limits of quantification^[6,163]. The linearity of a calibration curve is measured with R^2 and displays how closely the curve fits with the points. The accuracy in a calibration curve is obtained through the systematic error which relates to the closeness of agreement between the observed value and the reference value. The precision is derived from the random error within the curve and is obtained by the standard deviation of measurements. The calibration curves slope gives the sensitivity of the instrumentation. The limit of detection is the concentration to which smallest measurement can be detected with reasonable certainty for a given procedure. This is derived using the equation $b+x\sigma$ where the b is the background, σ is the noise and x is 3. The limit of quantification is derived from the same equation but in this instance x is 10. The limit of quantification is defined as the minimum concentration of sample that can be quantified with acceptable accuracy and precision.

Peak	759 cm ⁻¹	1378 cm ⁻¹	1461 cm ⁻¹
Calibration curve equation	y=0.1014x+0.0094	y=0.3046x+0.0821	y=0.0655x+0.0164
Sensitivity	0.1014	0.3046	0.0655
Noise Value (σ)	0.00539	0.00539	0.00539
Linearity (R^2)	0.9867	0.9954	0.9945
Background (I_b) equation	y=0.0183x+0.0066	y=0.0322x+0.0284	y=0.016x+0.0116
$3\sigma + I_b$ equation	y=0.0183x+0.0228	y=0.0322x+0.0445	y=0.016x+0.0278
LOD (I_s)	0.0258	0.0401	0.0315
LOD (%)	16.1	-13.8	23.0
$10\sigma + I_b$ equation	y 0.0183x+0.0605	y=0.0322x+0.0823	y=0.016x+0.0655
LOQ (I_s)	0.0718	0.0823	0.0814
LOQ (%)	61.5	0.07	99.2

Table 4.2.1. Instrument validation parameters derived from naphthalene in toluene calibration curve.

From the calibration curves produced in section 4.1 several instrument validation parameters can be obtained (Table 4.2.1). Using the calibration curves it can be determined that the sensitivity of the 1378 cm⁻¹ peak is three times greater than that at 759 cm⁻¹. The background intensities for all three peaks increase relative to naphthalene concentration increase. Instrument noise would produce constant background intensity regardless of sample concentration changes; therefore this increasing background must be a combination of instrument noise and sample noise. All three calibration curves are linear, with all peak intensities being within error range derived from noise. The limits of detection observed for peaks 759 cm⁻¹ and 1461 cm⁻¹ are both higher than expected due to the high intensity of noise within the spectrum masking several of the bands at lower concentrations. This is additionally further observed in the very high limit of quantification values observed for these peaks. A negative limit of detection is observed from the peak at 1378 cm⁻¹. Clearly this value cannot be possible and therefore an error is derived from the analysis. The cause of this error must be attributed to the sample and therefore to identify it the original spectra for the samples must be investigated.

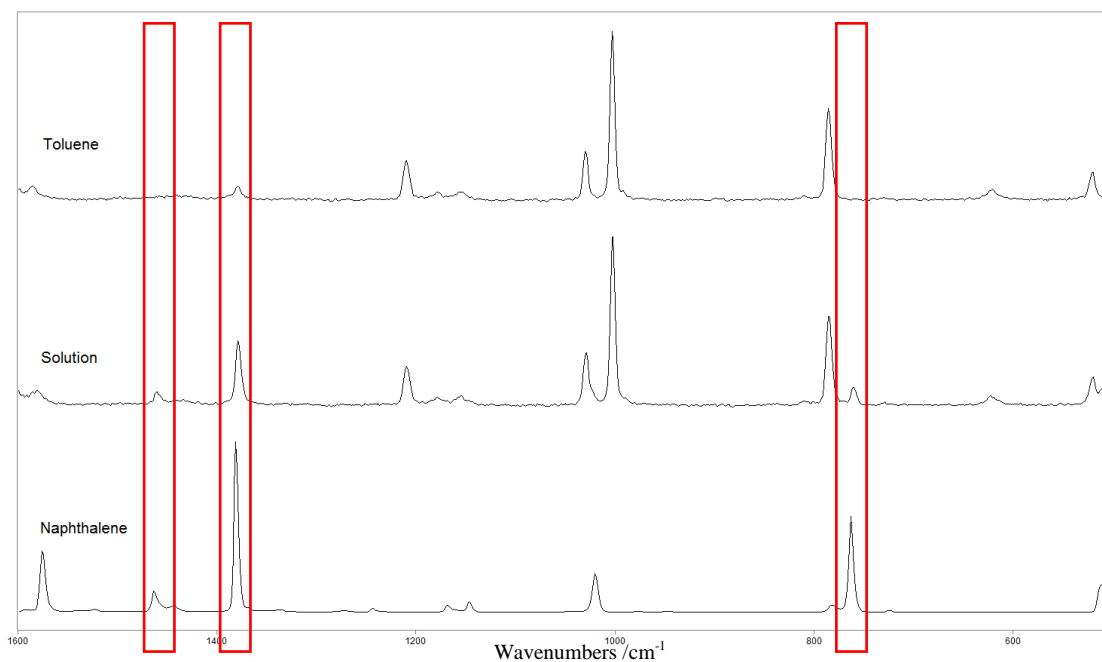


Figure 4.2.1. Spectrum of toluene, 100% w/v naphthalene in toluene and pure naphthalene samples

The spectra of the standards used within these samples are shown in figure 4.2.1. From these spectra two observations can be made regarding the toluene sample. Firstly the toluene bands have a very strong intensity and therefore will have the potential to mask naphthalene peaks. The second observation is that a small peak occurs within the toluene spectrum at 1378 cm^{-1} . This peak will have an additive effect to the naphthalene band and therefore even at 0% concentration in intensity greater than zero would be observed. This band can therefore be identified as the cause of the erroneous limit of detection. In an attempt to resolve this issue the toluene spectrum and background were subtracted from the solutions and calibration curves were plotted.

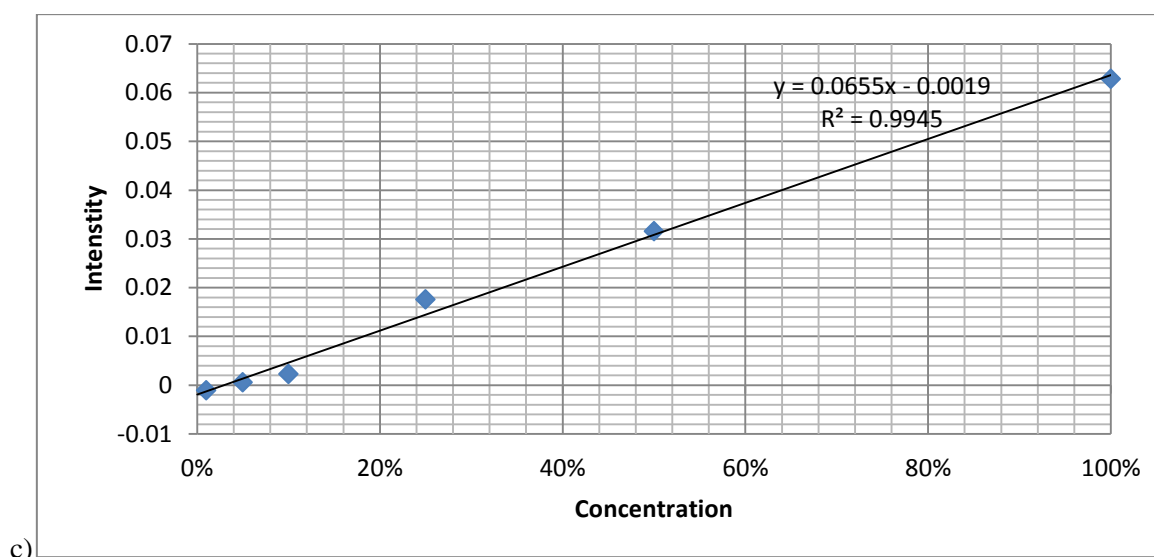
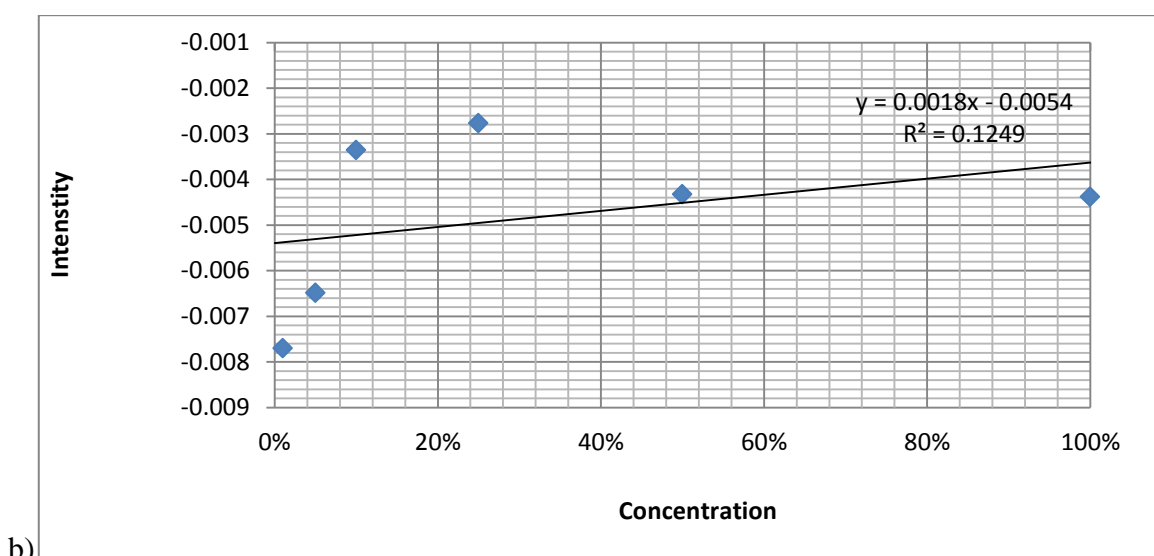
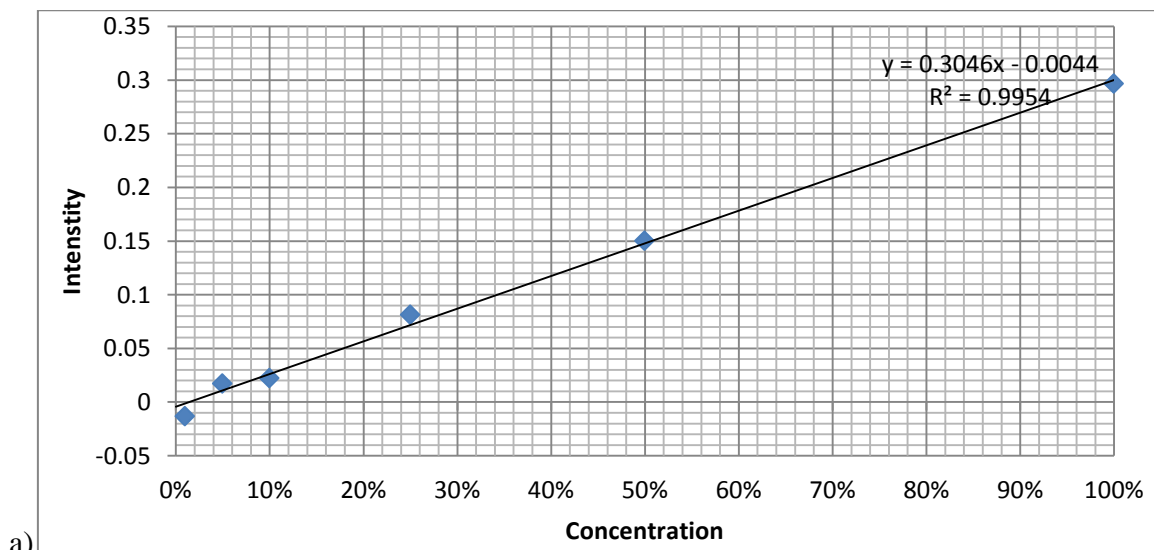


Figure 4.2.2. Concentration vs. intensity plot for naphthalene in toluene solutions with the background subtracted a) 1378 cm^{-1} b) 759 cm^{-1} and c) 1461 cm^{-1}

The calibration curves for the background and toluene subtracted spectra show several interesting features (Figure 4.2.2). In all three curves the intercept occurs at a negative value due to the removal of the background. This causes problems with calculating limits of detection and has potential to produce more negative results. Removing the background in this way also removes information relating to the types of background noise occurring in these samples. By processing the spectra in this way the curve for the 1378 cm^{-1} band fits more closely to the expected results. However the curve produced from the peak at 759 cm^{-1} creates a very different pattern when compared to the non-removed background and toluene spectra. This is due to a very weak and broad toluene band occurring across some of the naphthalene band. By subtracting the toluene spectrum a portion of the naphthalene band is removed and the erroneous curves are produced.

From these results it is clear that removal of backgrounds and solvent spectra will negatively impact instrument validation calculations. Therefore to produce a suitable standard an alternative solvent must be used. Acetone was deduced as an alternative due to its ability to dissolve naphthalene readily. As with the previous solutions spectra were obtained of the standards and the solutions

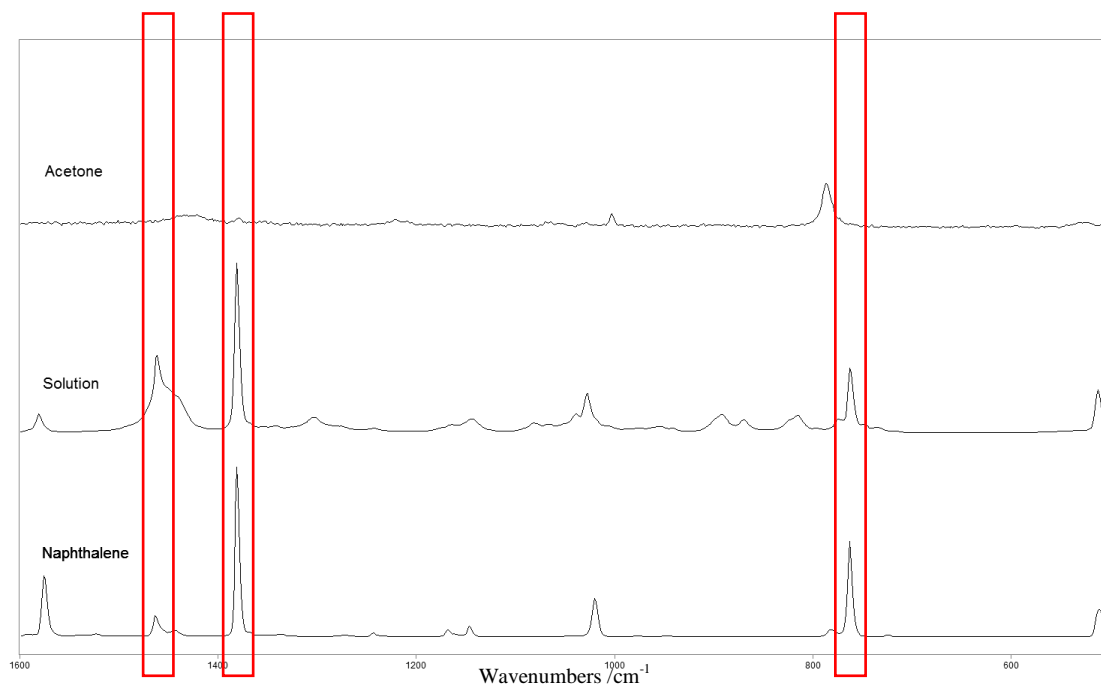


Figure 4.2.3. Spectrum of acetone, 100% w/v naphthalene in acetone and pure naphthalene samples

The spectra of acetone, naphthalene and a 100% w/v mixture are shown in figure 4.2.3. From these spectra it can be seen that there are two advantages of the use of acetone compared to toluene. Firstly the peaks in the acetone spectrum are much weaker than those observed in the toluene spectrum. This means they are less likely to mask any naphthalene peaks. The peak positions of acetone does not appear to occur in the same places as the naphthalene peaks at 1378 cm^{-1} , 759 cm^{-1} and 1461 cm^{-1} . Therefore similar negative limits of detect are unlikely to be observed.

◆	Raman band (I_{total})	—	Calibration curve (I_{total})	—	$3\sigma_{(point)} + I_b$
●	Background (I_b)	—	Calibration curve (I_b)	—	$3\sigma_{(RMS)} + I_b$

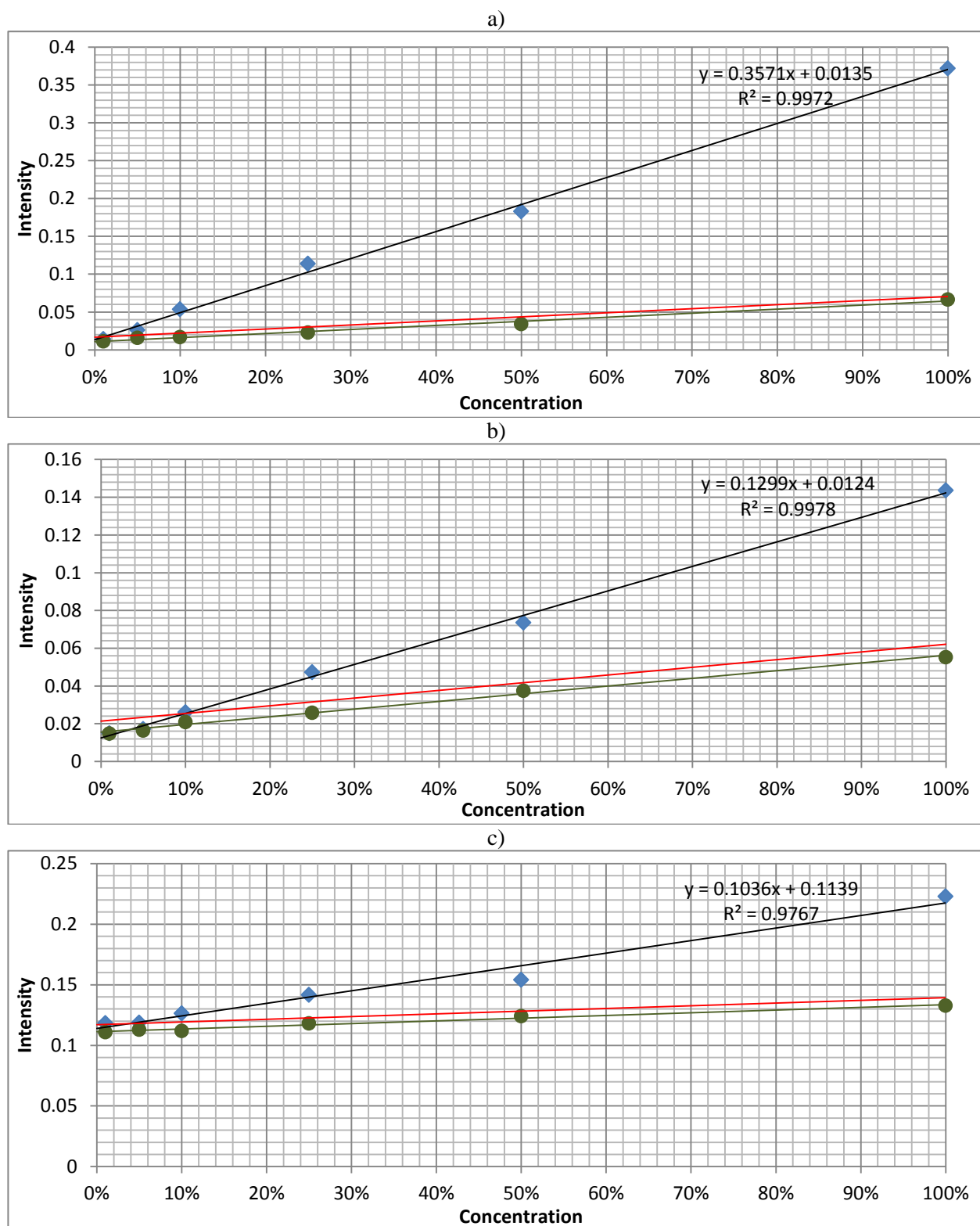


Figure 4.2.4. Concentration vs. intensity plot for naphthalene in acetone solutions at peaks a) 1378 cm^{-1} b) 759 cm^{-1} and c) 1461 cm^{-1}

Peak	759 cm-1	1378 cm-1	1461 cm-1
Calibration curve equation	$y=0.1299x+0.0124$	$y=0.3571x+0.0135$	$y=0.1036x+0.1139$
Sensitivity	0.1299	0.3571	0.1036
Noise Value (σ)	0.00194	0.00194	0.00194
Linearity (R^2)	0.9978	0.9972	0.9767
Background (I_b) equation	$y=0.0407x+0.0155$	$y=0.0537x+0.0109$	$y=0.0224x+0.1112$
$3\sigma + I_b$ equation	$y=0.0407x+0.0213$	$y=0.0537x+0.0167$	$y=0.0224x+0.1171$
LOD (I_s)	0.0254	0.0173	0.1180
OD (%)	10.0	1.1	3.9
$10\sigma + I_b$ equation	$y=0.0407x+0.0349$	$y=0.0537x+0.0303$	$y=0.0224x+0.1306$
LOQ (I_s)	0.0452	0.0333	0.1352
LOQ (%)	25.2	5.5	20.6

Table 4.2.2. Instrument validation parameters derived from naphthalene in acetone calibration curve.

The calibration curves for the naphthalene in acetone solution produce information of instrument validation parameters (Figure 4.2.4 and table 4.2.2). From the results it can be seen that they are much more reliable than the toluene curves. All the limits of detection occur as positive values and are low, meaning noise and background in these solutions does not mask the bands greatly. Due to this the limits of quantification are also much lower, which means the solutions can be quantified at a much lower concentration. The 1461 cm^{-1} peak contains a very large background in the spectrum due to a broad band occurring next to this peak and having additive effect. However this broad band has a weak intensity and therefore the limit of detection remains low. From this data it can therefore be determined that naphthalene in acetone would be a useful solution for comparing validation parameters of different instruments.

4.3. Evaluation of instrument resolution

The selectivity of an instrument is defined by the resolution in performance. Resolution of an instrument becomes important when comparing different instruments as poor resolution means that an instrument may be unable to distinguish between two different peaks within a small region. Therefore to test for instrument resolution a solid sample was devised of calcite and trehalose. Calcite has been investigated in previous chapters and has been shown to be a strong Raman scatterer with several strongly defined peaks. Several forms of trehalose are amorphous and therefore unsuitable in use as standards, however trehalose dihydrate does not display these properties and was therefore used in this section. Trehalose was used for two reasons; trehalose is a potential biomarker with relevance to astrobiology^[96] and trehalose produces many peaks in the Raman spectrum. Many of the peaks produced by trehalose occur in similar regions and therefore this sample is very useful in determining the limitations of an instruments resolution. The samples were used as a mixture due to calcites potential to mask trehalose peaks as much stronger scattering occurs from calcite bands compared to trehalose.

4.3.1. Trehalose as a standard

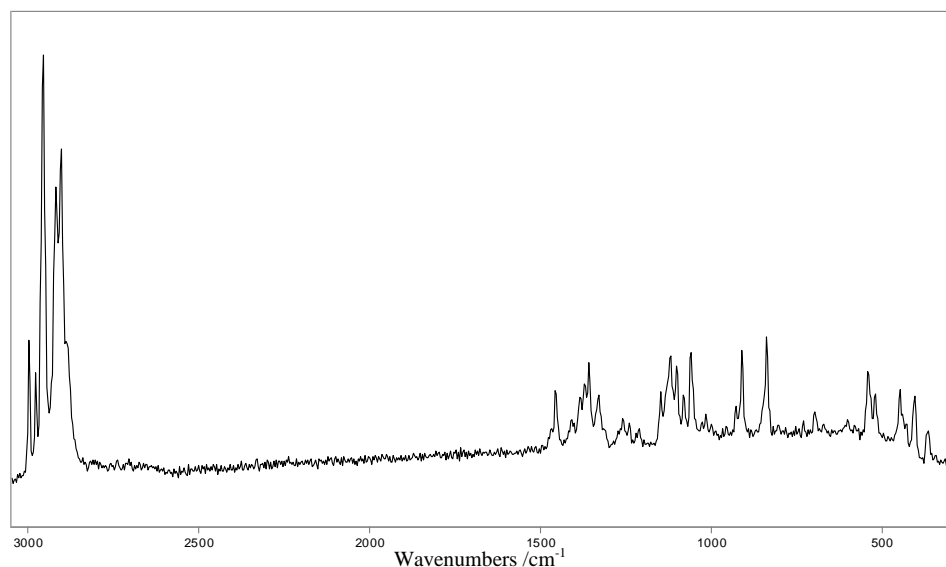


Figure 4.3.1. Raman spectrum of trehalose standard

The spectrum of trehalose features multiple peaks and features very little background (Figure 4.3.1). This gives several parameters to match when comparing instruments. The relative intensities, space between peaks, resolution and the limit of detection for seeing these peaks are all factors that can be investigated with this sample. For this work the bands at 540 cm^{-1} and 520 cm^{-1} will be used due to their close proximity to each other and isolation from other peaks. These peaks should appear more distinct with better instrument resolution.

4.3.2. Effect of accumulations on sample resolution

To obtain a comparable spectrum the samples must be optimized on the InVia Raman spectrometer. The first stage of this is to obtain an optimal number of accumulations.

The results of altering the number of accumulations can be seen in figure 4.3.2.

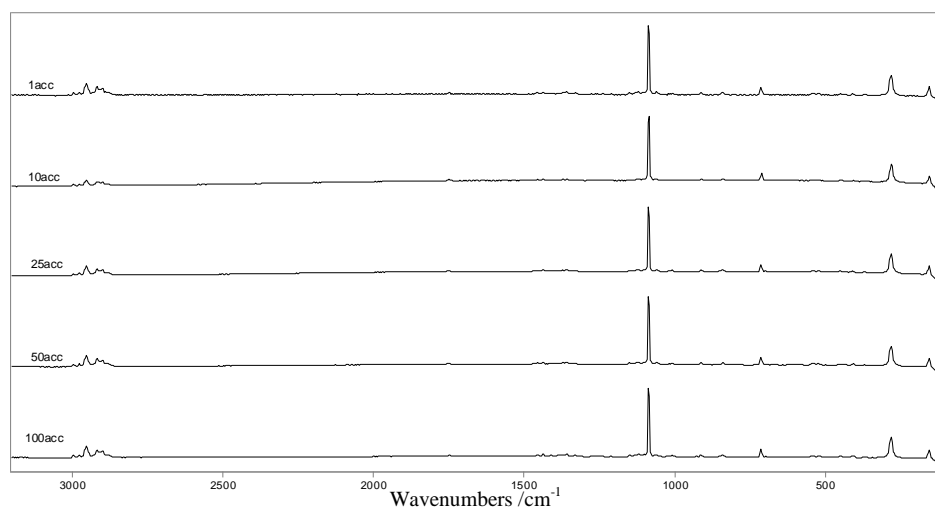


Figure 4.3.2. Raman spectra of calcite and trehalose 10% mixture using different accumulations

At 1 accumulation 8 peaks are clearly distinct from the noise and therefore not all peaks can be seen. When the number of accumulations is increased to 10, all the peaks which may be used in identification are visible. There is very little change from 25 accumulations on any major peaks. No changes can be seen, even on minor peaks, when 50 and 100 accumulations are used. Over the whole spectrum the trehalose peaks are not easily distinguishable. However by magnifying the region 600 cm^{-1} to 350 cm^{-1} the previously discussed 540 cm^{-1} and 520 cm^{-1} peaks can be identified.

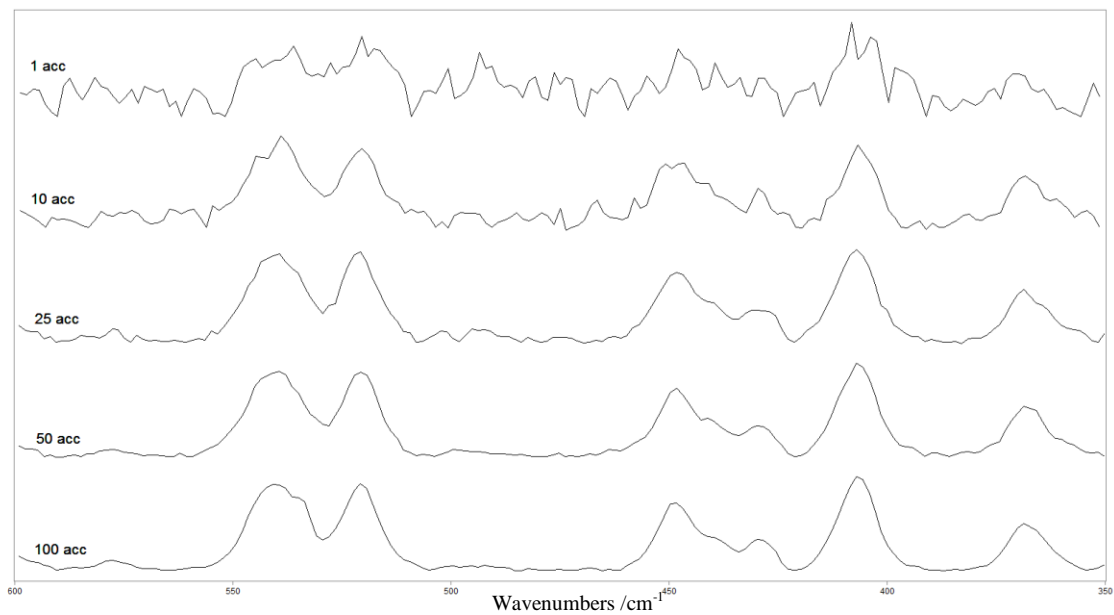


Figure 4.3.3. Raman spectra of calcite and trehalose 10% mixture using different accumulations over the 600 cm^{-1} to 350 cm^{-1} range

From the region 600 cm^{-1} to 350 cm^{-1} multiple peaks are observed from the trehalose within the mixture (Figure 4.3.3). The peaks within this region all appear within close proximity to each other and therefore at a low resolution are unlikely to be distinguishable. An example of this is observed in the 540 cm^{-1} and 520 cm^{-1} region whereby at higher accumulations an additional peak is observed which was previously masked by the 540 cm^{-1} peak. Additionally it is clear that at low accumulations very few of these trehalose peaks can be defined from the noise.

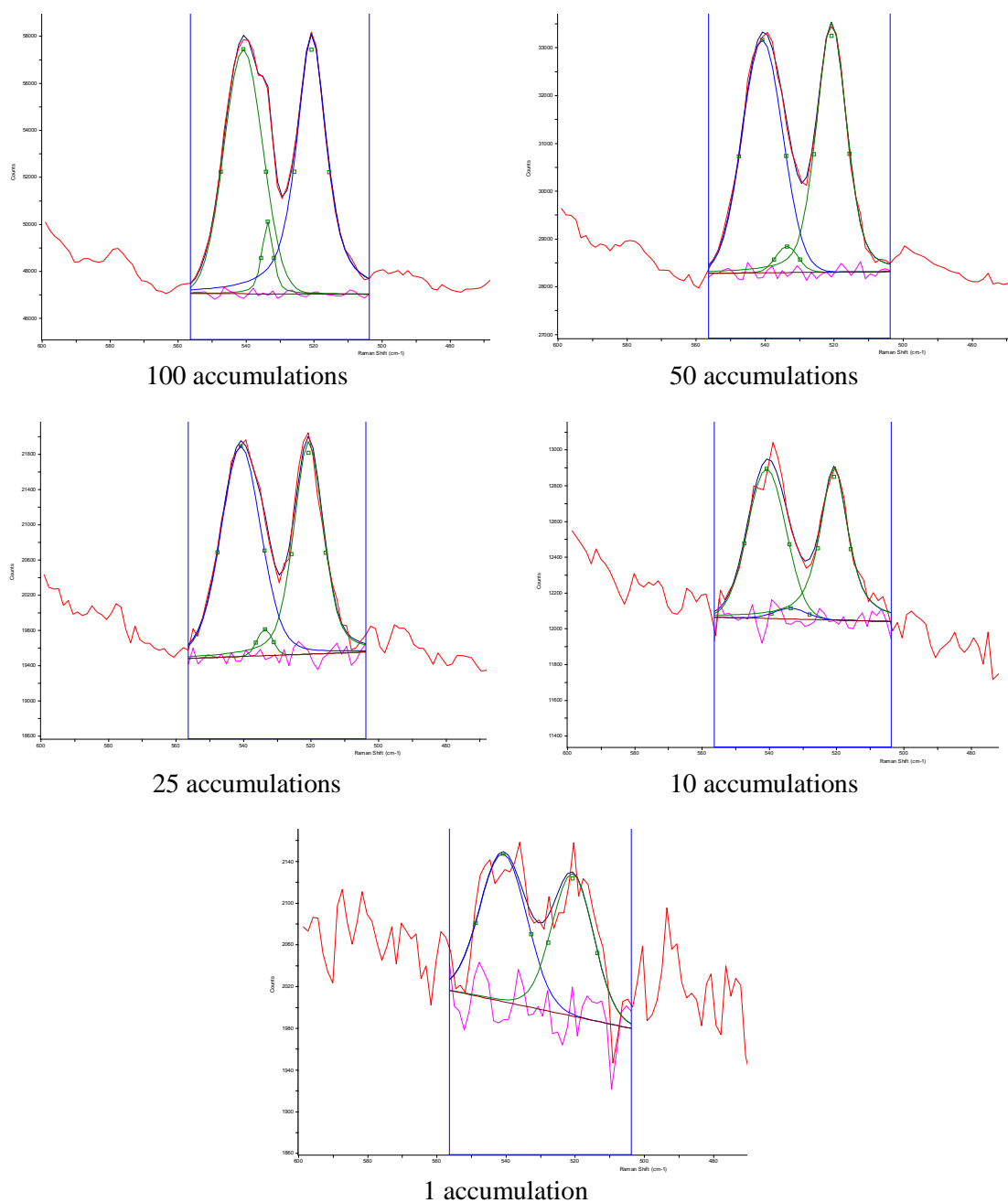


Figure 4.3.4. Raman spectra of calcite and trehalose 10% mixture with peaks at 540 cm^{-1} and 520 cm^{-1} fitted to spectrum. Original trace in red, fitted peaks in green, fitted trace in blue, baseline in brown and residual in violet.

Using the GRAMS/AI software the region the peaks at 540 cm^{-1} and 520 cm^{-1} were identified using peak fitting (Figure 4.3.4). The shape of these peaks within this spectrum were expected to be a mixture of the Gaussian form and Lorentz form^[2]. The form in which peaks occur affects the shape of the peaks base and half height width. Therefore for the fitted peaks, shifts in the peaks form indicate changes in the spectrum.

From the peak fits performed in figure 4.3.4 it is clear that noise is present predominantly within the 1 and 10 accumulation spectra and it has an additive effect on the peaks making them difficult to easily isolate from the noise. Additionally, there is a substantial background visible within these spectra, these fits therefore require the baseline to become sloped. The peak fitting occurring in the 1 accumulation spectrum is much weaker with the peaks becoming much broader than in the other spectra and it is also impossible to fit the minor 533.8 cm⁻¹ band in the 1 accumulation spectrum.

		1 acc	10 acc	25 acc	50 acc	100 acc
Fit parameters	Reduced Chi ²	0.7673	0.4681	1.4495	1.6663	0.8779
	Correlation R ²	0.8354	0.9641	0.9910	0.9971	0.9989
Band /cm ⁻¹						
540.8	Height	141.9	838.3	2391.1	4883.8	10396.1
	Width	16.0	13.4	13.9	13.7	13.3
	Area	2385.7	11892.5	36567.7	70867.0	147144.2
	Lorentz	0	0	0.2023	0	0.0112
533.8	Height		60.0	303.7	549.0	3075.8
	Width		11.2	5.3	7.5	3.8
	Area		715.0	1708.0	4404.2	15394.9
	Lorentz		0	0.0023	0	0.5623
520.8	Height	136.7	858.0	2417.1	5225.7	11038.5
	Width	14.1	9.7	10.2	10.2	10.2
	Area	2098.0	10762.8	29139.0	62320.3	144042.8
	Lorentz	0.0975	0.7442	0.4002	0.3488	0.6996

Table 4.3.1. Height, width, area and Lorentz of 3 fitted peaks within the spectrum of 10% calcite and trehalose mixture at different accumulations

Using the peak fits observed in figure 4.3.4, information can be gathered regarding these fits (Table 4.3.1). From the data it is clear that the heights for the bands at 520.8 cm⁻¹ and 540.8 cm⁻¹ are proportional to the number of accumulations. For all spectra, except the 1 accumulation sample, the widths of these bands are consistent. The 540.8 cm⁻¹ band is Gaussian in shape over all the accumulations and the overlap in the 533.8 cm⁻¹

and 540.8 cm^{-1} bands causes the unusual shape of these bands. The 533.8 cm^{-1} band at lower accumulations is masked and therefore the values relating to this band do not fit a linear pattern. The correlation of the fits increases with accumulations due to increase in the signal to noise ratios. Due to the non-changing widths of the samples, the resolution for the peaks appears relatively unchanged throughout all accumulations.

4.4. Laser power stability analysis

This section looks at the impact laser power has on samples and attempts to devise control standards for instrument validation which remain unaffected by laser power. For samples of astrobiological relevance the presence of a fluorescence background is often observed^[164-166]. This background often has the potential to mask any signals of importance within the Raman spectrum. The intensity of both the background and bands can both be directly affected by the laser power being applied to the sample. For materials of a biological nature the samples have the potential to fluoresce or degrade under high laser power^[3,164,167]. In such instances the laser power must be reduced, however if the laser power is reduced then any sample peaks can become indistinguishable from noise. Therefore it is important to look at the impact reducing laser power has on the intensity of Raman bands.

This work looks at the effect of altering laser power on the previously investigated calcite trehalose mixtures and naphthalene in acetone solutions. The trehalose is a useful compound for this analysis because it is a biomarker which also contains numerous peaks. These multiple peaks allow the different effects on altering the laser power to be seen for both major and minor bands in the spectrum. The calcite component of this mixture produces bands with strong Raman intensities which can be used to test for instrument response. However, as shown in chapter 3, solid mixtures display issues with homogeneity. Therefore to show comparability for homogenous mixtures the naphthalene acetone solutions were also analysed.

Samples of trehalose in calcite and naphthalene in acetone were prepared and analysed using Raman spectroscopy. The laser power of the instrument was altered to produce

spectra of the samples at 100%, 50%, 10%, 5%, 1% 0.5%, 0.1%, 0.05% and 0.0001%.

For each spectrum the sample position was not altered and so all spectra were from the same location of the sample.

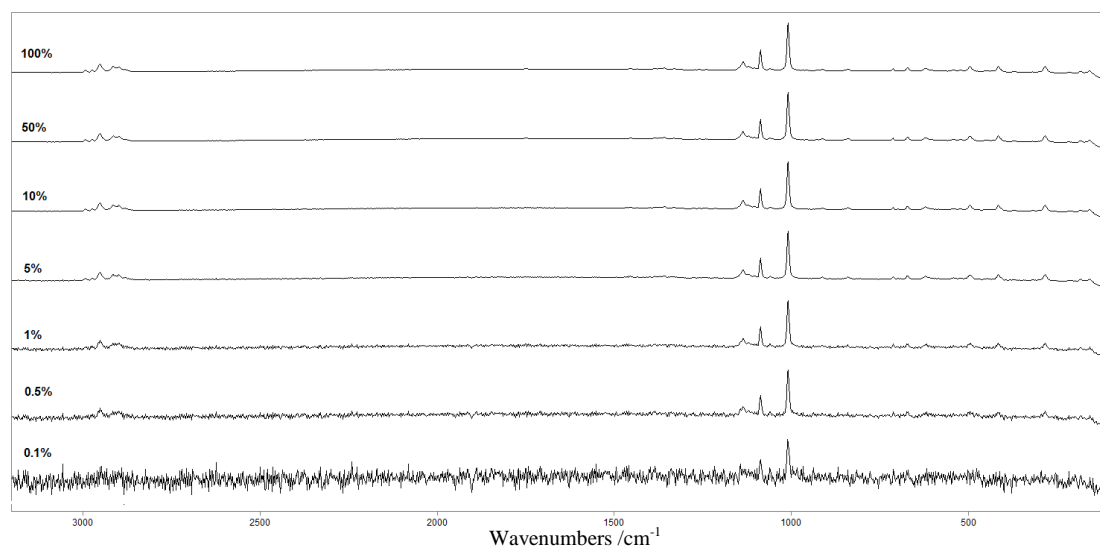


Figure 4.4.1 Raman spectra of calcite and trehalose mixtures analysed using different laser powers.

From the spectra of the calcite and trehalose mixtures at different laser powers very little variation can be seen within the sample (Figure 4.4.1). For trehalose the weaker peaks, between 1000 cm^{-1} and 200 cm^{-1} , remain visible until 0.5% laser power. The larger peaks of both trehalose and calcite, such as the ν_1 -Symmetric CO_3 stretching band at 1086 cm^{-1} , remain visible at 0.1% laser power. There are no visible peak shifts or changes in background due to heating. Therefore this sample would be useful as a control standard for analysis. However the comparability issues between different instruments remain present due to differences in homogeneity. To prevent this, the naphthalene in acetone solution discussed in section 4.2 must be investigated.

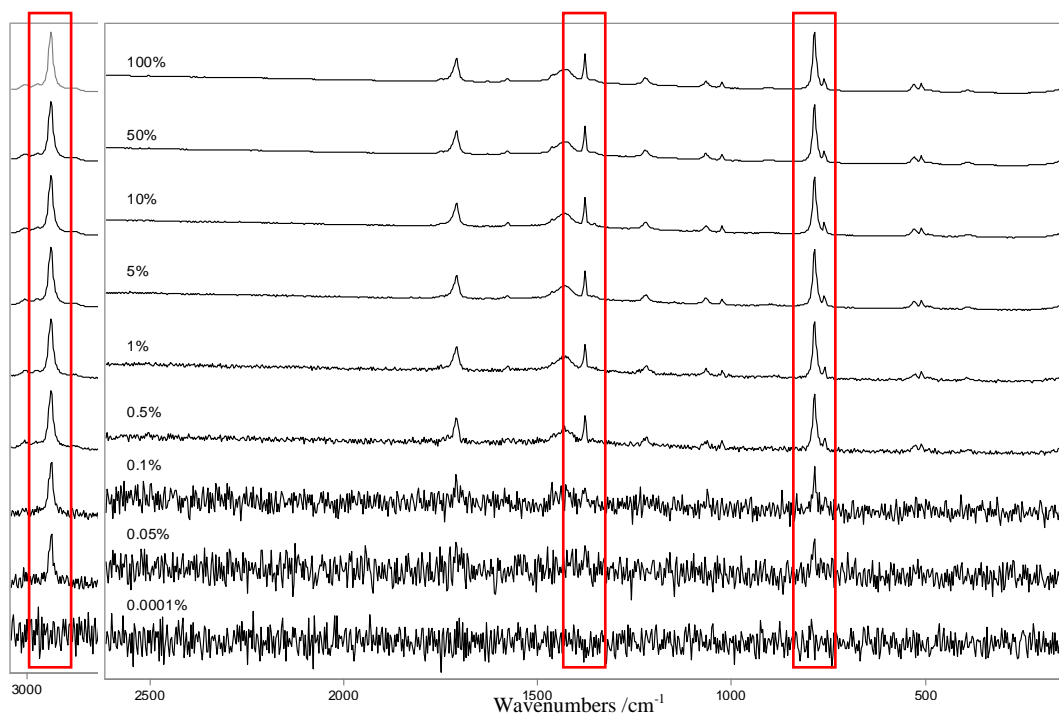


Figure 4.4.2. Raman spectra of naphthalene and acetone solution analysed using different laser powers with peaks relevant to this study highlighted.

To remove any potential issues derived from homogeneity of the samples a solution of naphthalene in acetone was prepared. The spectra for the naphthalene in acetone solutions are shown in figure. 4.4.2. As with the previous sample, the spectra were all obtained from the same location. In this sample the majority of the peaks became indistinguishable from the noise at 0.1% laser power. The only peak which remained visible at this power was at 2923 cm^{-1} . This peak, however, became indistinguishable from the noise at the next laser power; 0.05%.

	Naphthalene	Acetone	Acetone
%	1378	787	2923
100	134507	246670	1064850
50	65876	119883	518358
10	10113	18080	77751
5	4889	8751	37488
1	1129	2097	9077
0.5	600	1042	4333
0.1	70	160	854
0.05	64	98	368
0.0001	2	34	16

Table 4.4.1. Peak intensities for the three largest peaks within the spectrum at the different laser powers. Numbers in italic are values below the noise threshold

Using the spectra obtained in figure 4.4.2 the intensities for the three largest peaks within the spectrum were recorded and can be seen in table 4.4.1. The intensities can be seen for acetone at 787 cm^{-1} and 2923 cm^{-1} and naphthalene at 1378 cm^{-1} . From the values obtained the naphthalene peak remains visible until 0.05% power and the acetone peaks remain visible at lower laser power. The intensities recorded seem to show linear pattern relating to the laser power. To check this linearity, laser power was plotted against peak intensity.

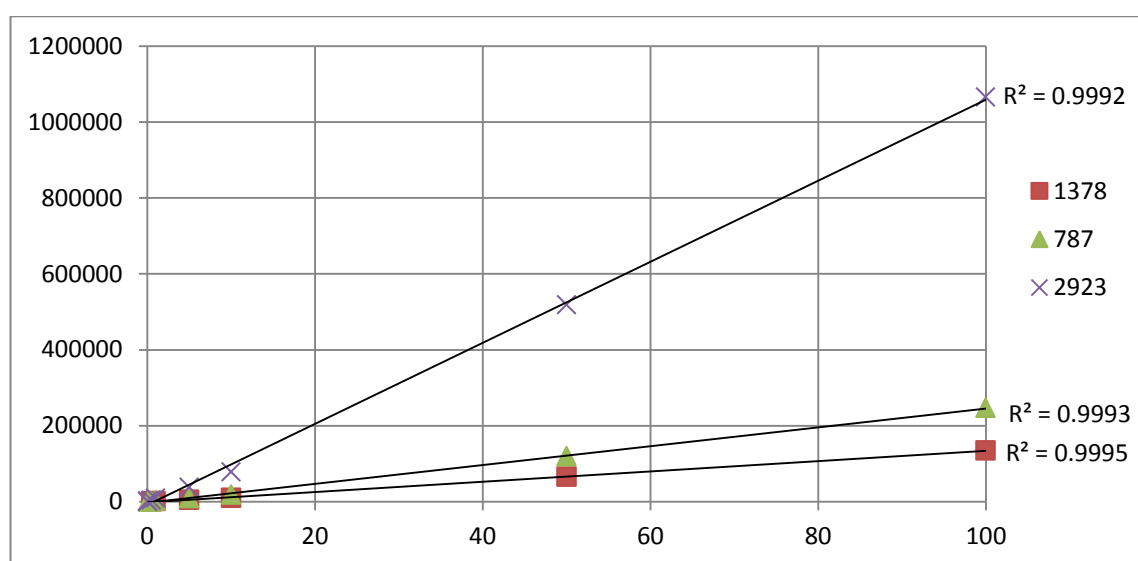


Figure 4.4.3. Graph showing laser power against peak intensity for peaks at 787 cm^{-1} , 1378 cm^{-1} and 2923 cm^{-1} .

Figure 4.4.3 shows the intensities of the largest peaks in relation to the laser power.

From the graphs it can be seen that there is a direct relationship between the laser power and the intensity of the peaks produced. The R^2 values for each peak intensity indicate that there is a minimal effect of laser power on the samples.

From these results it can be determined that these samples are suitable for analysis of instrument validation parameters across different instruments. They have been shown to be stable under increases in laser power. The calcite and trehalose mixture remain unaffected by the increases in laser power, however due to being solid samples they present issues with homogeneity. Therefore the naphthalene in acetone solutions is an alternative sample. They also do not alter when exposed to increased laser powers and do not have the homogeneity issues solid samples have. Therefore they would be ideal control standards of validation between different instruments.

4.5. Systematic identification of compounds

The previous sections have looked at identifying samples while considering factors which effect both signal and spectrum. Identification is based on the peaks present, intensities and position. This section looks at assigning the larger peaks within samples of importance to the search for life on Mars and devising an automated method for analysis. This automated identification would minimize human interaction with the sampling and data processing, thus increasing the robustness of the sampling. For this work samples were investigated with Raman spectroscopy as individual compounds rather than in mixture. Five different organics and four different inorganic samples were interrogated using a 633 nm laser. From the spectra obtained the most intense peaks were identified.

When the instrument is used on the surface of Mars there will be many samples and not enough time to analyse all the details on every single one. Therefore a method of quick identification of samples of interest is required. A database can be used for rapid identification of samples of interest. However database matching can have issues in samples where there are lots of signals, noise or large backgrounds. Therefore this section investigates using peaks in a protocol devised for rapid detection of samples which would be of interest for further analysis. For this work it is assumed that at least one of these peaks would be present in a sample of interest and that these are the only compounds present in the sample. This section uses this information in a systematic approach to identifying samples of importance.

4.5.1. Organic

Samples of anthracene, beta-carotene, naphthalene, phenanthracene and phenylalanine were all analysed using Raman spectroscopy. For each sample 5 peaks with the largest intensities were recorded and their positions assigned.

Wavenumbers /cm ⁻¹	Assignment
3057	CH stretching
3028	CH stretching
1557	CC stretching
1402	CC stretching
753	Ring antisymmetric deformation, bending CH

Table 4.5.1. Assignment of anthracene peaks

The anthracene spectrum produced several peaks with different intensities. The peak at 1402 cm⁻¹ was the largest detectable peak within the spectrum. The 4 other peaks were all approximately a third of the size of the main peak. All visible peaks within the spectrum were clearly distinct from the noise.

Wavenumbers /cm ⁻¹	Assignment ^[168]
1514	CC stretching
1155	ν (C-C) stretch
1007	In-plane rocking modes of (C-CH ₃)

Table 4.5.2. Assignment of beta-carotene peaks

The spectrum for beta-carotene produced a background which may potentially mask smaller peaks. Three distinct peaks were clearly visible at 1514, 1155 and 1007 cm⁻¹. While each peak was distinct from the noise, the peak at 1007 cm⁻¹ had a much smaller intensity and therefore has more potential to be masked by noise or background features.

Wavenumbers /cm ⁻¹	Assignment ^[159]
3055	CH stretching
1576	CC stretching
1381	CH in-plane bending
1020	CH out-of-plane bending
763	Ring antisymmetric deformation, bending CH

Table 4.5.3. Assignment of naphthalene peaks

The spectrum for naphthalene contains several peaks which are very distinct from the noise. The 5 main peaks at 3055, 1576, 1381, 1020 and 763 cm⁻¹ all have a very high signal-to-noise ratio. A sixth peak at 510 cm⁻¹ also has a similar intensity to the peak at 1576 cm⁻¹ and therefore could be used in identification of the sample.

Wavenumbers /cm ⁻¹	Assignment
1623	CC stretching
1441	CC stretching
1350	CH in-plane bending
1037	CH out-of-plane bending
710	Ring antisymmetric deformation, bending CH

Table 4.5.4. Assignment of phenanthracene peaks

The phenanthracene Raman spectrum contains numerous peaks which could potentially be used in identification. The spectrum contains 16 peaks which are clearly distinct from the noise. The largest peaks are at 1623, 1441, 1350, 1037 and 710 cm⁻¹.

Wavenumbers /cm ⁻¹	Assignment ^[169]
3062	CH stretching
1603	CO stretching
1213	CC stretch backbone carbon phenyl ring
1004	CC aromatic ring breathing
831	CCH deformation aliphatic

Table 4.5.5. Assignment of phenylalanine peaks

The largest peak for phenylalanine occurs at 1004 cm^{-1} and is approximately 4 times more intense than the next largest peak. The next four largest peaks occur at 3062, 1603, 1213 and 831 cm^{-1} . These peaks all have similar intensities and their intensities are similar to approximately 7 other peaks in the spectrum.

	1	2	3	4	5
Anthracene	1402.4	753.8	1557.4	3056.7	3028.2
Beta-carotene	1513.5	1155.1	1007.1		
Naphthalene	1381.2	3055.4	762.5	1020	1576.1
Phenanthracene	709.7	1349.8	1622.9	1440.8	1036.8
Phenylalanine	1004.1	3062.3	1213.2	1603	830.6

Table 4.5.6. Table showing peak positions of the 5 most intense peaks in each organic compound

Table 4.5.6 shows the different organic samples with their peaks ordered from 1 to 5, where 1 is the most intense peak. From this information it can be determined that if one of these samples is present in the sample then it would be likely to see one of these peaks present. The peak in the 1 column being present within the unknown would be a strong indication of that organic being present.

4.5.2. Inorganic

Samples of aragonite, calcite, gypsum and jarosite were all analysed using Raman spectroscopy. For each sample 5 peaks with the largest intensities were recorded and their positions assigned.

Wavenumbers $/\text{cm}^{-1}$	Assignment ^[170]
1084	ν_1 symmetric stretch
703	ν_4 symmetric deformation

Table 4.5.7. Assignment of aragonite peaks

The spectrum of aragonite contained only two peaks. Both peaks present were very intense and very narrow. Therefore the appearance of a similar spectrum should easily be identifiable as aragonite.

Wavenumbers /cm ⁻¹	Assignment ^[158]
1748	v ₁ and v ₄
1087	v ₁ -Symmetric CO ₃ stretching
713	v ₄ -Symmetric CO ₃ deformation
282	T(Ca, CO ₃)
155	T(Ca, CO ₃)

Table 4.5.8. Assignment of calcite peaks (T, translational lattice mode.)

The calcite spectrum contains several distinct very intense peaks. The strongest peak occurs at 1087 cm⁻¹. This peak can often be used in combination with the double peak at 282 and 155 cm⁻¹ to make a definitive identification of the compound.

Wavenumbers /cm ⁻¹	Assignment ^[154,155]
1141	v ₃ antisymmetric stretch vibration modes
1007	v ₁ symmetric stretch vibration modes of SO ₄
620	v ₄ antisymmetric bending vibration modes
494	v ₂ symmetric bending of SO ₄
415	v ₂ symmetric bending of SO ₄

Table 4.5.9. Assignment of gypsum peaks

The spectrum of gypsum is similar to the calcite spectrum in that it has one distinct peak which may be used in identification and several smaller peaks which can be used to confirm this. The largest peak occurs at 1007 cm⁻¹ and this peak can be used in combination with the peaks at 494 and 415 cm⁻¹ to make identification.

Wavenumbers /cm ⁻¹	Assignment ^[171]
1106	$\nu_3(\text{SO}_4)$
1009	$\nu_1(\text{SO}_4)$
622	$\nu_4(\text{SO}_4)$
438	$\nu_2(\text{SO}_4)$
223	O-Fe

Table 4.5.10. Assignment of jarosite peaks

The spectrum of jarosite contains many intense peaks and all below 1200 cm⁻¹. This sample can be easily distinguished from organic components due to the lack of peaks at higher wavenumbers. All the larger peaks at 1106, 1009, 622, 438 and 223 cm⁻¹ are of a similar intensity.

	1	2	3	4	5
Aragonite	1084	702.8			
Calcite	1086.6	281.5	154.9	712.5	1748
Gypsum	1007.2	493.8	1141.3	414.5	619.7
Jarosite	1105.9	1009.2	223.2	437.9	622.3

Table 4.5.11. Table showing peak positions of the 5 most intense peaks in each inorganic compound

Table 4.5.11 shows the different inorganic samples with their peaks ordered from 1 to 5, where 1 is the most intense peak. From this information it can be determined that if one of the samples is present then it would be likely to see one of the peaks present. The peak in the 1 column being present within the unknown would be a strong indication of that inorganic being present.

Using these peak intensities for organic and inorganic samples a table was created.

From this table the peaks and samples were ordered by intensity and grouped to show similarities and differences with positions.

Anthracene	3056.7	3028		1557	1402.4
Beta-carotene				1514	1155.1
Naphthalene	3055.4			1576.1	1381.2
Phenanthracene				1622.9	1441 1349.8
Phenylalanine	3062.3			1603	1213
Aragonite					
Calcite			1748		
Gypsum					
Jarosite					
	3062-3028		1748		1623-1155.1

Anthracene				753.8		
Beta-carotene				1007.1		
Naphthalene		1020		762.5		
Phenanthracene		1036.8				709.7
Phenylalanine				1004.1	830.6	
Aragonite	1084					712.5
Calcite	1086.6					
Gypsum	1141.3		1007.2			
Jarosite	1105.9		1009.2			
	1141.3-1084	1036.8-1020	1009.2-1007.2	1007.1-753.8	712.5	709.7

Anthracene					
Beta-carotene					
Naphthalene					
Phenanthracene					
Phenylalanine					
Aragonite	702.8				
Calcite				281.5	154.9
Gypsum	619.7	493.8	414.5		
Jarosite	622.3	437.9			223.2
				702.8-154.9	

Table 4.5.12. Table of combined peak intensities for organic and inorganic samples

Table 4.5.12 shows the peak positions as they are combined and ordered based on position. Inorganic peak positions are highlighted in red and organic in green. From the combined data it can be seen that there are distinct ranges of grouped peaks for the organics and inorganics.

Using the information above, it is possible to systematically identify samples by making some assumptions. The first assumption is that an unknown mixture contains one of the samples in the table. It also must be assumed that at least one of the 5 peaks is visible and not masked by noise or a background. A third assumption is made that the samples do not interact or cause shifts in the peaks. From the information in Table 4.5.12 a flow diagram was created.

Figure 4.5.1 and 4.5.2 show a flow diagram produced using the peak information collated in Table 4.5.12. Using this diagram it is possible to systematically identify the four inorganic compounds; aragonite, calcite, gypsum and jarosite and the five organic compounds; anthracene, beta-carotene, naphthalene, phenanthracene and phenylalanine. Using such a protocol on an unknown sample would allow for quick identification of samples which may be of importance to the search for life on Mars.

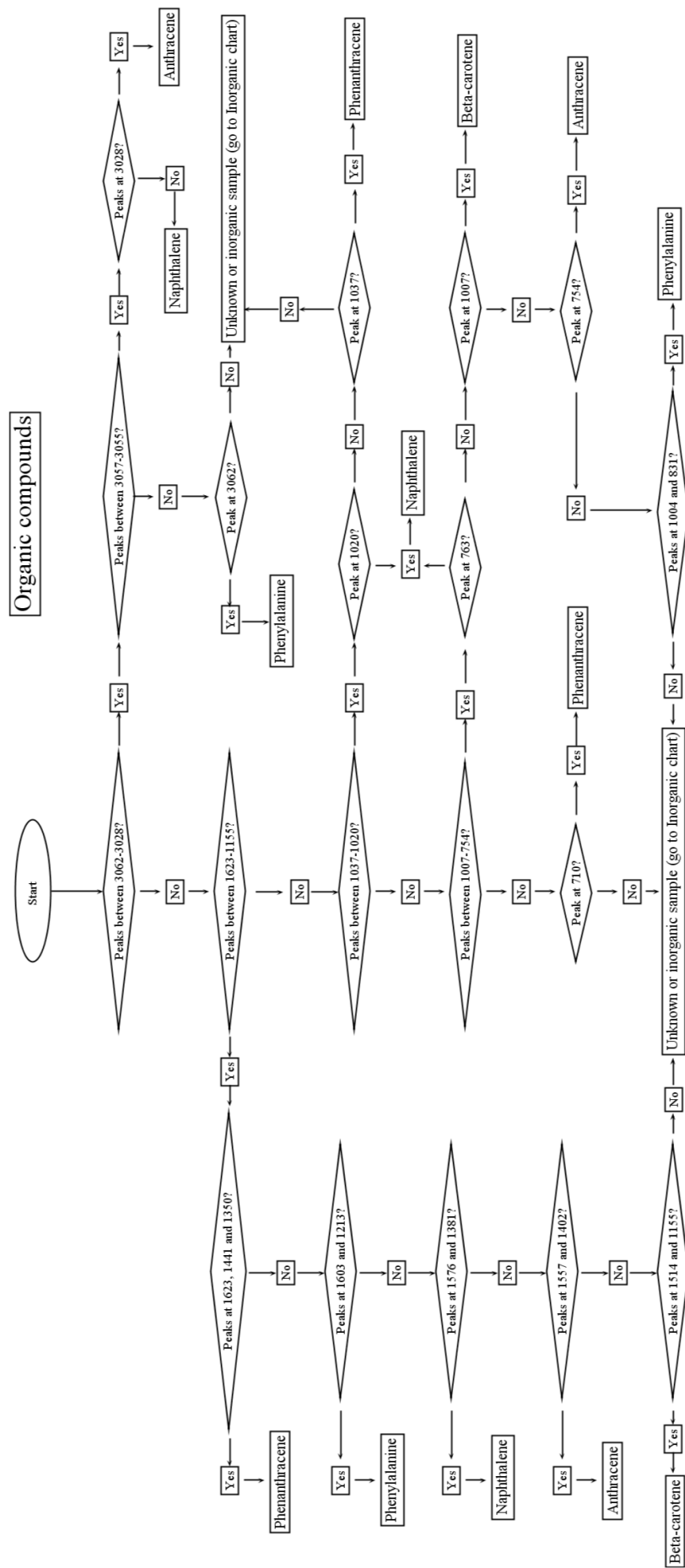


Figure 4.5.1. Flow diagram showing systematic identification of organic unknowns.

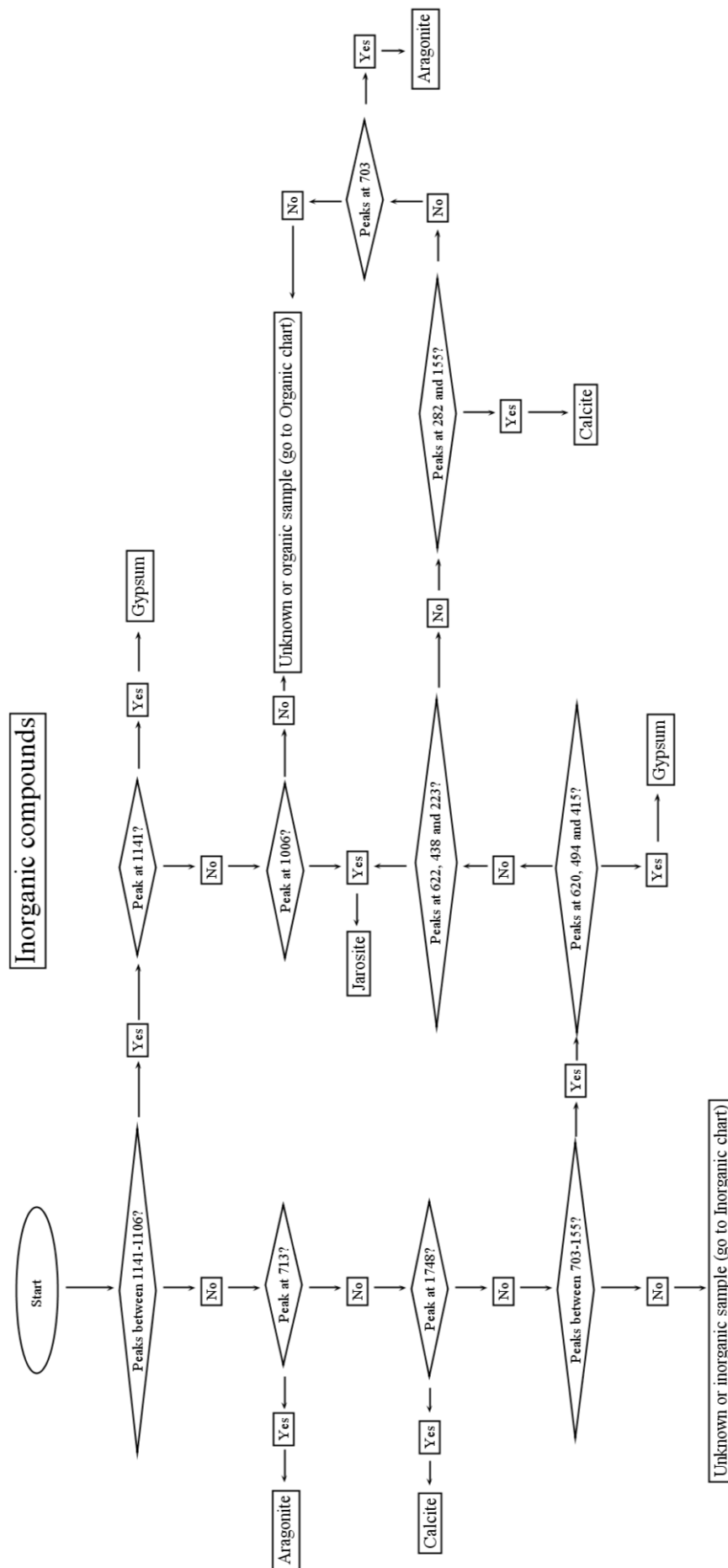


Figure 4.5.2. Flow diagram showing systematic identification of inorganic unknowns.

4.6. Conclusions

In this chapter the effects of altering different parameters within limit of detection calculations were investigated. Two different methods of calculating noise using varying points and areas were used to establish different limits of detection. The effects on limits of detection were additionally established whereby instrument validation parameters were assessed. The stability of standard samples under increasing laser power was additionally investigated. Using peak assignments of multiple different organic and inorganic samples a procedural method of identifying samples was devised. This method could be applied to mixtures of inorganic and organic materials to identify the compounds present.

Chapter 5

Instrument performance comparators

The aim of this chapter is to investigate the ability for comparable data to be produced between the InVia Renishaw Raman instrument and the MOB prototype instrument. To do this a method using a 3 by 3 grid system was interrogated. A slide mask was developed to allow for reproducible analysis of the same location between instruments. Spectra from the prototype and benchtop instrument were then compared.

5.1. Preparation for comparison of MOB instrument with InVia

In chapter 4 instrument validation parameters were discussed and suitable standards were devised based on these measurements. Key features that must be considered are robustness and sampling consistency between instruments. On the ExoMars rover the analysis will be automated by the rover and not prone to human error. However for comparisons between the standard benchtop Raman spectrometers and the prototype instrument these factors must be considered. To allow optimization of the MOB instrument standard spectra of samples must be produced. The instrument parameters can then be altered so that the resultant spectra match. Once such optimizations have occurred then the MOB instrument can be used to reliably obtain the same spectra that would be obtained on the InVia instrument.

In chapter 3 issues were identified within the homogeneity of samples. This could potentially be overcome by looking at solutions rather than solids, however, this would

not be representative of real Martian samples. For comparability it is required solid powders are used and a method for obtaining reliable comparable data from powdered mixtures is required. To do this the issue of homogeneity of the sample must be removed. For this, precise measurements were used so that the analysed region within each sample was exactly the same. For each sample a slide was produced which had space to look at a nine different locations within each sample.

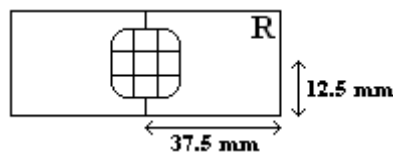


Figure 5.1.1. Image showing slide produced for sample analysis

Figure 5.1.1 shows the slide produced for each of the samples. An “R” was written onto the top right-hand corner of the slide to prevent rotation of the sample. The centre of the slide was measured to be in the position 37.5 mm by 12.5 mm.

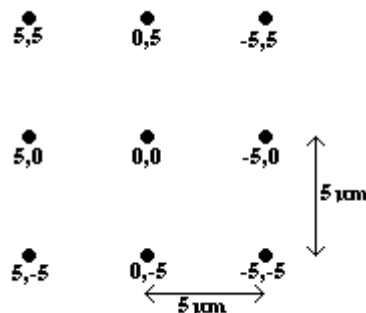


Figure 5.1.2. Image showing the grid system used in analysis

Figure 5.1.2 shows the grid used on all samples. 0,0 is the position of the origin in the centre of the slide. From this point all additional points were derived at 5 μm from this origin as shown in the diagram. A stage was prepared for the MOB instrument where the laser positions were pre-identified. The slide could be placed directly on the stage and the laser would be positioned at the location defined (0,0). A distinct mark was

drawn on the slide to allow easy movement to the middle of the slide. For these optimizations the solid mixture of calcite and trehalose evaluated as a standard in chapter 4, was used.

5.1.1. Sample variation observed on Renishaw InVia instrument

As detailed previously, homogeneity of these samples varies from location to location. With the nine different points it is possible to see the differences in this homogeneity. The concentration variation is important when optimizing the instrument using a known sample. By looking at the variation within a known sample over a small region the suitability of the sample as a standard can be established.

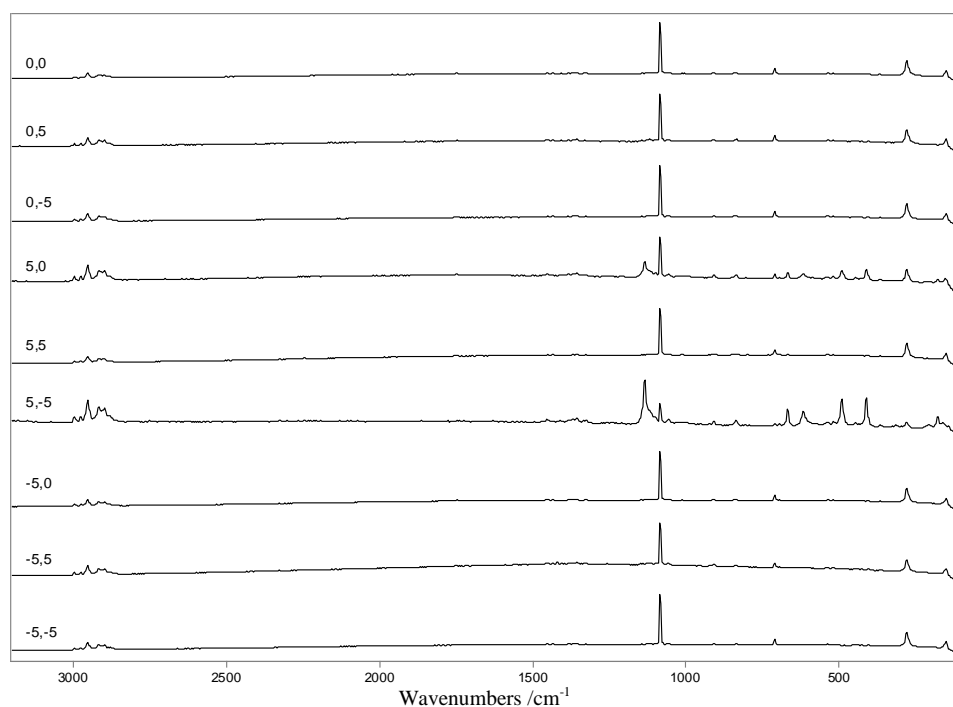


Figure 5.1.3. Raman spectra of calcite and trehalose 25% mixture at different locations

In the 25% mixture several regions of in-homogeneity occur. At both locations 5,0 and 5,-5 clear differences between the spectra can be seen. From the spectra obtained, at this high concentration there is a large variation within the sample over micron distances.

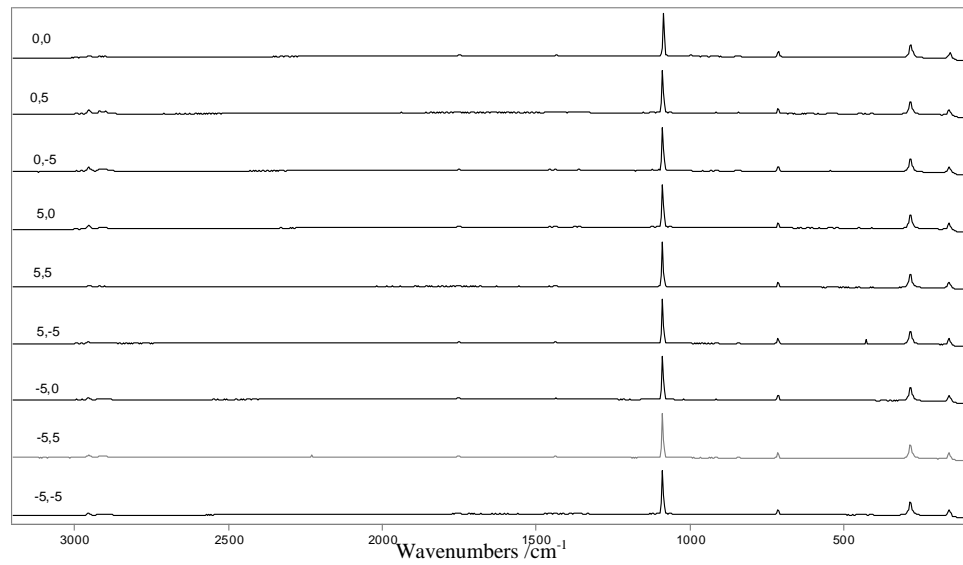


Figure 5.1.4 Raman spectra of calcite and trehalose 10% mixtures at different locations

The 10% mixture shows very little variation in the spectrum between each location. All locations show similar peaks present and there is very little difference in their relative intensities. In these spectra the concentration variation is much less than that observed in the higher concentration spectra. Therefore for use of this sample as a standard a lower concentration would be desirable.

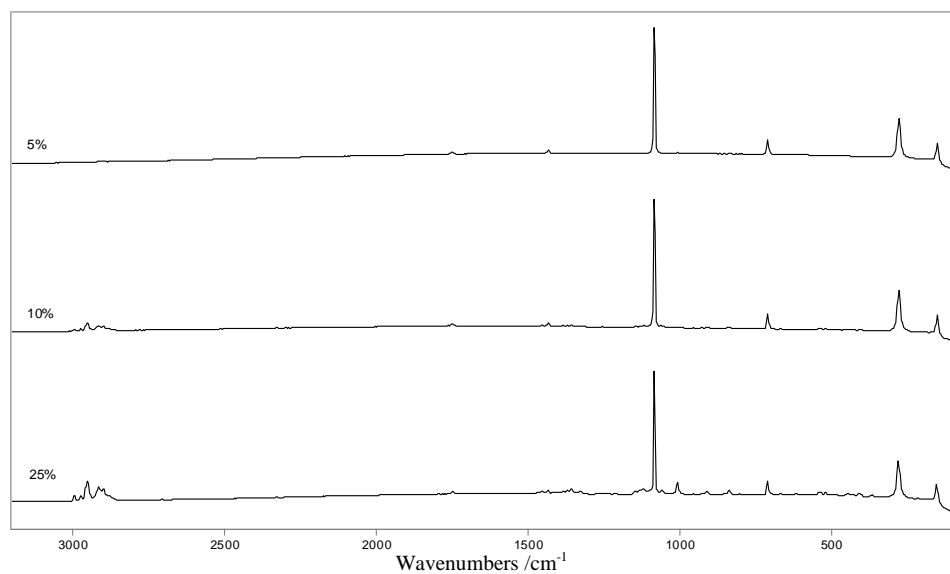


Figure 5.1.5 Calcite trehalose Raman spectra averaged over all points at 5%, 10% and 25% concentrations

All data from the 9 points was added together and averaged (Figure 5.1.5). This allowed for a more accurate LOD dataset. The difference between 10% and 5% showed very little change in peaks present and some minor peaks became visible. 25% shows multiple minor peaks in the spectrum. From this preliminary evaluation on the Renishaw InVia Raman spectrometer it is clear that representative spectra can be obtained from the same locations within the solid mixture. However for samples to be reproducible all points must be identical on the micron scale.

5.1.2. Comparison with prototype instrument

This section has looked at using 3 by 3 grids to compare different instruments. However such a method requires movement between two different instrument stages and this may potentially cause problems. While InVia instrument has a motorized stage and microscope the MOB instrument does not, therefore it is more prone to potential error. It has also been observed that only small micron changes in sample position can produce radically different spectra within higher concentration samples. Therefore the prototype instrument has the potential for reproducibility and accuracy issues.

An alternative method of comparing the instruments was therefore derived that would not have the potential for instrument error. This involved the use of a mask on the slide. A thin copper sheet of metal was supplied for potential use as a mask. To test; a hole was drilled in the slide 50um across.



Figure 5.1.6 Image of the slide used in previous section and new mask covering

Figure 5.1.6 shows the sample slide and the mask used for this section of work. The mask prevents sample analysis anywhere but where the hole is. The hole was made off-centre which allows for rotation 180° and flipping the mask over to get 4 different locations. The mask was also made to be the same size as the slide and therefore it simply covered the slide and would always have the hole in exactly the same position.

With the use of a mask covering the sample two factors will have an impact on the slides effectiveness for producing reliable data. These two factors relate to the laser spot size in relationship with the mask hole and the impact edge effects have upon the spectrum. For the mask to work effectively the laser spot size must be of similar size to the hole within the mask. If the laser spot is too small then the spectrometer will be capable of looking at different regions within the hole and thus positioning will again affect the resultant spectra. If the laser spot is too large then the edges of the slide will have more impact upon the resultant spectrum. For reproducible spectra the ideal laser spot and hole within the mask would be of equal size. Edge effects within a sample produce distortion and background features within the Raman spectrum^[2,5]. Therefore spectra obtained at the edges of the hole will produce additional artifacts. These artifacts could potentially mask spectral features from the sample and thus produce unidentifiable spectra. The impact of these edge effects caused by the mask must therefore be investigated.

Under the microscope the hole appeared to be visible across a diameter of 150 μm . The impact point was not a completely smooth circle and region around the circle edge appeared much darker. Therefore there were three distinct visible regions: Metal slide, hole and region of darker colour. Using mapping the regions at which the silicon could visibly be seen is shown in Figure 5.1.7.

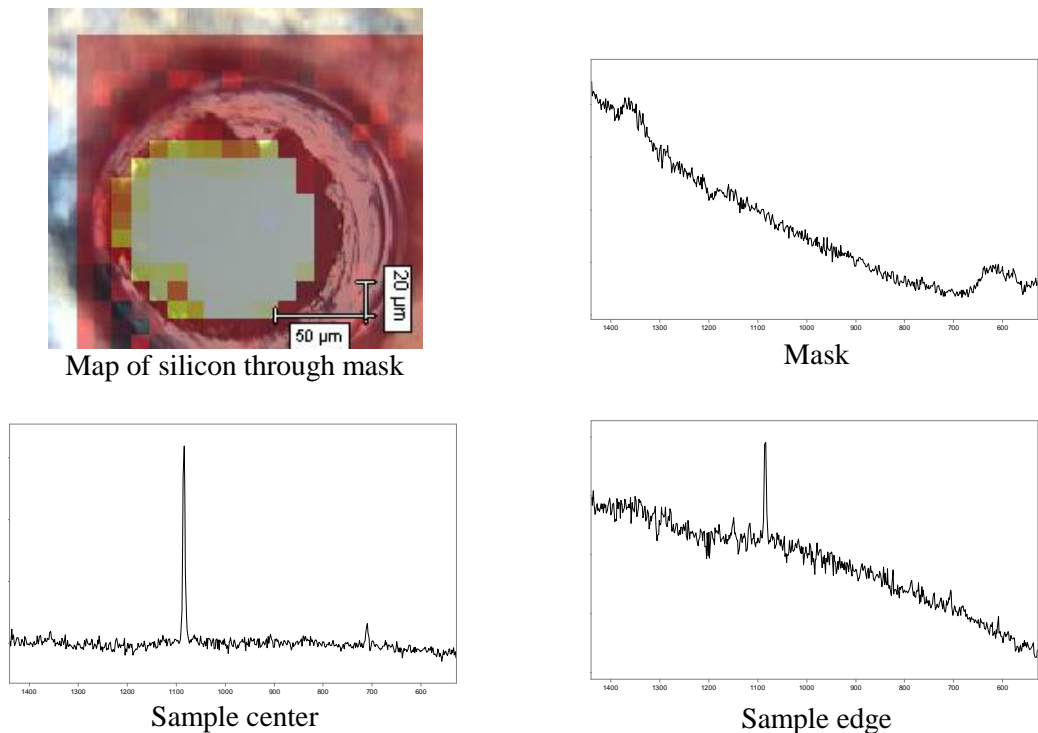


Figure 5.1.7. Map of silicon sample through the mask hole and spectra of mask, sample at the edge of the hole and sample at center of the hole.

Figure 5.1.7 shows the map obtained from the silicon with the mask overlaid and spectra obtained from the mask, sample at the edge of the hole and sample in the center of the hole. From the map produced it is clear that the region where the sample is visible is well defined. The slide produces no Raman bands and it only produces a weak background. The sample at the edge of the hole shows Raman bands with a weak background. The background at this position is not strong enough to mask any of the Raman bands. In the center of the hole the sample is clearly seen to be identifiable with no background or features derived from the mask.

5.1.3. Laser spot size and sampling

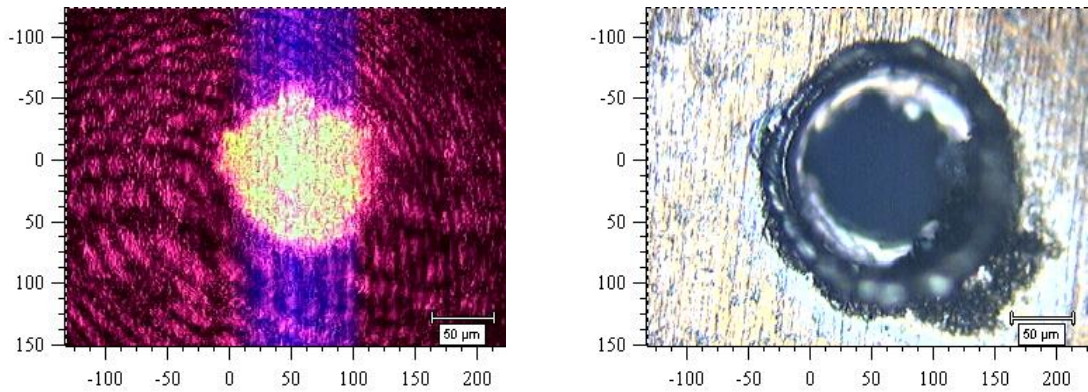


Figure 5.1.8. Laser spot size with comparison to mask hole size.

To establish the effects the mask may have on the laser the instrument was set up so that the laser spot would be directly in the centre of the mask hole. Figure 5.1.8 shows the image of the mask with and without the laser on. From the image only illumination of the sample through the hole can be seen. This means that the laser is hitting all the sample through the hole and thus the hole is of optimal size.

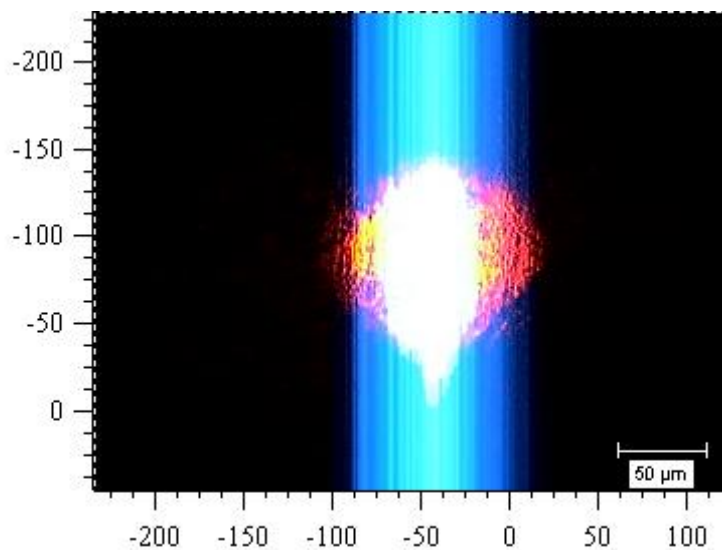


Figure 5.1.9. Image of laser spot size on surface of mask.

As a final confirmation of the laser spot size in relation to the hole in the mask an image was obtained focused directly onto the sample rather than the mask. Figure 5.1.9 shows the image of the laser as it was fired directly onto the sample through the mask. No illumination of the mask is visible and thus it can be confirmed that all signal obtained at this location would be from the sample rather than the mask.

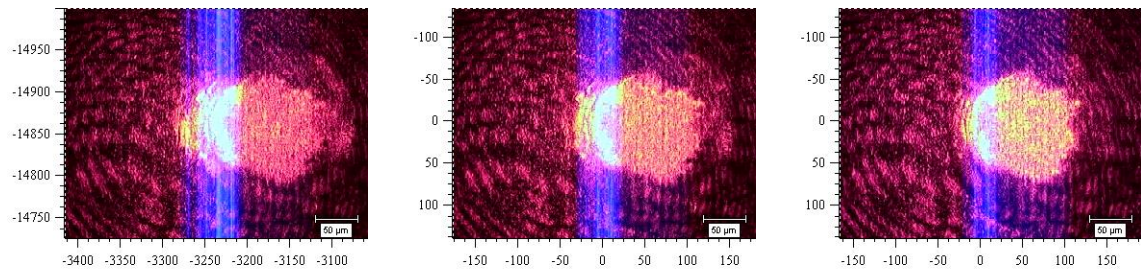


Figure 5.1.10. Laser run along the edge of the sample at 10um distances.

To confirm the effects of the laser on the edge of the slide images were obtained from the laser as it passes from the edge of the hole onto the sample (Figure 5.1.10.). From the images obtained it is clear that when the laser hits the edge of the slide the image of the spot is different from that is obtained when the laser does not. From these results it can be confirmed that in figure 5.1.8 the laser is focusing on the edge of the slide.

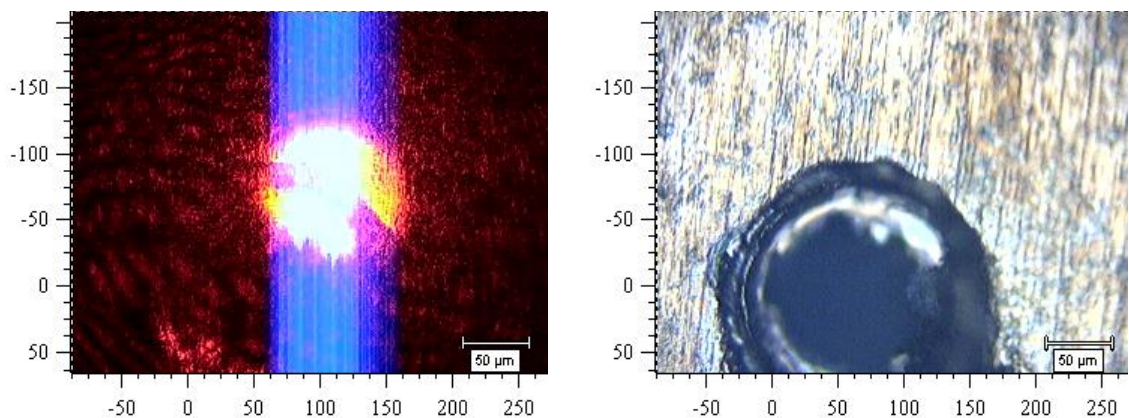


Figure 5.1.11. Laser spot on edge of mask sample hole

Figure 5.1.11 shows the laser as it directly hits the edge of the slide. From the image it can be seen that there is a clearly distinct region at the edge of the mask through the laser spot size. This means that at the edge of the slide the signal from the sample will directly cut off and thus the spurious signals cannot be from interactions at the edge of the slide.

5.1.4. Comparison of data collected with and without mask

The effect the mask has on the resultant spectra must also be considered for it to be used reliably on multiple instruments. For this the 25% calcite trehalose mixtures used in chapter 4 were used again. The sample was set up with the mask in position, a spectrum of the sample was obtained and then the mask was removed and the spectrum was obtained a second time.

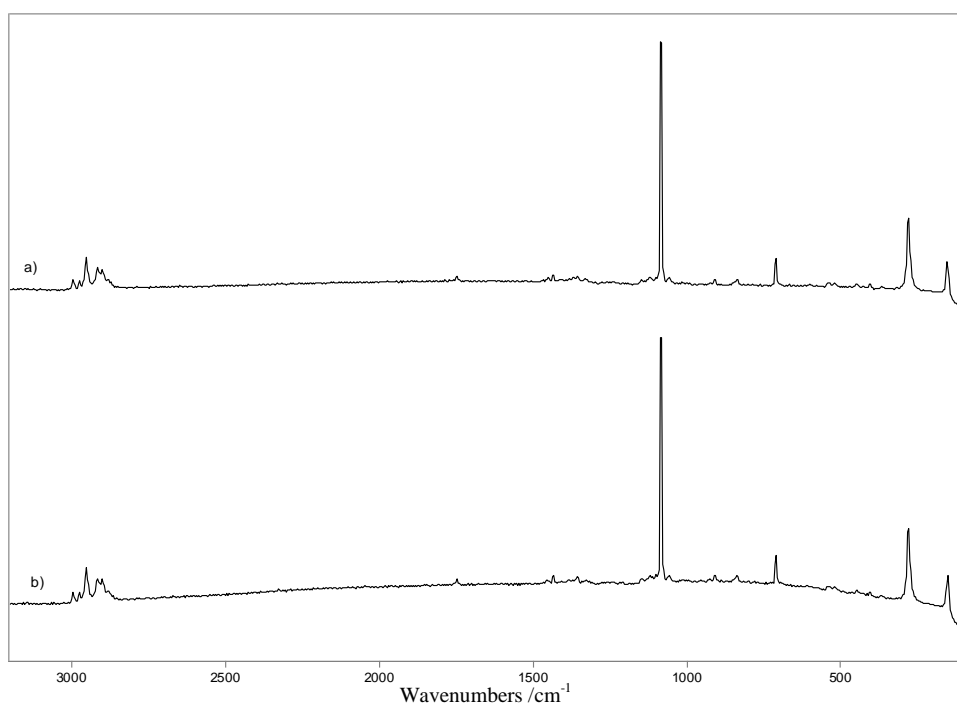


Figure 5.1.12. Stack plot of spectrum of 25% calcite trehalose a) without mask and b) with mask through x5 objective.

From the spectrum of the sample obtained (Figure 5.1.12.) it can clearly be seen the effect the slide has on the sample is minimal. All the same peaks, including the weaker ones, are present in both the spectra. A minor background is present in the spectrum obtained through the mask. This is likely due to the laser being slightly defocused as the laser must go through the mask.

From the spectra obtained and information relating to the laser spot size, the implementation of a sample mask appears to be an optimal to obtain reliable reproducible results. This method allows easily repeatable comparisons of samples on different Raman instruments without issues with the homogeneity of the samples becoming an issue. Edge effects do add a minor background, however this background does not appear to have any significant effect on band identification of a sample.

5.2. Comparison of Spectra Obtained from Prototype Raman instrument with a laboratory Raman instrument.

This section looks at the issues with comparing two different Raman instruments and getting reproducible results. This involves looking at the differences between spectra produced between instruments and deducing methodology to minimize these differences.

When the ExoMars rover goes to Mars it will collect data from samples on the Martian surface, this data will need to be processed and samples of importance identified. To do this reliably, consistent results between different instruments are required or there is potential for discarding samples of importance simply because the rover instrument was not setup correctly to see the spectrum from a sample of importance. To test the effectiveness and to calibrate the prototype instrument a control sample is needed.

5.2.1. Instrument Comparison

For this section similar data acquisition to the samples in Chapter 3 was repeated. Several mixtures of organic and inorganic compounds at various different compounds were observed. These spectra were recorded on both the MOB instrument and the InVia instrument for comparison. This allowed the very basic differences to be observed within the spectra produced for known samples. From these spectra it should be possible to alter parameters of the MOB instrument to obtain similar spectra.

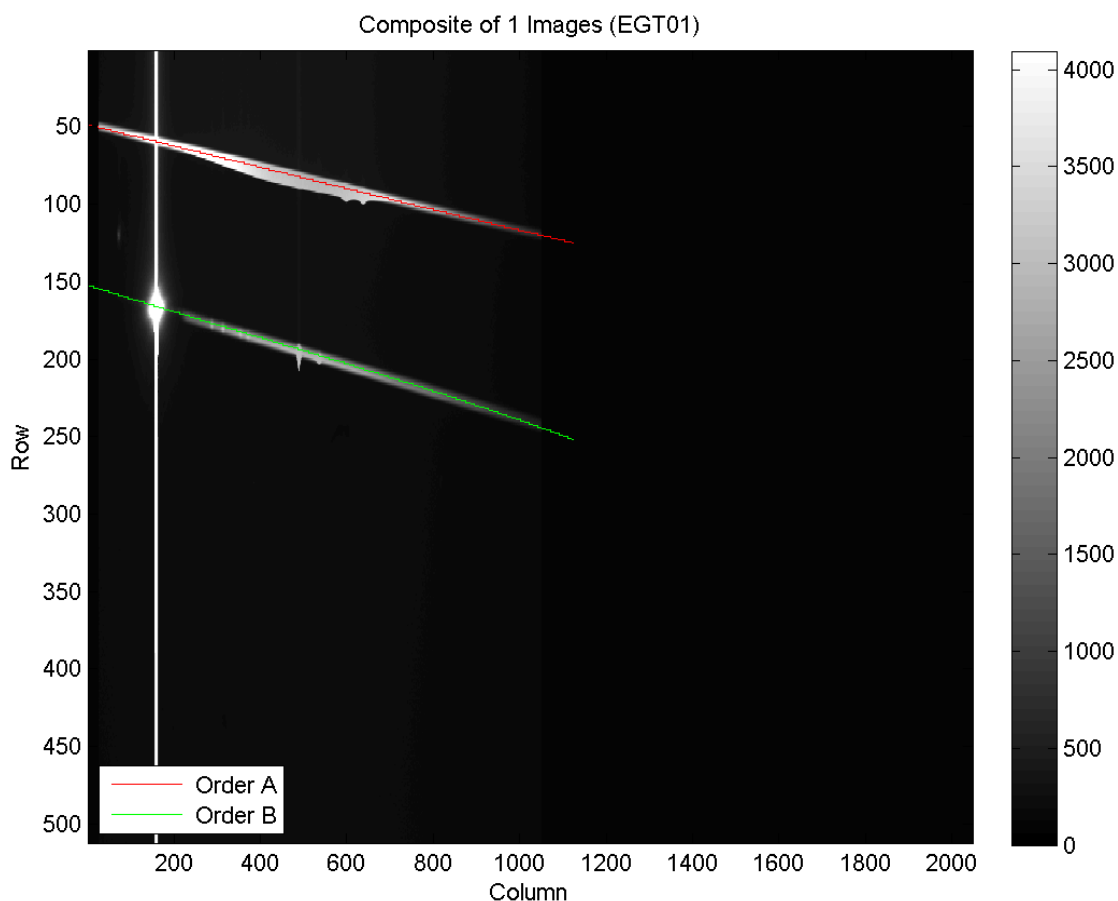


Figure 5.2.1. Image of the CCD from prototype Raman instrument produced from 1% gypsum and trehalose mixture

Figure 5.2.1 shows the CCD image, produced by the prototype instrument, of gypsum and trehalose mixture. From this image a polynomial fit was applied to the two visible orders and these fits were shown as red and green lines. Order A occurs over the 2000 cm^{-1} to 4500 cm^{-1} range and order B over the 0 cm^{-1} to 2250 cm^{-1} range. The brightness of each point along these fits was then plotted onto a graph.

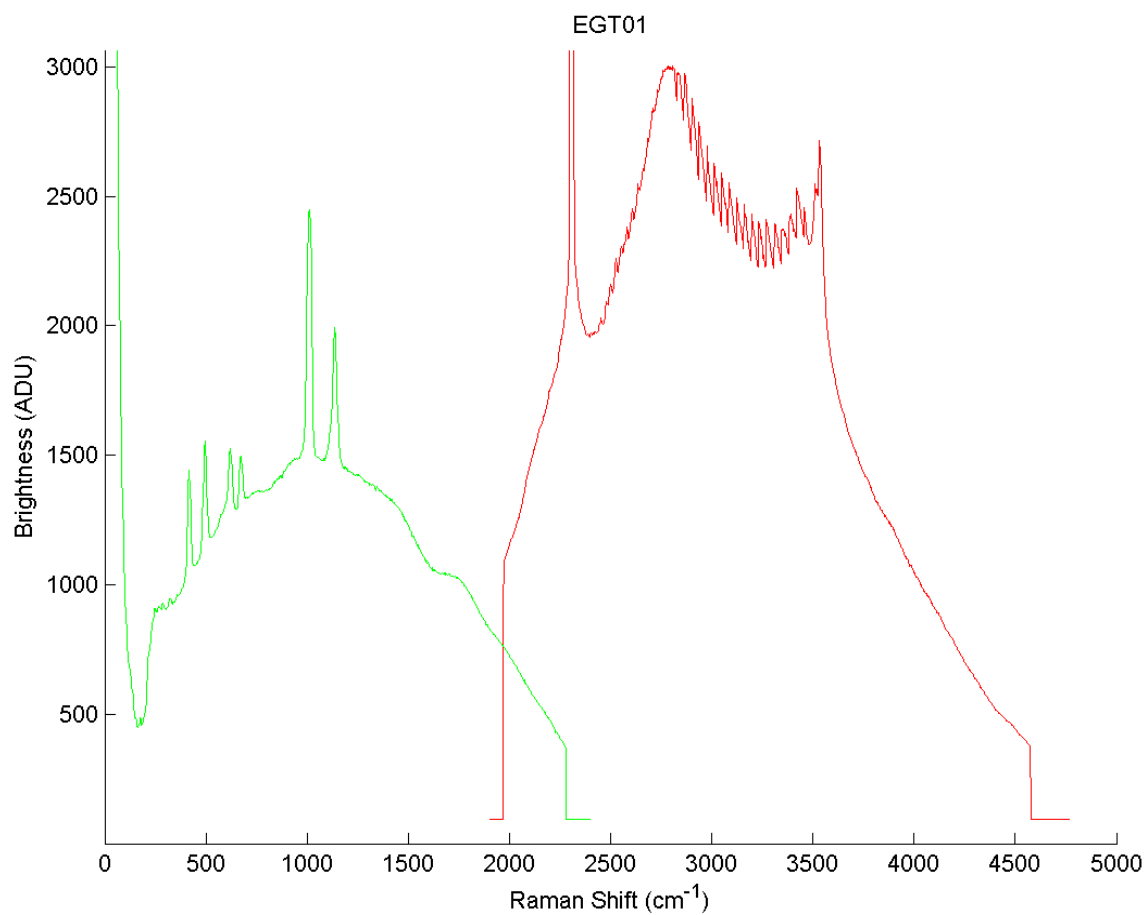


Figure 5.2.2. Spectrum derived from the CCD image of 1% gypsum and trehalose mixture

The spectra produced from the CCD images can be seen in figure 5.2.2. The spectra produced from each order were then baseline corrected and combined to produce spectra over the whole spectral region of 0 cm⁻¹ to 4500 cm⁻¹ wavenumbers. The resultant spectra were then compared with the spectra obtained using the Renishaw InVia instrument for the mixture and pure standards.

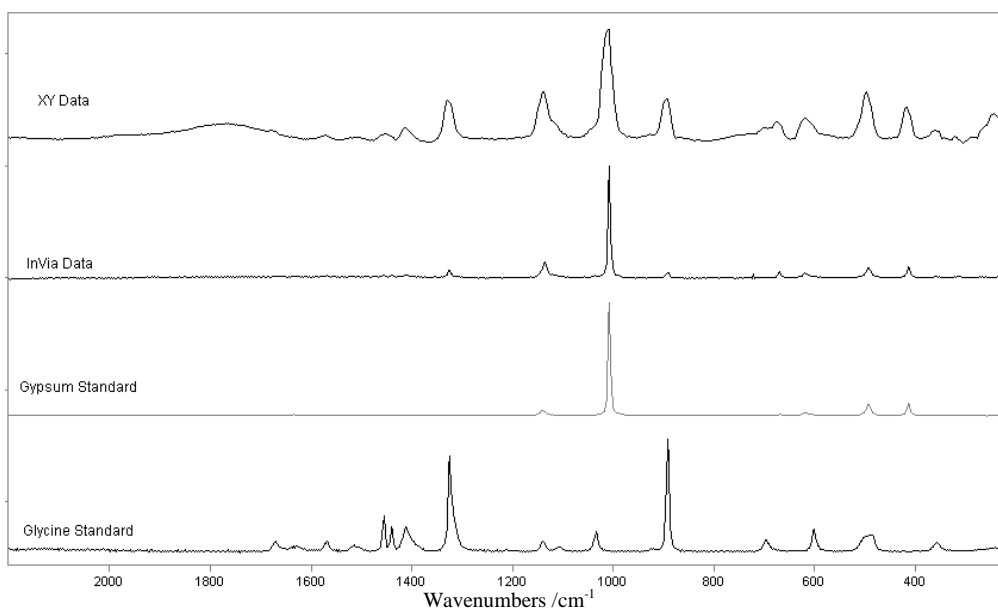


Figure 5.2.3. Raman spectrum of 25% mixture of gypsum and glucose

From the spectra obtained of the sample 25% mixture of gypsum and glucose (Figure 5.2.3) it was clear that there were several major differences between the XY data from the MOB instrument and the .SPC data from the InVia instrument. One of the first noticeable features is the broadness of the peaks obtained from the MOB. This was primarily due to the resolution of the MOB instrument being set to lower than that of the InVia instrument. Several broad bands are also visible at 1800 cm^{-1} ; however these features are produced through manipulation of the data through baseline correction. This processing was required because of the background within the original spectrum.

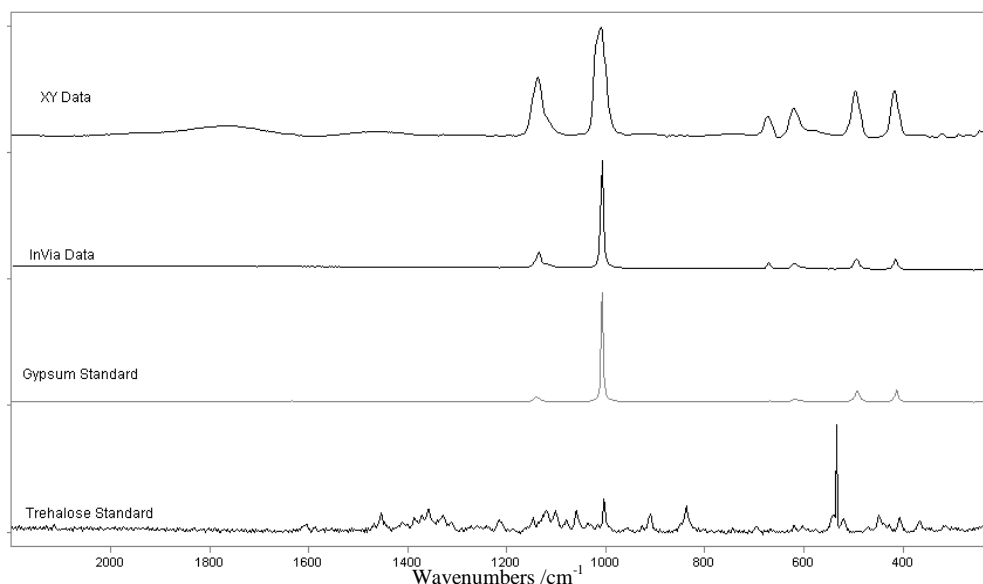


Figure 5.2.4 Raman spectrum of 1% mixture of gypsum and trehalose

From the spectra obtained of the sample 1% mixture of gypsum and trehalose (Figure 5.2.4.) the differences between the InVia Raman instrument and the MOB Raman instrument were not as clear as in the 25% gypsum glycine. In this sample the peaks corresponding to the trehalose were not present and so the spectrum produced was expected to have similarities to the gypsum standard. The spectra produced by the MOB instrument had a lower resolution than that of the InVia instrument and thus the peaks appeared broader. The main difference visible in the spectra produced on the different instruments was the relative intensities of the gypsum peaks to the main peak at 1007cm^{-1} . In the InVia spectrum the ratio of peak at 1007cm^{-1} to the peak at 1141cm^{-1} is approximately 6:1 but in the MOB spectrum this ratio is 2:1. This may be attributed to a number of factors including the baseline correction of the data or the way in which the resolution of the spectrum will cause peaks to be broader and less intense.

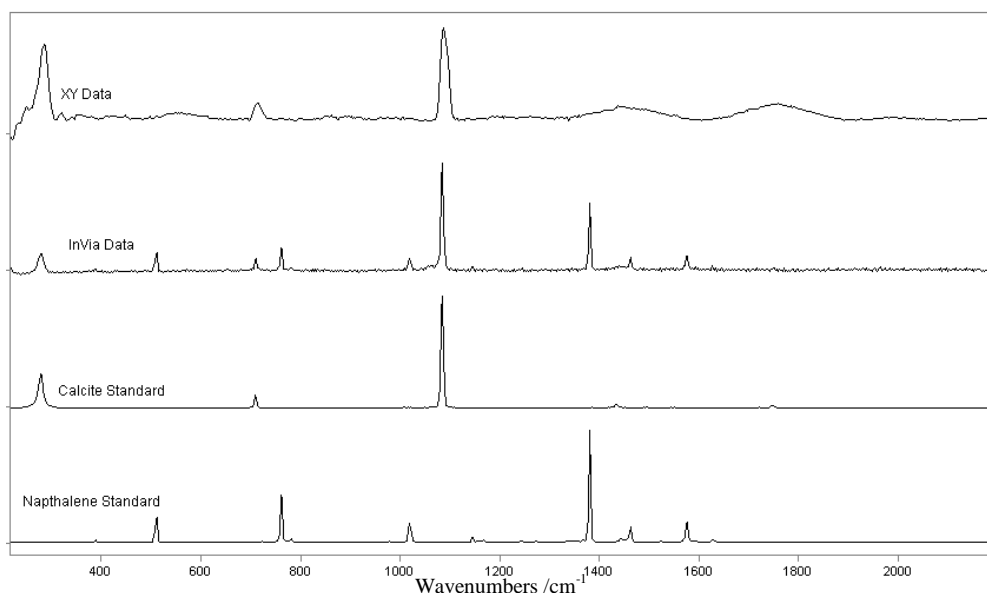


Figure 5.2.5 Raman spectrum of 10% mixture of calcite and naphthalene

The spectrum of 10% mixture of calcite and naphthalene shows a difference between the peaks present in the InVia spectrum and the peaks present in the MOB spectrum (Figure 5.2.5). While the InVia data clearly shows the presence of both the calcite and naphthalene, the MOB data only shows the presence of the calcite. This may be explained by the background within the MOB spectrum masking the naphthalene. In the case of the most intense naphthalene peak, at 1380cm^{-1} , this seems unlikely to be the sole reason for the absence. The absence of this peak could be attributed to the weaker intensity due to instrument resolution and the difference in peak intensity ratios.

From this data it was clear that several issues arose. The ratio of organic to inorganic peaks differed based on the instruments used to obtain the spectrum. Additional peaks were present within the organic spectrum but not the InVia spectrum is visible within the MOB spectrum. The background and the resolution related to the MOB instrument additionally caused differences within the spectral features observed. To quantify and deduce the cause of these differences it is required that the differences are recorded

fits are not as accurate on the prototype instrument, as can be seen by the residual component in the InVia data being much smoother than in the prototype data.

		CN01		CN03	
		Prototype	Renishaw	Prototype	Renishaw
Fit parameters	Reduced χ^2	4.0384	0.6285	4.3644	0.2770
	Correlation R^2	0.9806	0.9979	0.9626	0.9982
Band / cm^{-1}					
282.5	Height	625.8	1983.8	260.7	2728.1
	Width	11.5	12.0	29.5	11.6
	Area	10138.8	33616.7	9431.2	44153.3
	Lorentz	0.8094	0.8094	0.5401	0.7718
709.5	Height	155.3	709.3	58.7	1189.5
	Width	15.7	7.1	19.1	6.6
	Area	3006.5	6218.5	1572.3	10018.9
	Lorentz	0.3396	0.3396	0.6893	0.4116
1081.6	Height	885.1	6459.4	270.5	10913.8
	Width	12.1	5.9	11.7	5.6
	Area	14815.8	42383.5	3375.1	69322.0
	Lorentz	0.7033	0.0966	0.0006	0.1424

		GT01				GT01	
		MOB	InVia			MOB	InVia
Fit parameters	Reduced χ^2	1.4251	0.8418		Reduced χ^2	1.4251	0.8418
	Correlation R^2	0.9749	0.9987		Correlation R^2	0.9749	0.9987
Band / cm^{-1}				Band / cm^{-1}			
414.2	Height	338.3	2153.0	664.0	Height	195.2	1186.0
	Width	12.6	10.7		Width	13.1	8.2
	Area	4534.4	24557.5		Area	3979.6	11574.4
	Lorentz	0	0		Lorentz	1	0.2425
493.3	Height	383.7	2196.1	1007.8	Height	976.1	23247.9
	Width	17.6	12.2		Width	23.7	7.0
	Area	7520.1	36615.7		Area	25730.0	214211.4
	Lorentz	0.1003	0.6185		Lorentz	0.1006	0.5020
612.0	Height	251.3	1163.7	1135.5	Height	478.3	3387.0
	Width	17.1	16.2		Width	16.2	12.9
	Area	6648.9	29237.0		Area	11406.0	65158.4
	Lorentz	1	1		Lorentz	1	1

Table 5.2.1. Peak fit data from the prototype and InVia instrument for the 1% and 10% calcite and naphthalene samples and 1% gypsum and trehalose sample.

From the peak fitted data (Table 5.2.1.) the prototype instrument had much weaker correlation than the InVia. The peak heights were much weaker on the prototype instrument and their relative intensities also varied significantly compared to the InVia. The Lorentz values were similar between instruments however the widths were different. This shows that the resolution of the prototype instrument was much worse than the InVia and therefore for samples with numerous peaks, such as trehalose, distinguishing of some peaks would be difficult.

From the data observed there are several differences between the two instruments. For comparable data analysis the cause of these differences must be identified. The correction methods appear to affect the resultant spectra produced for the prototype instrument. Therefore the correction methods need to be optimized and an instrumental background obtained which can be removed from all spectra. The instruments will need to be calibrated with several known standards to optimize positioning of bands across the whole spectrum. This can be achieved with more sample analysis and comparisons. The resolution and sensitivity must also be enhanced by increasing the signal-to-noise ratio observed by the instrument.

5.3. Conclusion

In this section the method for grid system of data acquisition could be applied to the MOB instrument was interrogated. Due to the limitations of the prototype instruments sample stage, the reproducibility and accuracy of the positioning became an issue. Therefore a slide cover and mask was developed. Using this mask, spectra could only be obtained through the hole in the slide and therefore the location would be exactly the same on all instruments. Spectra obtained between the different instruments were interpreted and similarities and differences were observed between the instruments.

Chapter 6

Exemplar systems

In this chapter the utility of Raman spectroscopy to provide comprehensive information for a range of astrobiological samples will be demonstrated. A range of exemplar materials were investigated which were derived from relevant interplanetary scenarios. Samples were investigated in increasing molecular complexity as a demonstration of the specificity of Raman spectroscopy in these contexts. Molecular biomarker systems were investigated using hopanoid, sterane and steroid systems. Geological specificity was investigated using Raman spectroscopy in the identification of unknown evaporite minerals. Cellular systems were analysed and the effect of irradiation upon these samples. The detection of bio-geological inclusions was also investigated and the impact of crushing and grinding samples upon detection.

6.1. Identification of mineralogical samples

Raman spectroscopy has a range of applications in astrobiology. It was originally implemented on board the ESA ExoMars rover due to its utility for identification of mineralogical content. This section looks at the specificity of Raman spectroscopy in the detection of geological samples. The samples used in this section are evaporite minerals from Lake Magadi, relevant to astrobiology due to their indication of water presence.

To demonstrate Raman spectroscopy's utility in the identification and confirmation of mineralogy an unknown sample, supplied by University College London, from Lake

Magadi in Kenya was investigated. The sample was believed to be a trona, a material commonly associated with the location from which the sample was sourced. Trona is the common name for trisodium hydrogencarbonate dihydrate, $\text{Na}_3\text{H}(\text{CO}_3)_2 \cdot 2\text{H}_2\text{O}$ and this compound is primarily located as a deposit on lake beds^[172]. The presence of trona indicates a source of water and liquid water is requirement for life. Trona is therefore an important material in the investigation of life on Mars. Raman spectroscopy was required to confirm whether or not this sample had been correctly identified.

For the purpose of this work the Raman spectrum of the unknown sample was compared against standards of trona, sodium bicarbonate (present with sodium carbonate in natron) and thermonatrite. Natron, like trona, also occurs in lake beds and is a mixture of both sodium carbonate and sodium bicarbonate. Thermonatrite forms when trona or natron are exposed to high temperatures^[172].

6.1.1. Standards

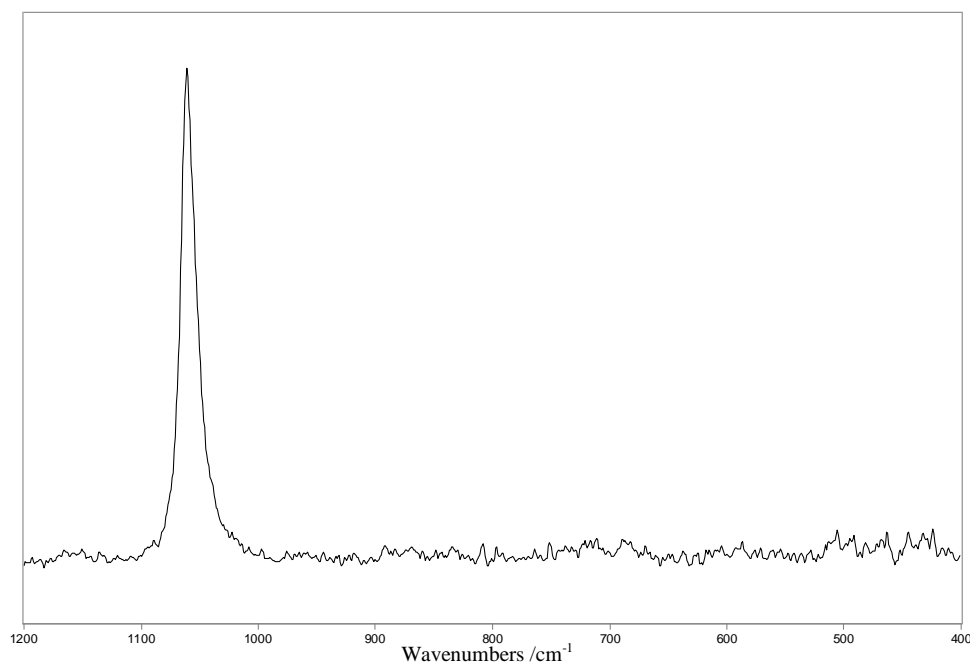


Figure 6.1.1. Raman spectrum of trona standard

The spectrum of trona (Figure 6.1.1) contains very few spectral features. Only a single peak occurs in the spectrum at 1061 cm^{-1} . No other features, such as backgrounds, are present and the signal to noise ratio of this peak is high enough that the noise has no potential to mask the peak.

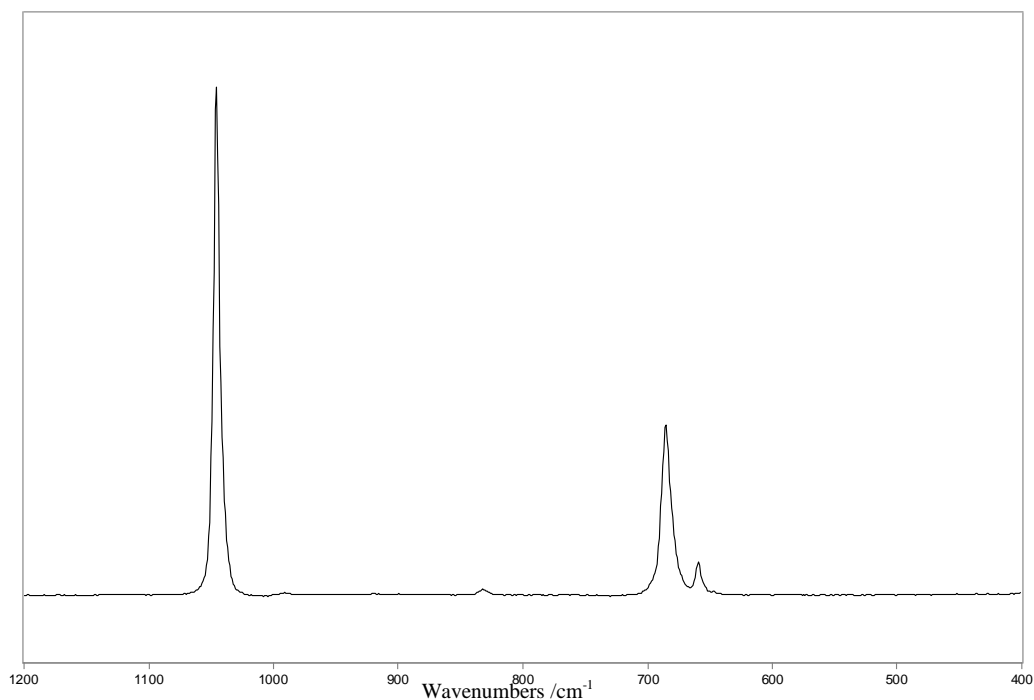


Figure 6.1.2. Standard sodium bicarbonate (NaHCO_3) Raman spectrum

The sodium bicarbonate spectrum (Figure 6.1.2.) also contains very few spectral features. The signal to noise ratio of this compound means that distinguishing peaks from the noise is possible and there is no background present within the spectrum. As with the trona, a single peak occurs, shifted slightly, to 1046 cm^{-1} and two additional peaks occur at 685 cm^{-1} and 659 cm^{-1} . This compound is easily distinguishable from trona due to the additional peaks and the shift in peak position.

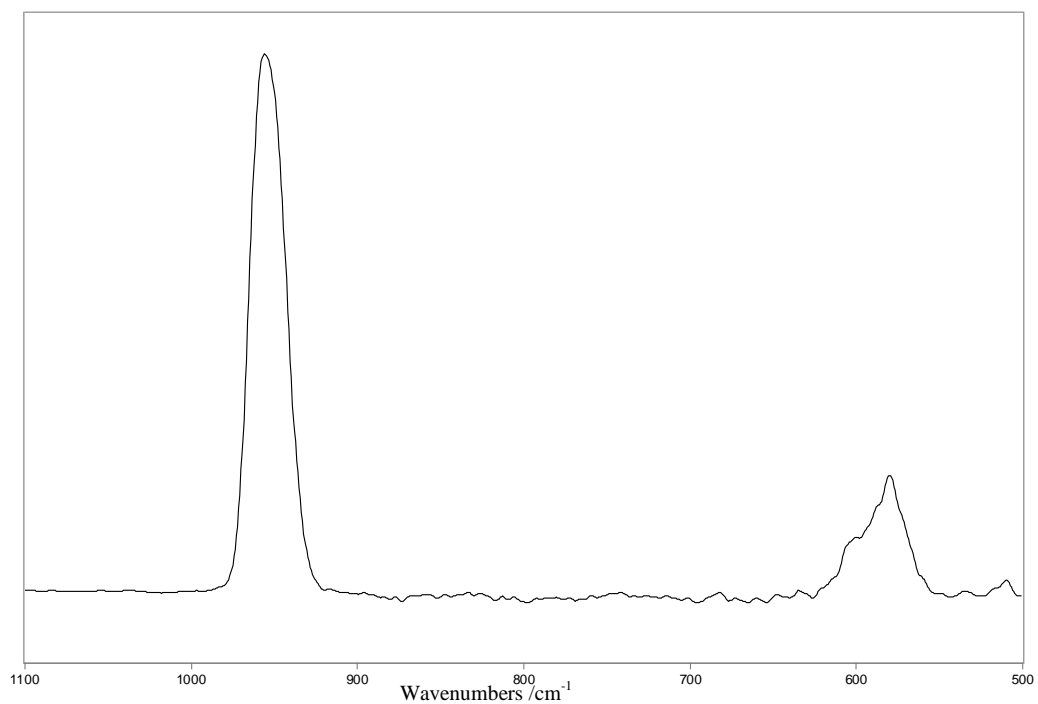


Figure 6.1.3. Standard thermonatrite (Na₂CO₃·H₂O) Raman spectrum

The spectrum of the thermonatrite (Figure 6.1.3.) contains a minor background and more noise than the previous spectra. As with the previous samples a single peak is present, occurring at 956 cm⁻¹ in this sample, additionally the peak is much broader. Two smaller peaks at lower wavenumbers overlap and occur at about 579 cm⁻¹ and 602 cm⁻¹. This sample is distinct from the spectrum of trona due to the shift in wavenumbers of the peaks, broadness of the peaks and minor peaks at lower wavenumbers.

6.1.2. Lake Magadi sample

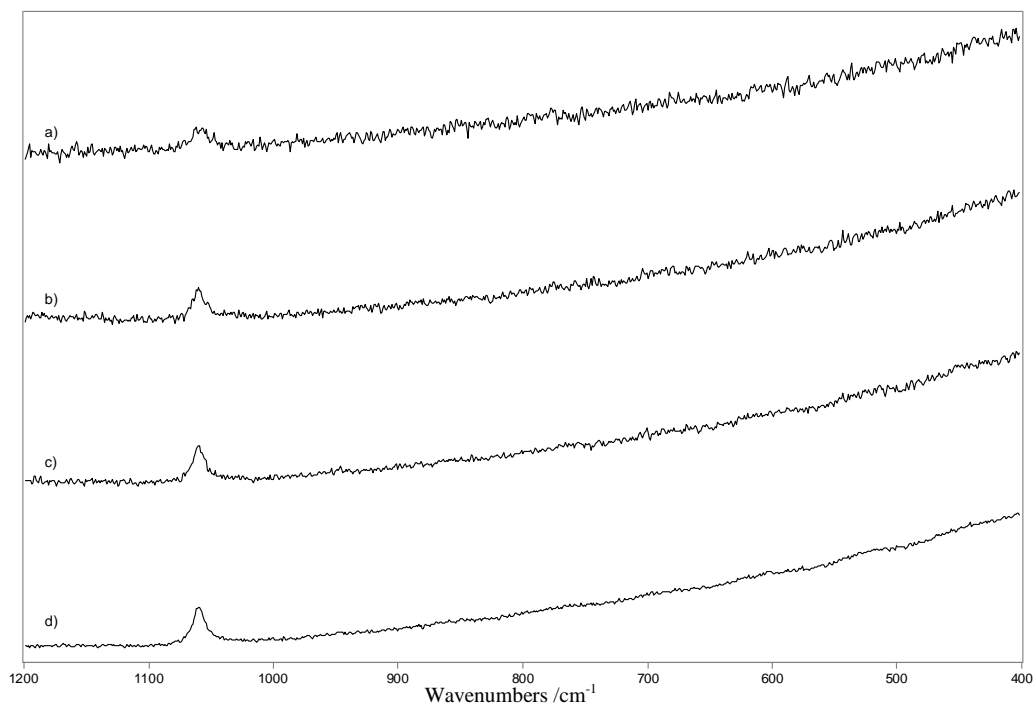


Figure 6.1.4. Raman spectra of proposed trona compound a) 1 accumulation 10% laser power, b) 1 accumulation 50% laser power, c) 1 accumulation 100% laser power, d) 10 accumulation 100% laser power

The spectrum of the unknown compound (Figure 6.1.4) produced a much larger background and a poorer signal to noise ratio. This background was likely derived from impurities within the sample due to its natural origin. The unknown sample featured only one peak and therefore could not have been thermonatrite and sodium bicarbonate. The single peak indicates that the unknown may be trona.

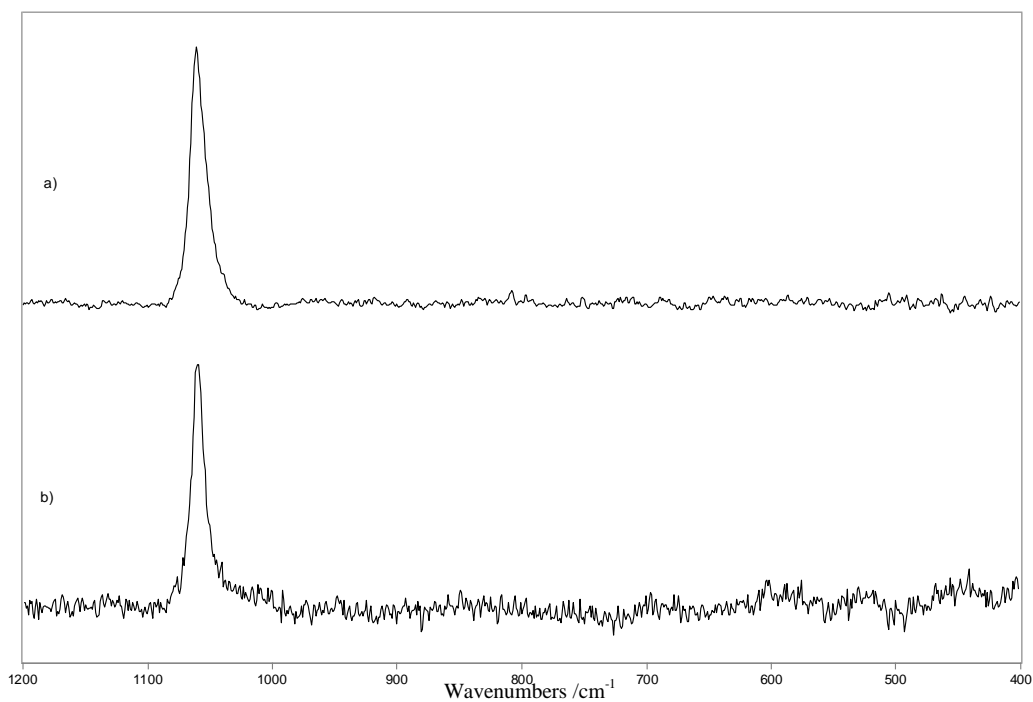


Figure 6.1.5. Raman spectra of a) standard trona, and b) suspected trona sample

Figure 6.1.5 shows a comparison of the unknown sample and the trona standard. In both spectra only one peak occurs at 1061cm^{-1} . Therefore the unknown is likely to be trona. Differences with the signal-to-noise ratios can be identified as deriving from the impurities in the natural sample compared to the standard spectrum.

6.2. Raman analysis of potential life biomarkers

On Earth there are several Mars analogue sites from which life can be studied and one such site is in the McMurdo Dry Valleys in Antarctica^[173]. Raman spectroscopy has been used at these sites to produce many biomarker signatures which may be used for comparison with samples from Mars. In these cold deserts endolithic communities have been found which contain biomarker molecules which may be used in the identification of extinct life on Mars^[174,175]. There have been numerous studies of biomarkers of relevance to ExoMars^[86,90-92,94,96,99,101,103,104,110,114,140,146,174-178]. However there has been very little investigation of steranes, sterols and hopanoids using Raman spectroscopy. Therefore this work looks at these samples using Raman spectroscopy to analyse these biomarkers.

Previous research has primarily focused on cyanobacteria, lichens and algae which are capable of surviving extreme conditions^[101]. For survival in these environments UV and photosynthetic protective pigments are often present in the form of; chlorophyll (photosynthesis), β -carotene (radiation damage repair) and scytonemin (UV protection). These compounds are essential biomarkers for proof of extant or extinct life^[137,179] and have all been analysed by Raman spectroscopy.

A list of 63 potential biomarkers was produced in 2007 based on Earth fossils and meteorite records^[96]. Using this list, four biomolecules of interest were identified to share the same polycyclic structure. These biomolecules are; ABC tricyclic terpane, gammacerane, steranes and hopanes. Due to the high stability of this structure these compounds are all important Mars relevant biomarkers.

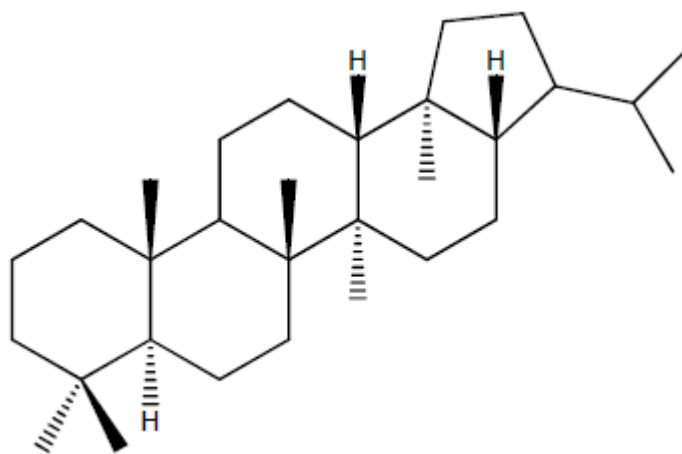


Figure 6.2.1. Chemical structure of hopane

Hopanoids are pentacyclic organic molecules which aid bacteria in their adaption to extreme environments. They are found within cell membranes and primarily function to control cell membrane permeability. Hopanoids are based on the chemical structure of hopanes which can be seen in figure 6.2.1. Hopanes have been detected in ancient fossils which indicate that even before the atmosphere became oxidising, oxygenic photosynthesis had evolved^[176]. The presence of these hopanoids within fossils demonstrates that they are among the most stable of the organic biomarkers. They have also shown strong persistence and chemical stability within rocks and shales where microbial remains are fossilised^[114]. Hopanoids have also been detected within prokaryote organisms^[180]. For these reasons these molecules are classified as high priority targets in the search for Martian life.

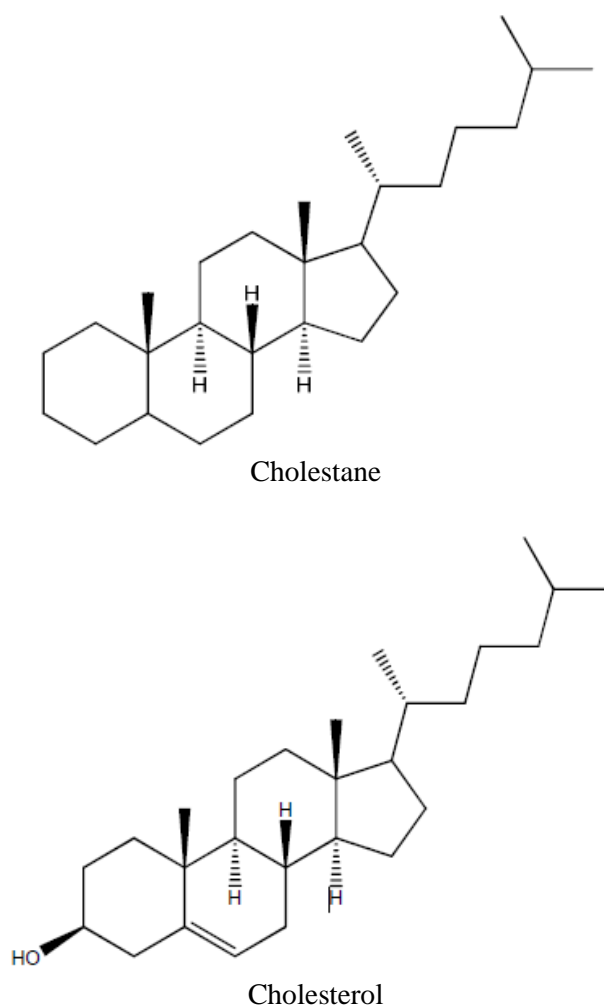


Figure 6.2.2. Chemical structures of cholestane and cholesterol

Steroid alcohols, sterols, occur naturally within animals, plants and fungi and are tetracyclic organic molecules. The structure of cholesterol and its reduction product cholestane can be seen in figure 6.2.2. Sterols aid in the control of cell membrane fluidity, however it is only a small number of bacteria found in eukaryote organisms undertaken this process^[181,182]. Both steranes and sterols are geologically stable^[183]. However sterols, unlike hopanoids, require the presence of oxygen for synthesis. For this reason they are a lower priority for detection than the hopanoids due to the lack of oxygen present on Mars^[89,96].

In this work the degradation products of biological origin are detected using Raman spectroscopy. Sterols, steranes and hopanoids were interrogated with Raman spectroscopy to assess the ability to differentiate the compounds based on structural differences. The limits of detection of these compounds are also established.

6.2.1. Standards

Raman spectra of the four powder samples were obtained at 1% laser power for 30 acquisitions. The spectra were baseline corrected using multiple points due to the presence of a large background emission. Due to fluorescence emission from the samples, the spectra obtained were subjected to baseline correction to ensure all the samples were clear and comparable at the different concentrations. The spectra obtained of the standards can be seen in figure 6.2.3.

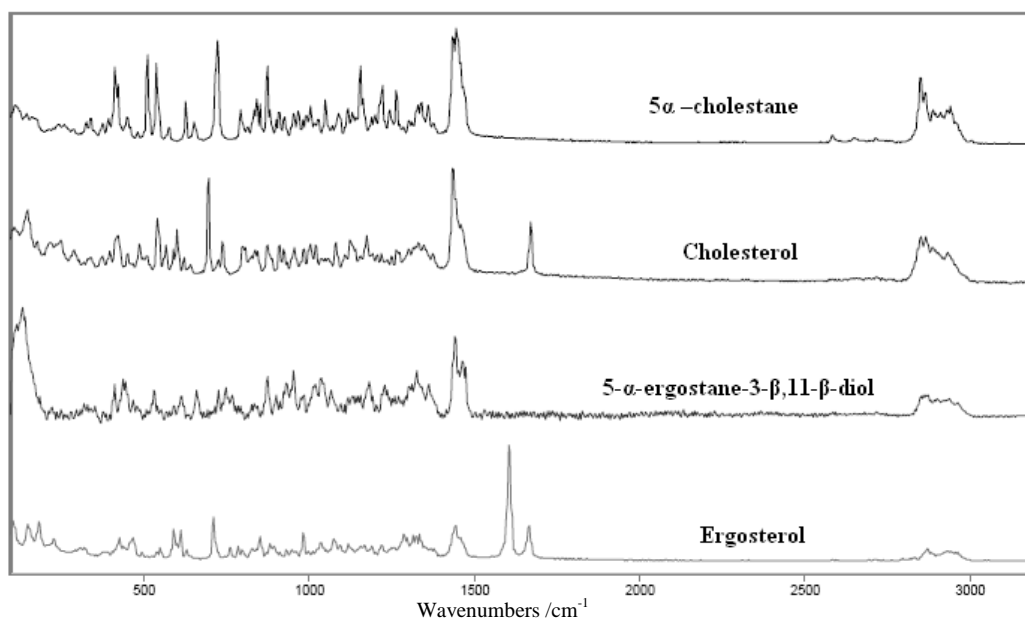


Figure 6.2.3 Raman spectrum of standards

In the spectra several Raman bands are common to multiple samples due to their structural similarities. The bands and assignments can all be seen in table 6.2.1. Similar peaks were observed between 2960 cm^{-1} and 2840 cm^{-1} , assigned as cyclic CH_2 stretching, 1445 cm^{-1} and 1430 cm^{-1} , assigned as cyclic CH_2 scissoring vibrations, 730 cm^{-1} and 700 cm^{-1} , assigned as aliphatic CH_2 vibrations, and 540 cm^{-1} and 525 cm^{-1} , assigned as cyclohexane/cyclopentane ring vibration.

Cholesterol	5-cholestane	Ergosterol	5- α -ergostane-3- β ,11- β -diol	Assignment
2933	2935	2931	2935	cyclic CH_2 stretching
2868	2864	2872	2870	cyclic CH_2 stretching
2851	2851			cyclic CH_2 stretching
1671		1668		conjugated C=C
		1606		C=C
1446	1445	1445	1444	cyclic CH_2 scissoring vibrations
1437	1437	1439	1440	cyclic CH_2 scissoring vibrations
	875		876	
541	539	539	535	ring vibration

Table 6.2.1 Raman peak positions and assignments for standards.

To distinguish between compounds several peaks were identified. For the sterane samples a peak at 875 cm^{-1} can clearly be seen. The conjugated C=C at 1670 cm^{-1} is unique to the sterols. In ergosterol a diagnostic peak occurs at 1606 cm^{-1} , assigned to C=C. Due to these peaks being unique to these compounds they can be used to easily distinguish and discriminate between these compounds.

6.2.2. Analysis of powder mixtures

Raman spectroscopy was used to analyse 13 mixed samples of ergosterol and cholestane of; 0, 1, 2, 5, 10, 25, 50, 75, 90, 95, 98, 99 and 100% w/w. Spectra were obtained at five different locations within the sample each 200 μm from the last

location. In this work the x5 objective was used to reduce homogeneity issues discussed in previous chapters. Figure 6.2.4 shows the spectra obtained for the samples and the spectra obtained appear to show a linear relationship between peak intensities and concentration of the samples.

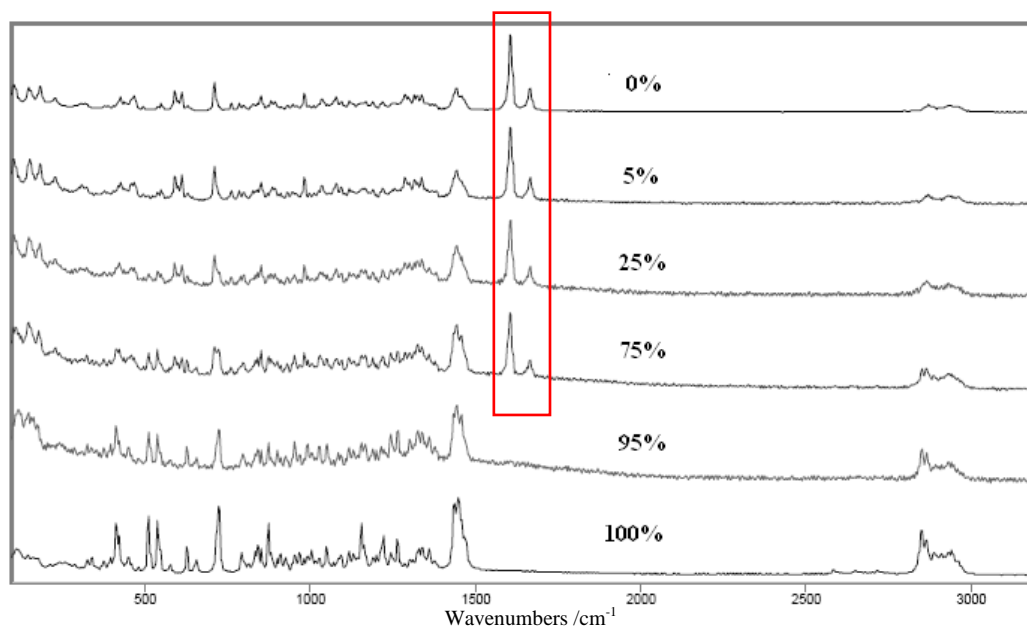


Figure 6.2.4. Raman spectra of ergosterol and cholestane mixtures

6.2.3. Analysis of hopanoids

Ergosterol was dissolved in dichloromethane to produce a solution to allow for sample analysis at varying concentrations without issues arising due to homogeneity.

Dichloromethane was chosen as a solvent due to its Raman spectrum only featuring two intense peaks at 699 cm^{-1} and 281 cm^{-1} which did not interfere with peaks from the ergosterol spectrum. Figure 6.2.5 shows the spectra obtained for ten solutions.

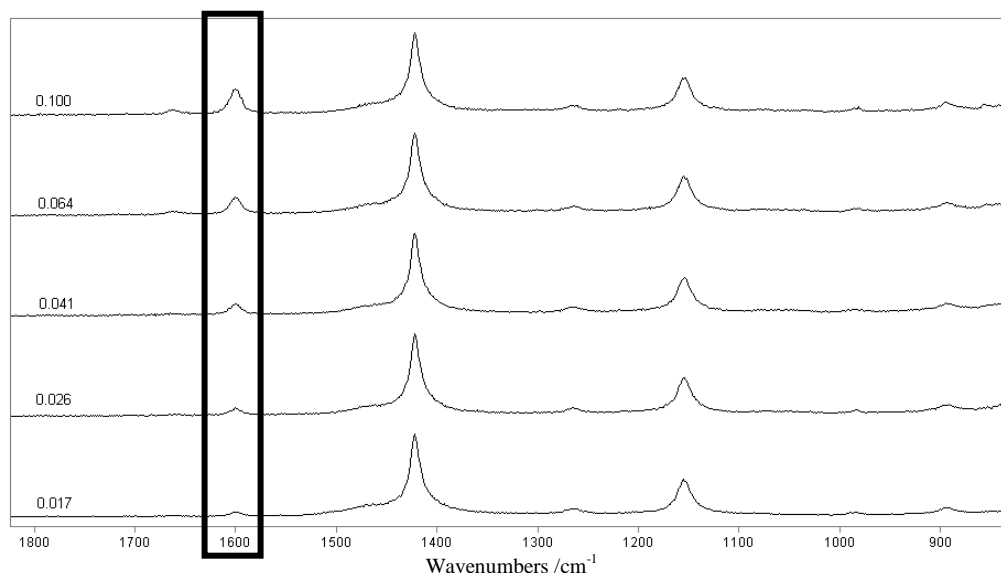


Figure 6.2.5. Spectra of liquid samples in concentration(mol/dm^3)

Using the previously defined peak positions in table 6.2.1 it is clear than in these samples only one peak is distinguishable; the C=C vibration at $\sim 1600 \text{ cm}^{-1}$. This peak shows a similar linear relationship to the peak intensity and concentration. Due to the noise within the spectrum, derived from the solvent spectrum, a limit of detection of $0.015 \text{ mol}/\text{dm}^3$ was obtained for these samples.

6.2.4. Conclusions

In this work clearly identifiable features within the Raman spectra of steranes and sterols were observed. The ability to distinguish between different types of steranes and sterols was also deduced with sample such as ergosterol, a peak indicative of the compound was visible at 1670 cm^{-1} (conjugated C=C bonds). The investigation of limits of detection using powder sample mixtures demonstrated the importance of homogeneity within mixed samples. The liquid samples of ergosterol mixtures resolved this issue and this can clearly be seen in the results produced for these solutions. While the intensity produced from the solvent bands in the spectrum dwarfed the signal from

the ergosterol, its presence was still detectible. Magnification of the relevant area in the spectrum allowed for clear identification of these peaks.

6.3. Effects of irradiation on bacterial species

The previous sections have all looked for signs of life using biomarkers. Biomarkers often show indications of life which had existed but is no-longer possible. It is possible that life may still exist on Mars in the form of extremophiles. These are bacteria which are highly durable and are far more resistant to extremes of environments such as those with high radiation levels similar to that of the Martian surface. This section looks at these extremeophiles on the cellular level.

The effect of radiation on different bacterial species and the changes in Raman spectra produced are investigated in this section. For this work, bacterial samples within culture and freeze dried cells, both irradiated and unirradiated. Table 6.3.1 shows the bacteria used and their amounts.

Bacterial strain	Label	Cell density in liquid culture	Mass of lyophilized powder
E.coli	EC	9×10^9 cells/ml	0.138 g
Deinococcus radiodurans	DR	3×10^7 cells/ml	0.102 g
Brevundimonas sp. MV.7	MV.7	3×10^8 cells/ml	0.053 g
Rhodococcus sp. MV.10	MV.10	9×10^6 cells/ml	--
Synechocystis sp. PCC6803 (cyanobacterium)	cyano	2×10^7 cells/ml	0.045 g

Table 6.3.1. Bacterial samples irradiated and their quantities.

E. Coli is a non-pigmented organism which is not defined as an extremeophile as it cannot withstand extreme environments. It was used in this investigation as a control sample. D. radiodurans is the most radiation-resistant organism currently known. It has a bright pink pigment which helps it to block ultraviolet radiation. Both Brevunidmonas and Rhodococcus are two strains isolated from the dry mineral soil of the Miers Valley in Antarctica. They both grow optimally in low temperature environments and are

pigmented orange and white respectively. Synechocystis is a cyanobacterium and so coloured a bright green due to the chlorophyll present.

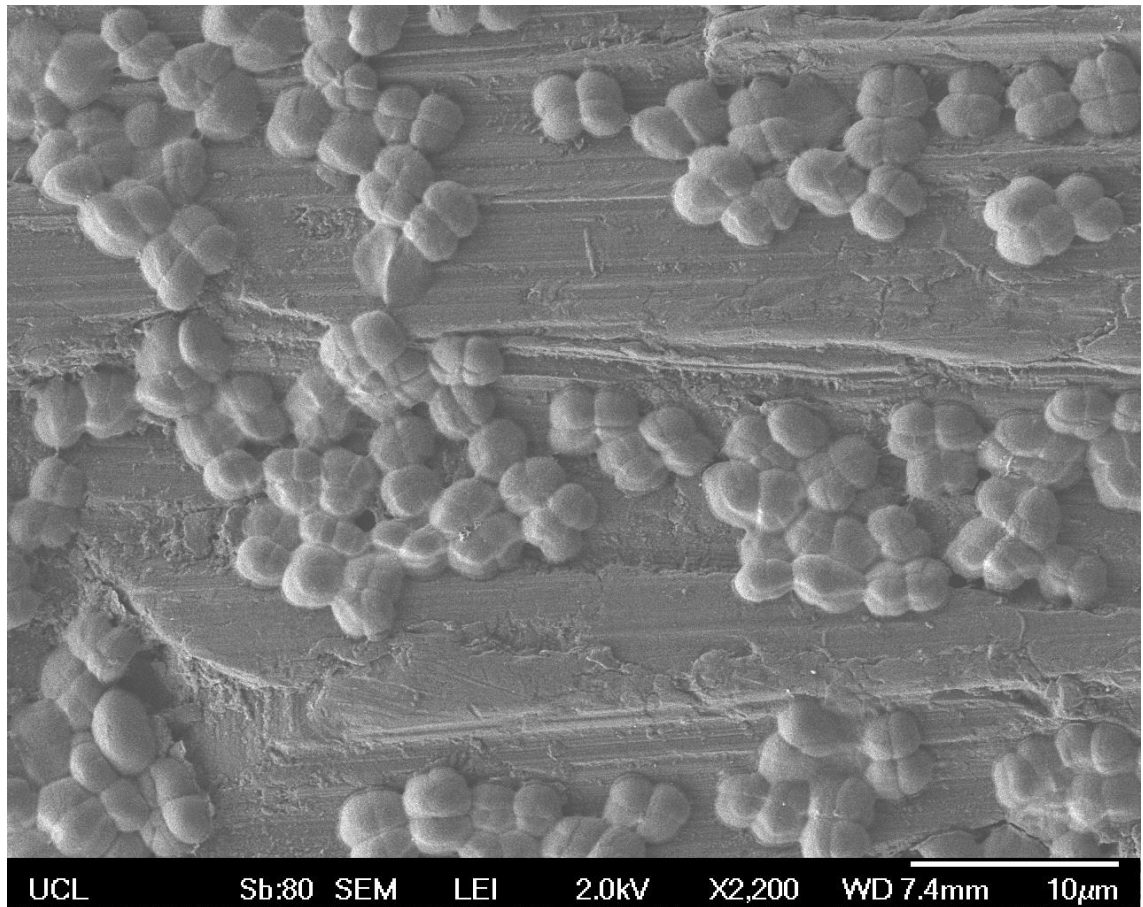


Figure 6.3.1. SEM image of Deinococcus cells on thin metal film

The Deinococcus cells were additionally proton-irradiated as a thin smear on an aluminium slide. Figure 6.3.1 shows an SEM image of the slide with the cells only having a thickness of 1-2 cells. The cells can be seen to cluster together with about 2 microns in diameter and a thickness approximately 5 microns.

6.3.1. Freeze dried

The freeze dried samples identified as EC, DR, MV7 and Cyano were analysed using Raman spectroscopy. Both the InVia spectrometer and Bruker IFS66/FRA 106 FT-Raman spectrometer were used to give spectra at a range of different wavelengths.

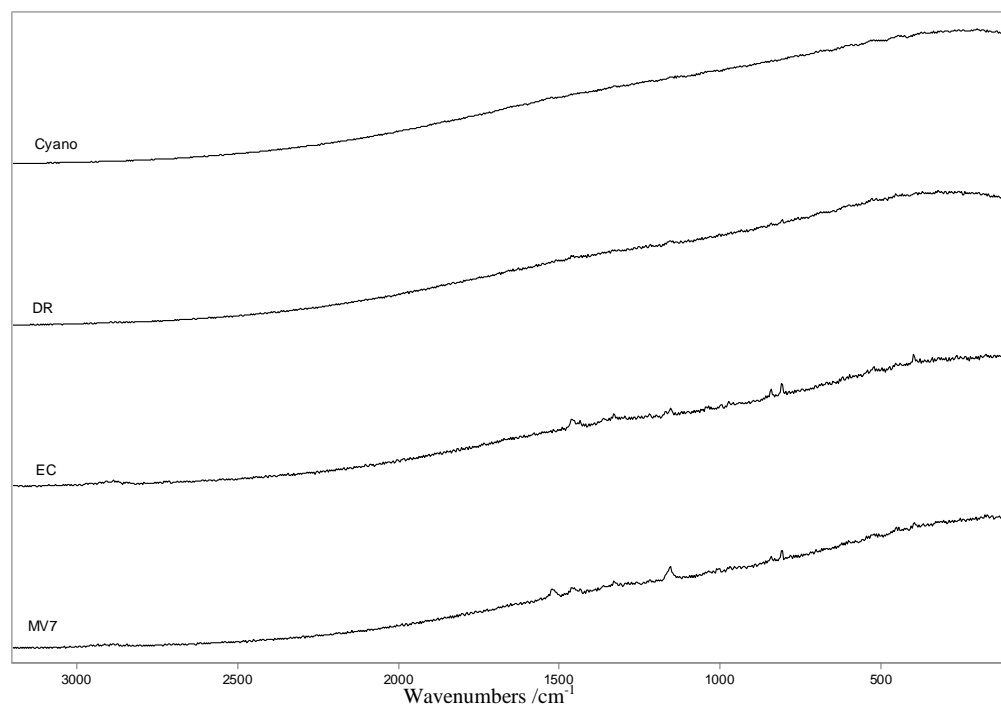


Figure 6.3.2. InVia spectra of solid freeze dried samples

The samples all produced a large background which masked the majority of signal present. This background could be attributed to the fluorescence of the samples and possible heating due to organic nature of the samples. Some features were present within the MV7 and EC spectra.

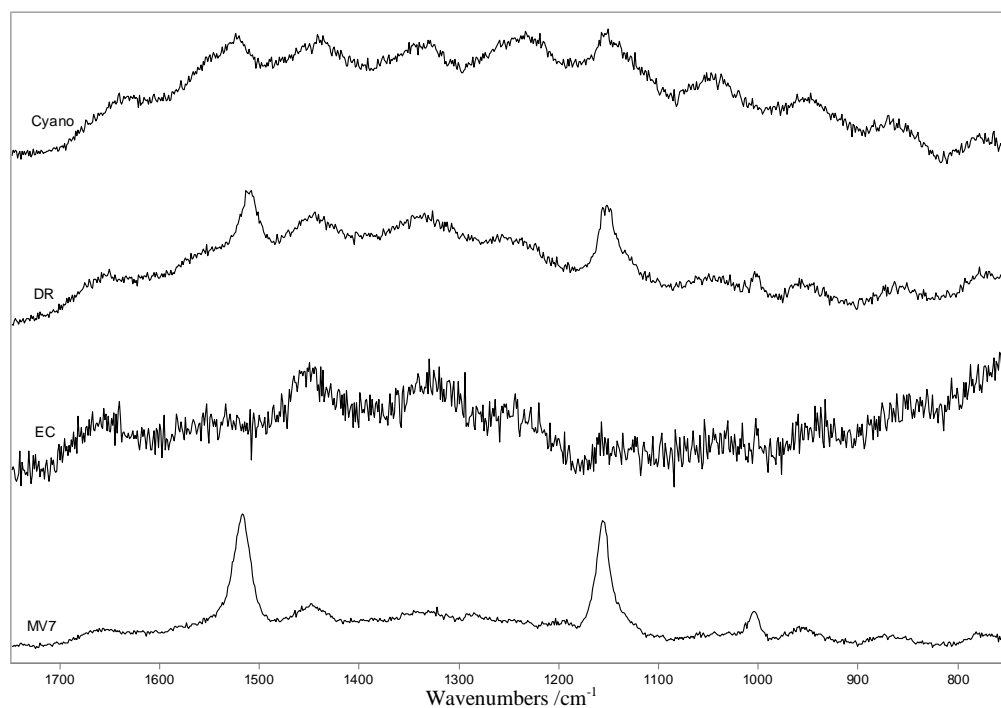


Figure 6.3.3. InVia spectra of solid freeze dried samples. (Background corrected)

Figure 6.3.3 shows the spectra of the dried samples baseline corrected over a smaller spectral range. While several features may be present within the samples are caused by the noise and baseline correction. However the two peaks at 1525 cm^{-1} and 1155 cm^{-1} present in DR and MV7 can be attributed to the samples. In the literature it has previously been established that β -Carotene also has vibrational bands at 1524 cm^{-1} and 1155 cm^{-1} therefore the visible peaks present can be attributed to the presence of carotenoids^[138].

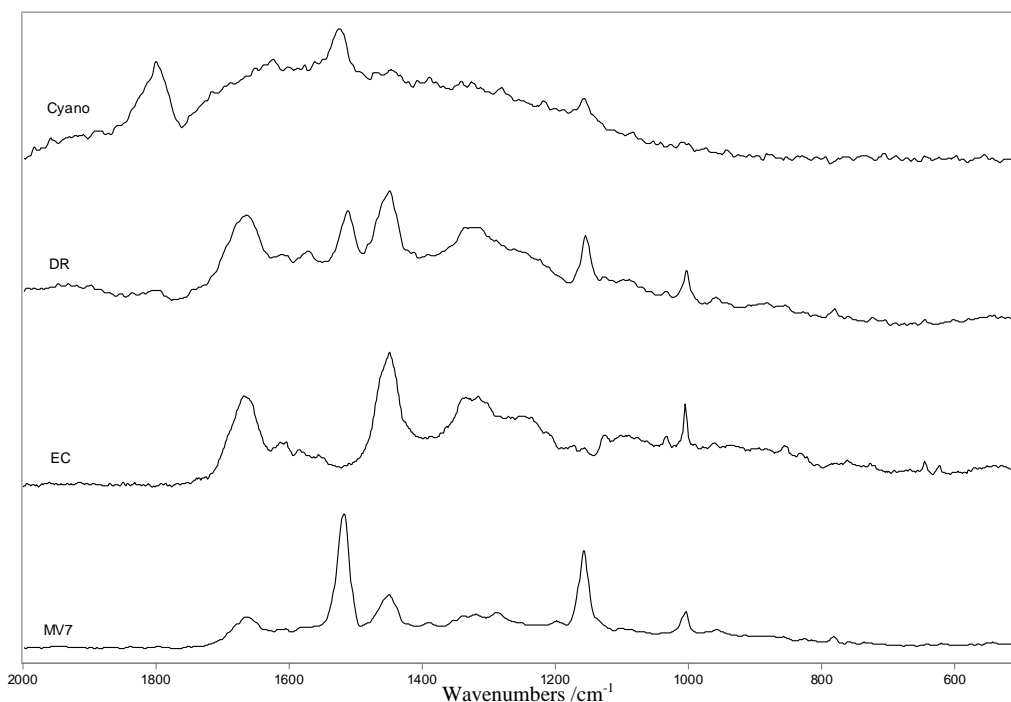


Figure 6.3.4. Bruker IFS66/FRA 106 FT-Raman spectra of solid freeze dried samples.

Using the 1064 nm laser removes the majority of the background features (Figure 6.3.4.). All samples display multiple peaks, several of which appear in multiple samples and some which are unique to individual species. The vibrational bands for the different samples can be seen in table 6.3.2.

Sample	Vibrational bands (cm ⁻¹)				
	a	b	c	d	e
Cyano		1525		1157	
DR	1667	1523	1449	1154	1002
EC	1665		1448		1003
MV7	1663	1521	1452	1160	1003

Table 6.3.2. Table detailing the peaks present in the Raman spectrum for the samples; cyano, DR, EC and MV7.

The Cyano spectrum has 3 distinct peaks, DR has 5, EC has 3 peaks and MV7 spectrum contains 5 peaks. The broad bands in column a can be attributed to ~ 1659 cm⁻¹ $\nu(\text{CO})$ Amide i and unsaturated lipids^[184,185]. From the previous observations of the spectra of DR and MV7 the signals in columns b, ~ 1524 cm⁻¹ $\nu(\text{C}=\text{C})$ Carotenoid, and d, ~ 1155 cm⁻¹ $\nu(\text{C}-\text{C})$ Carotenoid, can both be attributed to carotenoids^[138,184]. The bands seen in

column c can be attributed C-H₂ deformation while the sharp band in column e, at 1003 cm⁻¹, can be assigned to phenylalanine^[185].

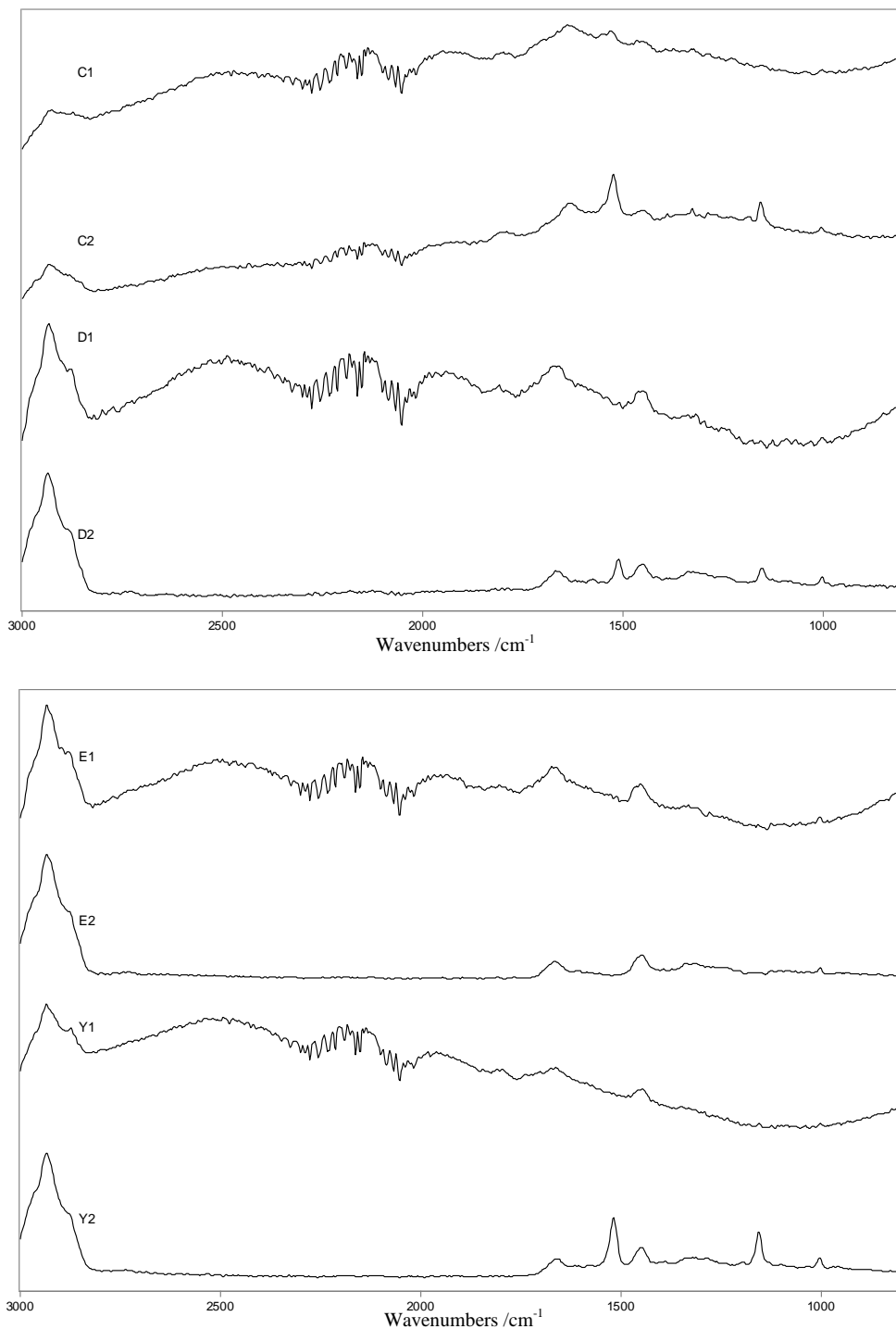


Figure 6.3.5. Bruker IFS66/FRA 106 FT-Raman spectra of freeze dried solid samples irradiated (1) and unirradiated (2) of Cyano (C), DR (D), EC (E) and MV 7 (Y).

Figure 6.3.5 shows the Raman spectra of the solid samples irradiated and non-irradiated. It is clear from the spectra that irradiation of the samples degrades the structure of all the species. The majority of all peaks present in the unirradiated sample are not present once irradiated due to an increase in noise, background and reduction of signal. Where vibrational bands are visible, they occur at 1524 cm^{-1} and 1155 cm^{-1} and therefore are likely to be derived from the carotenoids previously identified

6.3.2. Cells in culture

The live culture samples identified as EC, DR, MV7, MV10 and Cyano were analysed using Raman spectroscopy. Both the InVia spectrometer and Bruker IFS66/FRA 106 FT-Raman spectrometer were used to give spectra at a range of different wavelengths.

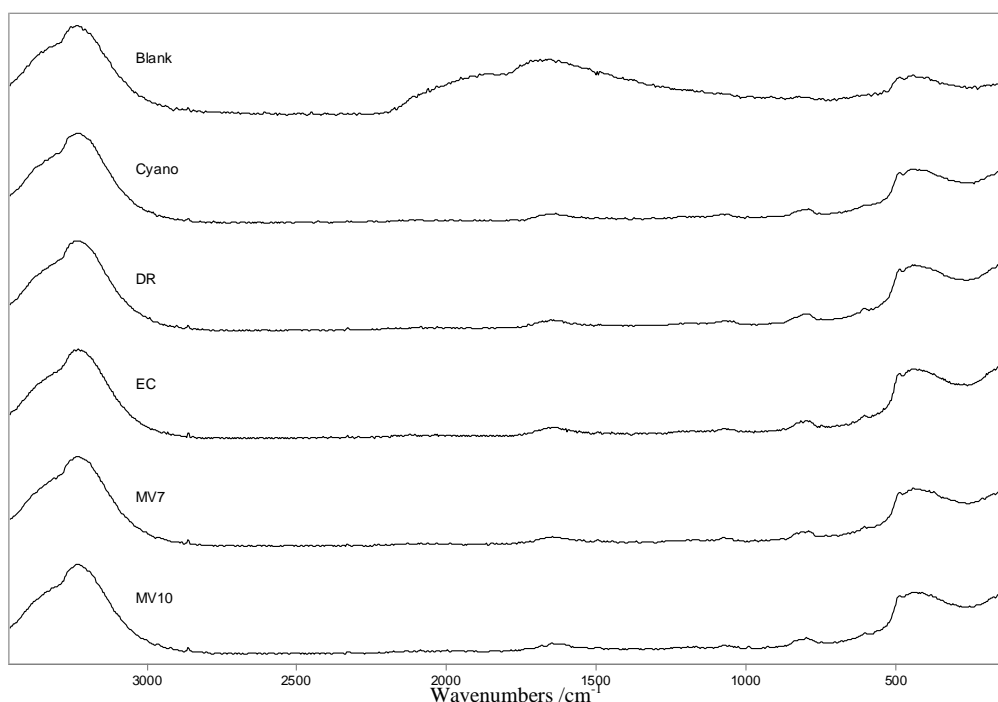


Figure 6.3.6. Bruker IFS66/FRA 106 FT-Raman spectra of cultures

From the Bruker FT-Raman spectra there were no spectral features present at 1064 nm for any samples (Figure 6.3.6). The resultant spectrum could primarily be attributed to

the presence of water, which gives a very weak signal. Therefore it is likely that the cultures had concentrations too low for analysis with Raman spectroscopy.

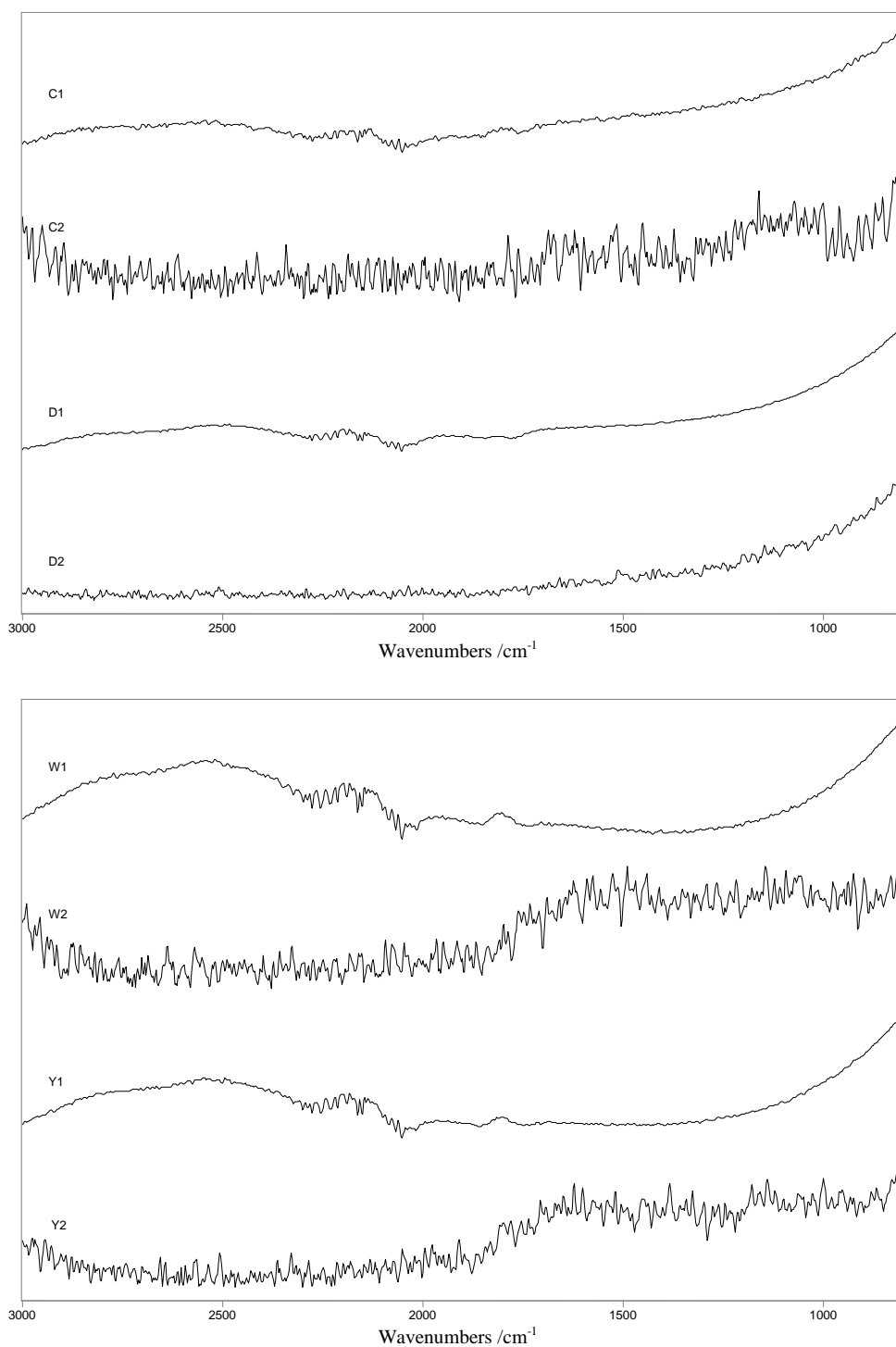


Figure 6.3.7. Bruker IFS66/FRA 106 FT-Raman spectra of bacterial cultures irradiated (1) and unirradiated (2) of Cyano (C), DR (D), MV 10 (W) and MV 7 (Y).

Irradiation of the samples produces a similar background to that observed with the solid samples (Figure 6.3.7.). However the sample signal is too weak to see any spectral features. Therefore identification of the degradation of the sample is not possible. The change in spectral features seen within the Raman spectra however could have been derived from the reduction in pigmentation of the samples after irradiation.

6.3.3. Cells grown on a metal slide

The proton-irradiated slide of *Deinococcus radiodurans* was also analysed using the InVia Raman instrument. This instrument allowed much easier analysis of the sample due to its microscope attachment and motorized stage. Due to the Bruker IFS66/FRA 106 FT-Raman instruments lack of either of these features it was not possible to obtain spectra of the samples. This was due to the size of the focal spot in relation to the cell distribution and thickness of the bacteria. The optimal conditions for obtaining Raman spectra of these samples using the InVia spectrometer was found to be 10s exposure, 1 accumulation, 100% laser power, x20 objective and at 633nm laser wavelength.

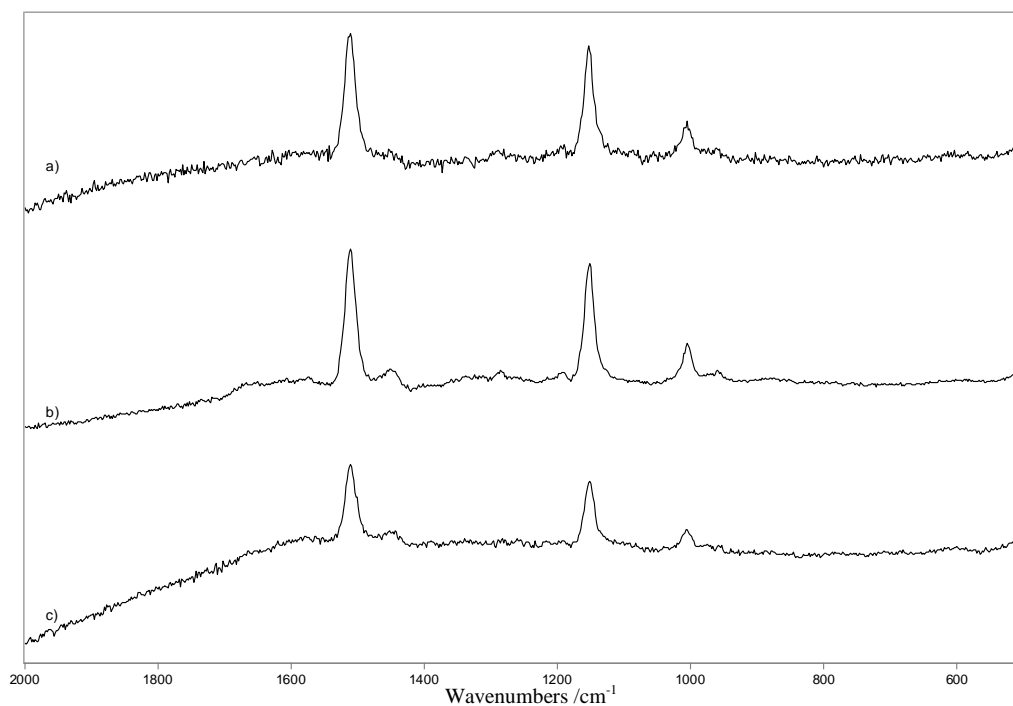


Figure 6.3.8. Spectra of slide obtained from unirradiated edge of sample at a) x5 b) x20 and c) x50.

Figure 6.3.8 shows the spectra obtained from the same location using different magnifications. The carotenoids can clearly be seen within the spectrum. From these spectra it is clear that optimal magnification is x20 due to the reduction in background and increase in peak intensities. In this sample it is likely that increasing the area to x5 increased the amount of background obtained in addition to the extra cells analysed. As seen with SEM, the cells were clumped together rather than distributed evenly; therefore the larger spot size is looking at more regions devoid of cells than regions with cells. The increased background seen with the x50 objective can be attributed to the increase in power over a smaller area. This increase in power has the potential to eliminate the background of the sample as well as the signal intensity and due to the higher localised power, the sample has greater potential for both heating and degradation.

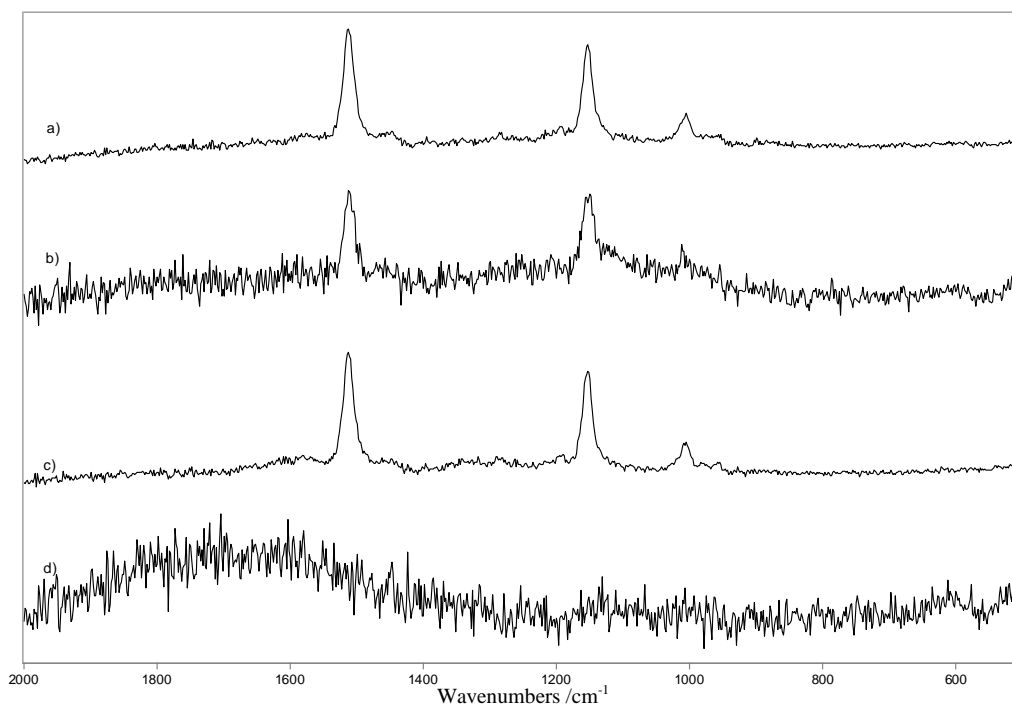


Figure 6.3.9. Spectra of slide from a) Unirradiated sample edge, b) Irradiated region, c) Unirradiated sample centre and d) Blank slide.

For these samples the blank clearly showed no spectral features which would affect identification of the bacteria. The edge of the sample and centre were both analysed due to differences in cell concentrations in these areas. These differences can be seen in the peak intensities but have a very limited effect and present no problems to identification of the samples. The irradiated region of the sample showed a similar result seen in the previous samples; the signal-to-noise ratio decrease and the background was increased. These changes, however, may potentially be derived from the differences in cell distribution at the irradiated region compared to other regions

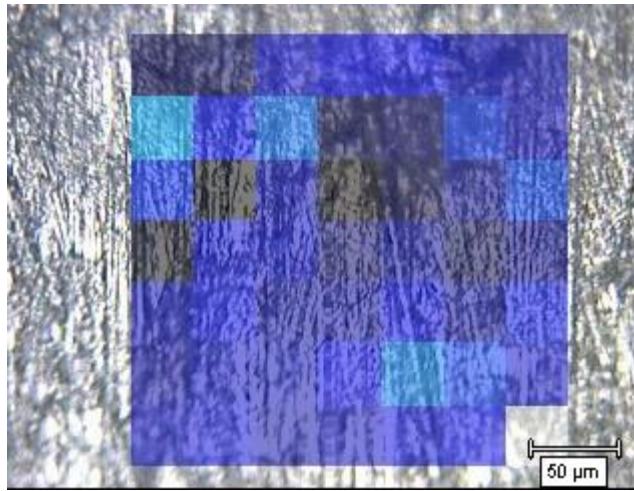


Figure 6.3.10. Spectral map of sample slide using x20 objective.

To investigate the differences in sample distribution across the slide and how this affects the Raman spectrum a map was created over a region of the slide. From the map produced it can be seen that some regions have weaker Raman intensities compared to others. These may be derived from the distribution of cells at these locations or the thickness of the cells.

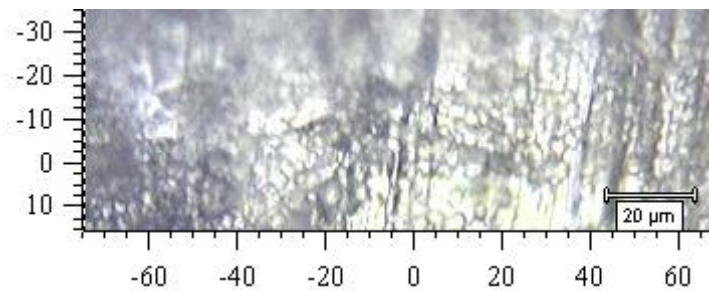


Figure 6.3.11. Image of the cells on the slide at x50 magnification.

Figure 6.3.11 shows an example of the cells in a region mapped under x50 magnification. From this image very few voids where no cells are present can be observed. Therefore the variations within the Raman spectrum at different locations are not due to these isolated clumps. The differences observed with the mapping must therefore be due to differences in the thickness of cell distribution across the slide.

6.4. Detection of life in extreme environments

In section 6.3, Raman spectroscopy was used to investigate extremeophiles on the cellular level. On the ExoMars rover however extremeophiles and biomarkers will be investigated *in situ*. Therefore for samples to be comparable, these biological materials must be investigated in a similar environment. This section looks at the ability of Raman spectroscopy to detect inclusions of cyanobacteria within geological materials. The samples used within this section have previously been investigated by Vitek *et al*^[186] and therefore are already well characterised. The bio-geological inclusions are ground to form a powder, as will occur using the ExoMars rover drill, and investigated a second time using Raman spectroscopy.

An analogue to looking for life on Mars is found in looking at extremophilic life in Antarctic cold deserts and the Atacama Desert in Chile. Work on this has primarily been based on cyanobacteria, lichens and algae which can survive in hostile environments such as those on Mars. Such life would require certain photosynthetic and UV-protective pigments such as scytonemin, chlorophyll and β -carotene. These chemicals are all considered essential biomarkers for proof of existing, extant or extinct life and have been analysed using Raman spectroscopy^[174,179,187-189]. The Atacama Desert is one of the driest places on Earth. Therefore for life to exist in such a place, such an organism would have to show extreme endurance and the ability to survive in completely inhospitable environments for normal organisms. If life exists in such a place like this then it is this type of life that could be found on Mars.

6.4.1. Inclusions

Samples were supplied by the Centre of Environmental Sciences, CSIC, Spain from the Yungay region of the Atacama Desert; therefore the samples are from one of the driest places on Earth. The rocks primarily consist of halite rock and are believed to contain endoevaporitic colonization. They feature characteristic endolithic patterns of colonization only a few millimetres below the surface.



Figure 6.4.1 Image of the sample Yungay_03 with locations analysed identified

Figure 6.4.1 shows a picture of Yungay_03 with the different regions marked. Region 1 is shown as the blue circle, region 2 as the green circle and region 3 was obtained from the yellow circle. A fourth location; region 4, was obtained from the colonization band at region 2 on the reverse on the sample. Beneath the white dense zone, region 1, a dark band indicating a colonization zone can be seen, region 2. With a stereoscopic microscope it is possible to identify the small dark spots corresponding to microorganism aggregates. Region 3 is the bedrock of the sample. In region 4, where the colonization zone is touching the surface, a dark band can be observed on the rock.

Raman spectra were obtained from the sample Yungay_03 at the four different locations. Laser power was kept at 10% to prevent degradation of the samples. After collection of the data, the background of the samples was removed to allow

identification of the peaks. Mapping was performed on the Yungay_03 sample over the region of colonization labelled region 2.

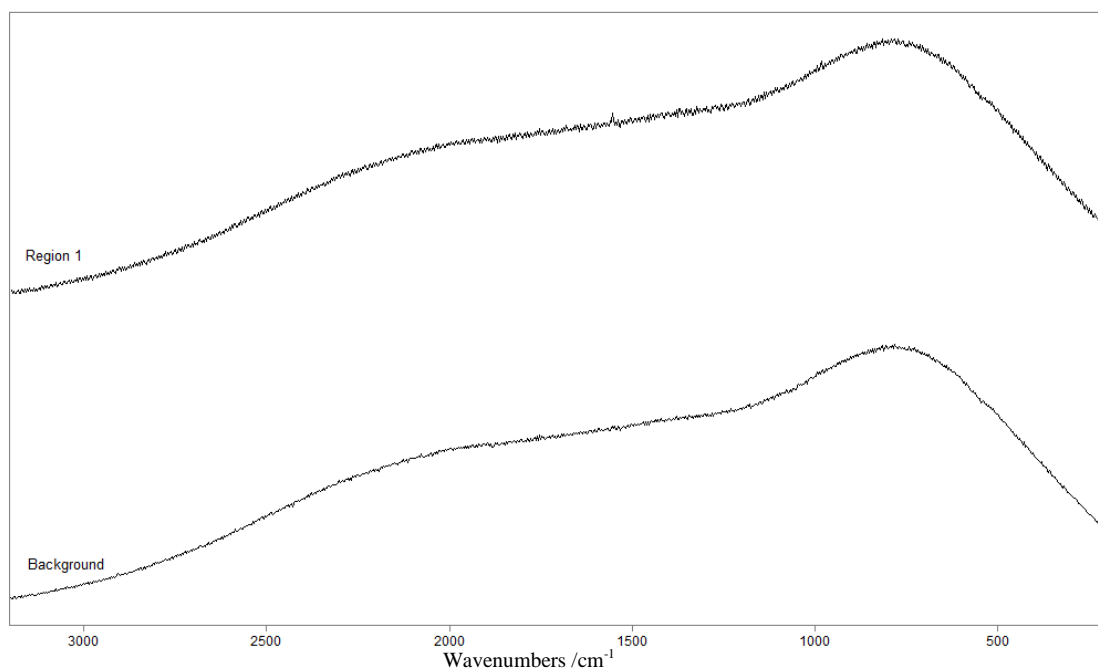


Figure 6.4.2. Raman spectrum of the halite rock background

Figure 6.4.2 shows the spectrum obtained of region 1 and the background obtained from the spectrum. The halites and silicates do not produce any distinguishable bands in the spectrum when analysed with Raman spectroscopy. The spectra contain only large background features and therefore in all the spectra obtained a large background was present. The background was removed using baseline subtraction and the resultant spectra can be seen in Figure 6.4.3.

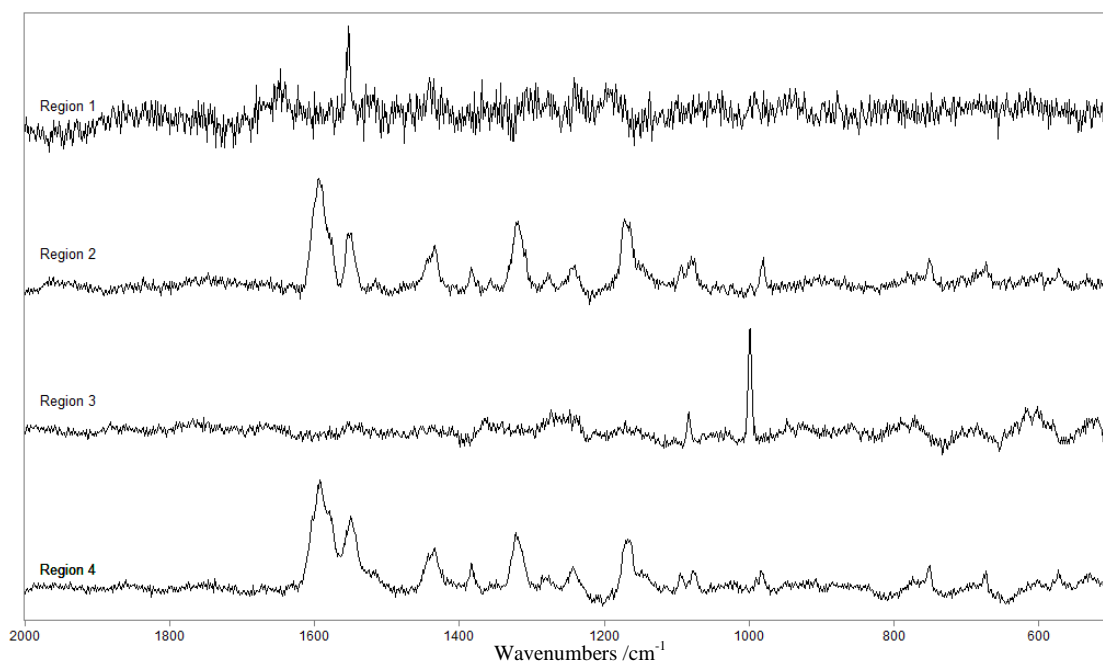


Figure 6.4.3. Raman spectrum of the regions on the sample Yungay_03

The spectra obtained of sample Yungay_03 at the four different regions clearly show differences in the Raman spectrum (Figure 6.4.3.). The spectrum of region 1 showed no identifiable signals, while two peaks are present they can be attributed to instrument artifacts and have a very low signal-to-noise ratio. In region 1 the spectrum is derived from the geological matrix itself. Region 2 was identified as a band of a black which was proposed to be scytonemin. Table 6.4.1 shows the peaks associated with a scytonemin spectrum.

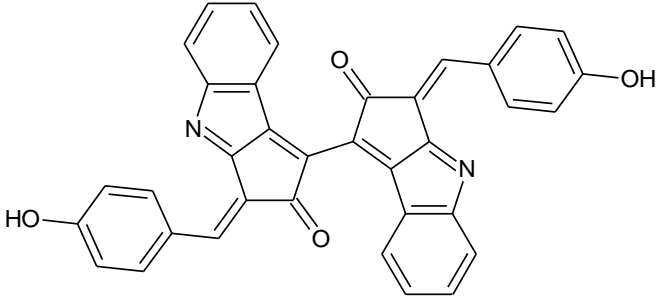
Peak	Assignment ^[190]	Structure
1592	ν (CCH) aromatic ring quadrant stretch	
1548	ν (CCH) <i>p</i> -disubstituted aromatic ring	
1433	δ (CCH)	
1378	ν (CCN) indole ring	
1314	ν (CN) indole ring	
1166	ν (CC) ring breathing pyrrole	
1096	ν (C–O) phenolic	
981	δ (CNC)	
748	δ (CCC:CCN) indole ring-puckering mode	
673	δ (CCN) pyrrole ring-puckering mode	
566	δ (CCN) aromatic ring indole system	

Table 6.4.1 Peak assignments and structure of scytonemin

In the spectrum obtained of region 2 peaks can clearly be seen indicating the presence of a compound not present in region 1. The most intense peaks at 1592cm^{-1} , 1548cm^{-1} and 1166cm^{-1} all are present within scytonemin. Additionally all the other peaks present in table 6.4.1 appear in the spectrum of region 2. Therefore this dark band seen on the sample can be identified as scytonemin, a compound present within cyanobacteria which absorbs UV radiation. The presence of such a compound would indicate the presence of life. Region 3 shows very little information due to the effect of the background on the sample. Region 4 is the spectrum of a cutaway section of the rock where the dark band observed in region 2 is present. Therefore the similarity seen in the spectrum of region 2 and 4 was to be expected.

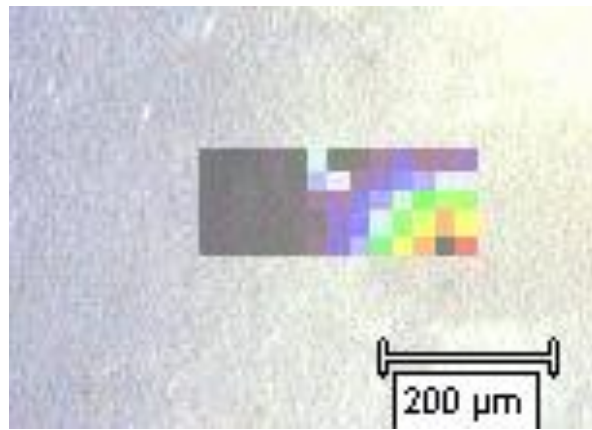


Figure 6.4.4. Map of a colonization area

While acquiring a spectrum for regions 2 and 4 several dark circular regions were observed on the surface of the samples and a Raman map was performed on the sample where these regions were present. The maps were obtained from 10 acc for 10 seconds at 25% laser power. The spectra were obtained using the x5 objective to obtain each spectrum over a larger spot area to reduce the effect of smaller regions of scytonemin on the map itself. The map was analysed using the components which make up the scytonemin and those regions are shown as the brightly coloured squares. From the map it is clear that the scytonemin is clearly located in one distinct space identified by the darker regions observed visually.

The presence of a biomarker within a sample obtained from the driest place on Earth clearly shows great potential for the detection of life on Mars. Scytonemin acts as a protective barrier from UV radiation for cyanobacteria. The presence of this compound suggests that this cyanobacterium may once have been present within this environment. If organisms can grow in these harsh environments then it is possible that organisms could grow in the similarly harsh environments found on Mars.

6.4.2. Ground samples

Using visual identification of regions of astrobiological importance a positive identification of biological material, using Raman spectroscopy, can occur. However onboard the ExoMars rover visual identification may not occur and the samples will be crushed and ground prior to analysis. Therefore the ability for Raman spectroscopy to detect the inclusions within these samples after processing must be determined.

For this investigation a small portion of the rock, where the inclusion was visibly present and detectible, was broken off and ground using a mortar and pestle. Once the sample particles were uniform in size the sample was mixed using a ball mill. In previous chapters it has been established that homogeneity within a solid mixture can produce problems with detection of organic material over a small region. Therefore as previously discussed, a 3 by 3 grid was implemented over a 400 μm by 400 μm range.

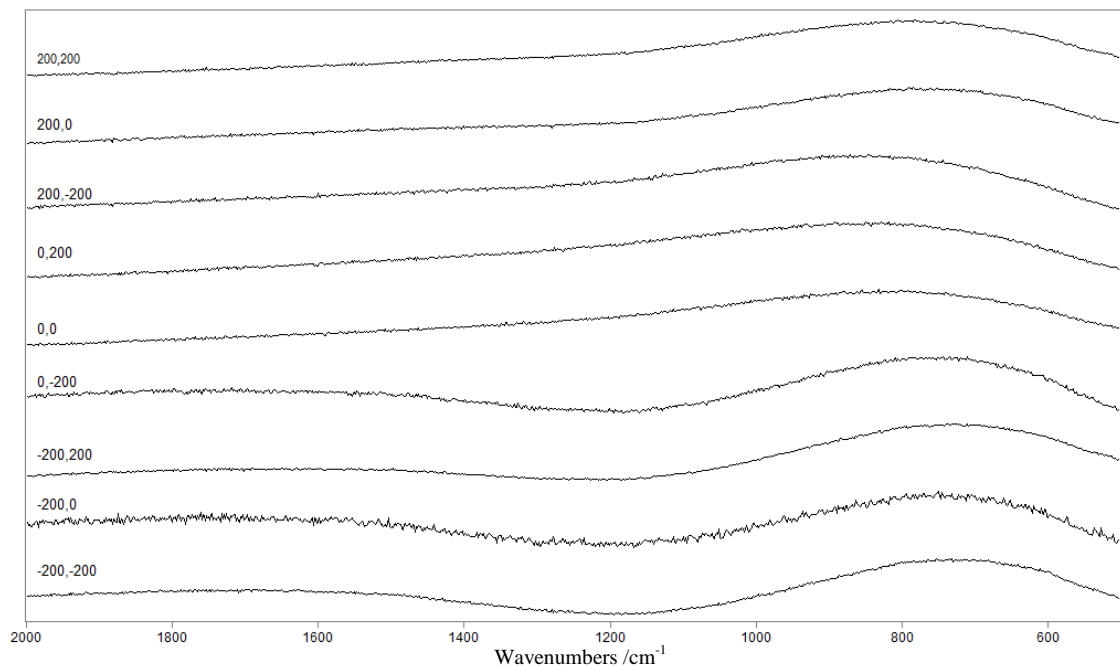


Figure 6.4.5. Raman spectra obtained from ground bio-geological at different points.

The Raman spectra of the sample showed no biological features at any of the nine points (Figure 6.4.5.). A large background occurred at all the locations derived from the geological material. This background masked any other features within the spectrum and therefore made detection of the organic impossible. Additionally the processing of the sample using grinding may heated and degraded the biological materials originally present.

These results demonstrate the issues with detection of organic material within the inorganic material previously observed in chapter 3. By grinding the sample the organic material is spread throughout the mixture rather than isolated in single locations, producing much stronger Raman bands. From this work it is clear that drilling, crushing and grinding geological materials has a negative impact on the ability for Raman spectroscopy to detect organic inclusions. Therefore for optimal use of Raman spectroscopy in astrobiology visual identification of potential organic samples is required followed by *in situ* analysis of these samples.

6.5. Conclusion

In this chapter the ability to distinguish between hopanoids, steranes and sterols has been established and the ability for Raman spectroscopy to identify and distinguish between evaporite minerals has been demonstrated. The ability for Raman spectroscopy to detect bacterial cells and identify differences between irradiated and unirradiated samples has been displayed. The impact of grinding and processing of bio-geological inclusions has also been investigated and the optimal sampling of astrobiological materials established.

Chapter 7

Conclusions and Further work

The aim of this study was to evaluate Raman spectroscopy as an analytical tool for interplanetary studies. This was achieved by establishing a protocol for sample analysis, determining optimal standards using instrument validation techniques and then optimizing analysis between a commercially available benchtop Raman instrument and a prototype Raman spectrometer. This information was then used in the analysis of a range of samples of astrobiological relevance.

Using multiple synthetic organic and inorganic samples, relevant to astrobiology, limits of detection were attempted to be deduced. However during this work the effect of sample inhomogeneity was clearly visible. Therefore analysis of different matrix formation methods was performed. This was achieved through producing mixtures using solid-solid, solid-solution and solution-solution mixing techniques. From these different techniques very little difference within the homogeneity of the mixtures was observed. To compensate for the constant presence of inhomogeneity within the samples a method of taking 9 points through a 3 by 3 grid system was developed. By taking the spectra from the 9 points and averaging them the spectra obtained became more representative of the whole sample. This was then applied to analysis of goethite and Martian soil simulate mixtures to display the capability for Raman spectroscopy to identify the organic component within these mixtures.

Instrument validation parameters were then applied to potential control standards of astrobiological relevance. These standards were required for optimization between instrument comparisons and therefore had to fulfil multiple parameters. The samples were required to be optimal for testing sensitivity, range, limit of detection, limit of quantification, robustness, selectivity, linearity, accuracy and precision of the instruments. This was achieved through calculating noise effects, limits of detection and peak fitting data. From this work calcite and trehalose mixtures and naphthalene in acetone solutions were devised as the optimal standards. To address the robustness of the instrument validation, a way of removing human error was developed through an automated identification method.

Having established the optimal sampling techniques and standards this information was then applied to comparative instrument optimization. This involved using a prototype instrument, devised to match the specifications of the instrument onboard the ESA ExoMars rover, and comparing the data obtained with a commercially available benchtop Renishaw InVia Raman spectrometer. To do this the 3 by 3 grid system was interrogated by the InVia instrument. It was determined that due to variation within samples on the micron scale, this technique could not simply be transferred to the prototype instrument. Therefore a sample mask with a hole was devised to cover the sample slides and mask the whole sample except for one region. This region would be exactly the same on both instruments and therefore allow for analysis of exactly the same area to be analysed on both spectrometers. Using this mask a range of samples were analysed on both instruments and data compared. From this data it was clear that the prototype instrument needed several optimizations to be comparable with the primary difference being related to the spectral resolution.

To display the application of Raman spectroscopy a range of astrobiological samples were interrogated. Geological, biomarker, cellular and bio-geological inclusions were analysed with increasing molecular specificity. For the geological sample an evaporite mineral of trona was used to demonstrate the capability of distinction between similar geological materials. The biomarkers; hopanoids, sterols and steranes had not previously been interrogated using Raman spectroscopy and in this study the ability to identify and distinguish between them was displayed. After establishing Raman spectroscopy capability to identify samples on the molecular level this was then scaled up to the cellular level. The ability for Raman spectroscopy to identify between irradiated and unirradiated bacterial species was investigated. This was then scaled up again to investigate geological inclusions of cyanobacteria colonization of geological materials in an extreme environment; the Atacama Desert. Using a rock sample featuring an inclusion the organic material was identified and then the sample was crushed and ground and analysed a second time. From this ground sample it was clear that processing the geological materials in this way, such as will happen onboard the ExoMars rover causes the inorganic sample background to mask Raman bands from the organic material. Therefore an external probe on board the ExoMars rover would be required for the optimal use of Raman spectroscopy on Mars.

From this study there are several areas where further work is required. For the synthetic mixture samples expanding the range of mixtures used would allow for more detailed information on the range of potential samples which may be encountered on Mars. Additional mixing techniques would be desirable to optimize homogeneity of the samples. Also by using a wider range of organic and inorganic materials the samples will become more representative of those likely to be found on the Martian surface. From this it would be possible to expand the control samples used in the instrument

validation methods and allow for additional measurement parameters to be recorded. From the prototype instrument the analysis of a greater range of samples is also desirable and analysis of the same samples after optimization of the instrument. This would then allow the prototype instrument to begin looking at exemplar systems and geological samples with the aim of eventually moving to use of the instrument outside the laboratory environment. This would require the investigation of further geological materials and potential biomarkers. For the cellular systems further analysis using the 1064 nm wavelength would be desirable to identify further features within the irradiated spectra. Additionally for the bio-geological inclusions further work is needed on the effects of crushing and grinding the samples and methods to optimize sampling of materials which undergo this process.

References

1. Armstrong CL (1995) Several pharmaceutical applications of fourier-transform raman spectroscopy. University of Bradford,
2. Dieing T, Hollricher O, Toporski J Confocal raman microscopy. Springer, Heidelberg ; London
3. Mirabella FM (1998) Modern techniques in applied molecular spectroscopy. Wiley, New York ; Chichester
4. Pelletier MJ (1999) Analytical applications of raman spectroscopy. Blackwell Science, Oxford
5. Sasic S, Ozaki Y Raman, infrared, and near-infrared chemical imaging. Wiley, Oxford
6. Skoog DA, Holler FJ, Crouch SR (2007) Principles of instrumental analysis. 6th ed. / Douglas A. Skoog, F. James Holler, Stanley R. Crouch. edn. Thomson Brooks/Cole, Belmont, CA ; United Kingdom
7. Lewis IR, Edwards HGM (2001) Handbook of raman spectroscopy : From the research laboratory to the process line. Marcel Dekker, New York
8. Gardiner DJ (1989) Practical raman spectroscopy. Springer Verlag,
9. Willock DJ (2009) Molecular symmetry. Wiley ; Chichester : John Wiley [distributor], Hoboken, N.J.
10. Flexner SB (1987) The random house dictionary of the english language. 2nd ed., unabridged. edn. Random House, New York
11. Wallace A (1907) Is mars habitable? A critical examination of professor percival lowell's book "Mars and its canals.", an alternative explanation
12. Chambers P (1999) Life on mars: The complete story.

13. Chevrier V, Mathe PE (2007) Mineralogy and evolution of the surface of mars: A review. *Planetary and Space Science* 55 (3):289-314
14. Hamilton VE, Christensen PR, Bandfield JL (2003) Volcanism or aqueous alteration on mars? *Nature* 421 (6924):711-712
15. McSween HY, Wyatt MB (2002) Spectral evidence for weathered basalt as an alternative to andesite in the northern lowlands of mars. *Nature* 417 (6886):263-266
16. McSween HY (2002) The rocks of mars, from far and near. *Meteoritics & Planetary Science* 37 (1):7-25
17. Larsen KW, Arvidson RE, Jolliff BL, Clark BC (2000) Correspondence and least squares analyses of soil and rock compositions for the viking lander 1 and pathfinder landing sites. *Journal of Geophysical Research-Planets* 105 (E12):29207-29221
18. McSween HY, Murchie SL, Crisp JA, Bridges NT, Anderson RC, Bell JF, Britt DT, Bruckner J, Dreibus G, Economou T, Ghosh A, Golombek MP, Greenwood JP, Johnson JR, Moore HJ, Morris RV, Parker TJ, Rieder R, Singer R, Wanke H (1999) Chemical, multispectral, and textural constraints on the composition and origin of rocks at the mars pathfinder landing site. *Journal of Geophysical Research-Planets* 104 (E4):8679-8715
19. Bandfield JL, Hamilton VE, Christensen PR (2000) A global view of martian surface compositions from mgs-tes. *Science* 287 (5458):1626-1630
20. Christensen PR, Bandfield JL, Bell JF, Gorelick N, Hamilton VE, Ivanov A, Jakosky BM, Kieffer HH, Lane MD, Jakosky BM, Kieffer HH, Lane MD, Malin MC, McConnochie T, McEwen AS, McSween HY, Mehall GL, Moersch JE, Nealson KH, Rice JW, Richardson MI, Ruff SW, Smith MD, Titus TN, Wyatt MB (2003) Morphology and composition of the surface of mars: Mars odyssey themis results. *Science* 300 (5628):2056-2061

21. Hamilton VE, Christensen PR (2005) Evidence for extensive, olivine-rich bedrock on mars. *Geology* 33 (6):433-436
22. Bibring JP, Langevin Y, Gendrin A, Gondet B, Poulet F, Berthe M, Soufflot A, Arvidson R, Mangold N, Mustard J, Drossart P, Team O (2005) Mars surface diversity as revealed by the omega/mars express observations. *Science* 307 (5715):1576-1581
23. Morris RV, Klingelhofer G, Schroder C, Rodionov DS, Yen A, Ming DW, de Souza PA, Fleischer I, Wdowiak T, Gellert R, Bernhardt B, Evlanov EN, Zubkov B, Foh J, Bonnes U, Kankeleit E, Gutlich P, Renz F, Squyres SW, Arvidson RE (2006) Mossbauer mineralogy of rock, soil, and dust at gusev crater, mars: Spirit's journey through weakly altered olivine basalt on the plains and pervasively altered basalt in the columbia hills. *Journal of Geophysical Research-Planets* 111 (E2)
24. McLennan SM, Bell JF, Calvin WM, Christensen PR, Clark BC, de Souza PA, Farmer J, Farrand WH, Fike DA, Gellert R, Ghosh A, Glotch TD, Grotzinger JP, Hahn B, Herkenhoff KE, Hurowitz JA, Johnson JR, Johnson SS, Jolliff B, Klingelhofer G, Knoll AH, Learner Z, Malin MC, McSween HY, Pockock J, Ruff SW, Soderblom LA, Squyres SW, Tosca NJ, Watters WA, Wyatt MB, Yen A (2005) Provenance and diagenesis of the evaporite-bearing burns formation, meridiani planum, mars. *Earth and Planetary Science Letters* 240 (1):95-121
25. Bishop JL, Murad E (2004) Characterization of minerals and biogeochemical markers on mars: A raman and ir spectroscopic study of montmorillonite. *Journal of Raman Spectroscopy* 35 (6):480-486
26. Bish DL, Carey JW, Vaniman DT, Chipera SJ (2003) Stability of hydrous minerals on the martian surface. *Icarus* 164 (1):96-103
27. Fialips CI, Carey JW, Vaniman DT, Bish DL, Feldman WC, Mellon MT (2005) Hydration state of zeolites, clays, and hydrated salts under present-day martian surface

- conditions: Can hydrous minerals account for mars odyssey observations of near-equatorial water-equivalent hydrogen? *Icarus* 178 (1):74-83
28. Tokano T, Bish DL (2005) Hydration state and abundance of zeolites on mars and the water cycle. *Journal of Geophysical Research-Planets* 110 (E12)
29. Forget F, Pierrehumbert RT (1997) Warming early mars with carbon dioxide clouds that scatter infrared radiation. *Science* 278 (5341):1273-1276
30. Nakamura T, Tajika E (2001) Stability and evolution of the climate system of mars. *Earth Planets and Space* 53 (8):851-859
31. Pollack JB, Kasting JF, Richardson SM, Poliakov K (1987) The case for a wet, warm climate on early mars. *Icarus* 71 (2):203-224
32. Phillips RJ, Zuber MT, Solomon SC, Golombek MP, Jakosky BM, Banerdt WB, Smith DE, Williams RME, Hynek BM, Aharonson O, Hauck SA (2001) Ancient geodynamics and global-scale hydrology on mars. *Science* 291 (5513):2587-2591
33. Catling DC (1999) A chemical model for evaporites on early mars: Possible sedimentary tracers of the early climate and implications for exploration. *Journal of Geophysical Research-Planets* 104 (E7):16453-16469
34. Fairen AG, Fernandez-Remolar D, Dohm JM, Baker VR, Amils R (2004) Inhibition of carbonate synthesis in acidic oceans on early mars. *Nature* 431 (7007):423-426
35. Kahn R (1985) The evolution of co₂ on mars. *Icarus* 62 (2):175-190
36. King PL, Lescinsky DT, Nesbitt HW (2004) The composition and evolution of primordial solutions on mars, with application to other planetary bodies. *Geochimica Et Cosmochimica Acta* 68 (23):4993-5008
37. Marion GM, Catling DC, Kargel JS (2003) Modeling aqueous ferrous iron chemistry at low temperatures with application to mars. *Geochimica Et Cosmochimica Acta* 67 (22):4251-4266

38. Morse JW, Marion GM (1999) The role of carbonates in the evolution of early martian oceans. *American Journal of Science* 299 (7-9):738-761
39. Booth MC, Kieffer HH (1978) Carbonate formation in mars-like environments. *Journal of Geophysical Research* 83 (Nb4):1809-1815
40. Gooding JL (1978) Chemical weathering on mars - thermodynamic stabilities of primary minerals (and their alteration products) from mafic igneous rocks. *Icarus* 33 (3):483-513
41. Bandfield JL, Glotch TD, Christensen PR (2003) Spectroscopic identification of carbonate minerals in the martian dust. *Science* 301 (5636):1084-1087
42. Christensen PR, Ruff SW, Fergason RL, Knudson AT, Anwar S, Arvidson RE, Bandfield JL, Blaney DL, Budney C, Calvin WM, Glotch TD, Golombek MP, Gorelick N, Graff TG, Hamilton VE, Hayes A, Johnson JR, McSween HY, Mehall GL, Mehall LK, Moersch JE, Morris RV, Rogers AD, Smith MD, Squyres SW, Wolff MJ, Wyatt MB (2004) Initial results from the mini-tes experiment in gusev crater from the spirit rover. *Science* 305 (5685):837-842
43. Moore JM (2004) Mars - blueberry fields for ever. *Nature* 428 (6984):711-712
44. Bell JF, McSween HY, Crisp JA, Morris RV, Murchie SL, Bridges NT, Johnson JR, Britt DT, Golombek MP, Moore HJ, Ghosh A, Bishop JL, Anderson RC, Bruckner J, Economou T, Greenwood JP, Gunnlaugsson HP, Hargraves RM, Hviid S, Knudsen JM, Madsen MB, Reid R, Rieder R, Soderblom L (2000) Mineralogic and compositional properties of martian soil and dust: Results from mars pathfinder. *Journal of Geophysical Research-Planets* 105 (E1):1721-1755
45. Foley CN, Economou T, Clayton RN (2003) Final chemical results from the mars pathfinder alpha proton x-ray spectrometer. *Journal of Geophysical Research-Planets* 108 (E12)

46. Rieder R, Economou T, Wanke H, Turkevich A, Crisp J, Bruckner J, Dreibus G, McSween HY (1997) The chemical composition of martian soil and rocks returned by the mobile alpha proton x-ray spectrometer: Preliminary results from the x-ray mode. *Science* 278 (5344):1771-1774
47. Bell JF, Mccord TB, Owensby PD (1990) Observational evidence of crystalline iron-oxides on mars. *Journal of Geophysical Research-Solid Earth and Planets* 95 (B9):14447-14461
48. Morris RV, Golden DC, Bell JF, Shelfer TD, Scheinost AC, Hinman NW, Furniss G, Mertzman SA, Bishop JL, Ming DW, Allen CC, Britt DT (2000) Mineralogy, composition, and alteration of mars pathfinder rocks and soils: Evidence from multispectral, elemental, and magnetic data on terrestrial analogue, SNC meteorite, and pathfinder samples. *Journal of Geophysical Research-Planets* 105 (E1):1757-1817
49. Klingelhofer G, Fegley B, Morris RV, Kankeleit E, Held P, Evlanov E, Priloutsii O (1996) Mineralogical analysis of martian soil and rock by a miniaturized backscattering mossbauer spectrometer. *Planetary and Space Science* 44 (11):1277-&
50. Klingelhofer G, Morris RV, Bernhardt B, Rodionov D, de Souza PA, Squyres SW, Foh J, Kankeleit E, Bonnes U, Gellert R, Schroder C, Linkin S, Evlanov E, Zubkov B, Prilutski O (2003) Athena mimos ii mossbauer spectrometer investigation. *Journal of Geophysical Research-Planets* 108 (E12)
51. Dyar MD, Schaefer MW (2004) Mossbauer spectroscopy on the surface of mars: Constraints and expectations. *Earth and Planetary Science Letters* 218 (3-4):243-259
52. Wdowiak TJ, Klingelhofer G, Wade ML, Nunez JI (2003) Extracting science from mossbauer spectroscopy on mars. *Journal of Geophysical Research-Planets* 108 (E12)
53. Morris RV, Golden DC, Bell JF (1997) Low-temperature reflectivity spectra of red hematite and the color of mars. *Journal of Geophysical Research-Planets* 102 (E4):9125-9133

54. Morris RV, Golden DC, Bell JF, Lauer HV, Adams JB (1993) Pigmenting agents in martian soils - inferences from spectral, mossbauer, and magnetic-properties of nanophase and other iron-oxides in hawaiian palagonitic soil pn-9. *Geochimica Et Cosmochimica Acta* 57 (19):4597-4609
55. Christensen PR, Bandfield JL, Clark RN, Edgett KS, Hamilton VE, Hoefen T, Kieffer HH, Kuzmin RO, Lane MD, Malin MC, Morris RV, Pearl JC, Pearson R, Roush TL, Ruff SW, Smith MD (2000) Detection of crystalline hematite mineralization on mars by the thermal emission spectrometer: Evidence for near-surface water. *Journal of Geophysical Research-Planets* 105 (E4):9623-9642
56. Tardy Y, Nahon D (1985) Geochemistry of laterites, stability of al-goethite, al-hematite, and fe-3+-kaolinite in bauxites and ferricretes - an approach to the mechanism of concretion formation. *American Journal of Science* 285 (10):865-903
57. Nahon DB (1991) Self-organization in chemical lateritic weathering. *Geoderma* 51 (1-4):5-13
58. Koch CB, Morup S, Madsen MB, Vistisen L (1995) Iron-containing weathering products of basalt in a cold, dry climate. *Chemical Geology* 122 (1-4):109-119
59. Catling DC, Moore JA (2003) The nature of coarse-grained crystalline hematite and its implications for the early environment of mars. *Icarus* 165 (2):277-300
60. Wade ML, Agresti DG, Wdowiak TJ, Armendarez LP, Farmer JD (1999) A mossbauer investigation of iron-rich terrestrial hydrothermal vent systems: Lessons for mars exploration. *Journal of Geophysical Research-Planets* 104 (E4):8489-8507
61. Bishop JL, Froschl H, Mancinelli RL (1998) Alteration processes in volcanic soils and identification of exobiologically important weathering products on mars using remote sensing. *Journal of Geophysical Research-Planets* 103 (E13):31457-31476
62. Torrent J, Barron V (2002) Evidence for a simple pathway to maghemite in earth and mars soils. *Geochimica Et Cosmochimica Acta* 66 (15):2801-2806

63. Morris RV, Golden DC, Shelfer TD, Lauer HV (1998) Lepidocrocite to maghemite to hematite: A pathway to magnetic and hematitic martian soil. *Meteoritics & Planetary Science* 33 (4):743-751
64. Kirkland LE, Herr KC (2000) Spectral anomalies in the 11 and 12 μm region from the mariner mars 7 infrared spectrometer. *Journal of Geophysical Research-Planets* 105 (E9):22507-22515
65. Morris RV (1998) Goldenrod pigments and the occurrence of hematite and possibly goethite in the olympus-amazonis region of mars. *Icarus* 134 (1):1-10
66. Burns RG, Fisher DS (1990) Iron-sulfur mineralogy of mars - magmatic evolution and chemical-weathering products. *Journal of Geophysical Research-Solid Earth and Planets* 95 (B9):14415-14421
67. Burns RG (1993) Rates and mechanisms of chemical-weathering of ferromagnesian silicate minerals on mars. *Geochimica Et Cosmochimica Acta* 57 (19):4555-4574
68. Chevrier V, Rochette P, Mathe PE, Grauby O (2004) Weathering of iron-rich phases in simulated martian atmospheres. *Geology* 32 (12):1033-1036
69. Gellert R, Rieder R, Anderson RC, Bruckner J, Clark BC, Dreibus G, Economou T, Klingelhofer G, Lugmair GW, Ming DW, Squyres SW, d'Uston C, Wanke H, Yen A, Zipfel J (2004) Chemistry of rocks and soils in gusev crater from the alpha particle x-ray spectrometer. *Science* 305 (5685):829-832
70. Baird AK, Toulmin P, Clark BC, Rose HJ, Keil K, Christian RP, Gooding JL (1976) Mineralogic and petrologic implications of viking geochemical results from mars - interim-report. *Science* 194 (4271):1288-1293
71. Economou T (2001) Chemical analyses of martian soil and rocks obtained by the pathfinder alpha proton x-ray spectrometer. *Radiation Physics and Chemistry* 61 (3-6):191-197

72. Rieder R, Gellert R, Anderson RC, Bruckner J, Clark BC, Dreibus G, Economou T, Klingelhofer G, Lugmair GW, Ming DW, Squyres SW, d'Uston C, Wanke H, Yen A, Zipfel J (2004) Chemistry of rocks and soils at meridiani planum from the alpha particle x-ray spectrometer. *Science* 306 (5702):1746-1749
73. Wang A, Haskin LA, Squyres SW, Jolliff BL, Crumpler L, Gellert R, Schroder C, Herkenhoff K, Hurowitz J, Tosca NJ, Farrand WH, Anderson R, Knudson AT (2006) Sulfate deposition in subsurface regolith in gusev crater, mars. *Journal of Geophysical Research-Planets* 111 (E2)
74. Bishop JL, Lane MD, Dyar MD, Parente M, Roach LH, Murchie SL, Mustard JF (2008) Sulfates on mars: How recent discoveries from crism, omega and the mers are changing our view of the planet. *Geochimica Et Cosmochimica Acta* 72 (12):A86-A86
75. Fan CJ, Schulze-Makuch D, Fairen AG, Wolff JA (2008) A new hypothesis for the origin and redistribution of sulfates in the equatorial region of western mars. *Geophysical Research Letters* 35 (6):-
76. Fernandez-Remolar DC, Prieto-Ballesteros O, Gomez F, Amils R, Gomez D, Osburn MR, Friedlander L, Arvidson R, Morris R (2007) Massive production of sulfates on mars through an oxidation event: The rio tinto mars model. *Astrobiology* 7 (3):500-500
77. Golden DC, Ming DW, Morris RV, Mertzman SA (2005) Laboratory-simulated acid-sulfate weathering of basaltic materials: Implications for formation of sulfates at meridiani planum and gusev crater, mars. *Journal of Geophysical Research-Planets* 110 (E12):-
78. Langevin Y, Poulet F, Bibring JP, Gondet B (2005) Sulfates in the north polar region of mars detected by omega/mars express. *Science* 307 (5715):1584-1586
79. Klingelhofer G, Morris RV, Bernhardt B, Schroder C, Rodionov DS, de Souza PA, Yen A, Gellert R, Evlanov EN, Zubkov B, Foh J, Bonnes U, Kankeleit E, Gutlich P,

- Ming DW, Renz F, Wdowiak T, Squyres SW, Arvidson RE (2004) Jarosite and hematite at meridiani planum from opportunity's mossbauer spectrometer. *Science* 306 (5702):1740-1745
80. Clark BC, Morris RV, McLennan SM, Gellert R, Jolliff B, Knoll AH, Squyres SW, Lowenstein TK, Ming DW, Tosca NJ, Yen A, Christensen PR, Gorevan S, Bruckner J, Calvin W, Dreibus G, Farrand W, Klingelhofer G, Waenke H, Zipfel J, Bell JF, Grotzinger J, McSween HY, Rieder R (2005) Chemistry and mineralogy of outcrops at meridiani planum. *Earth and Planetary Science Letters* 240 (1):73-94
81. Squyres SW, Grotzinger JP, Arvidson RE, Bell JF, Calvin W, Christensen PR, Clark BC, Crisp JA, Farrand WH, Herkenhoff KE, Johnson JR, Klingelhofer G, Knoll AH, McLennan SM, McSween HY, Morris RV, Rice JW, Rieder R, Soderblom LA (2004) In situ evidence for an ancient aqueous environment at meridiani planum, mars. *Science* 306 (5702):1709-1714
82. Philips T (2001) The solar wind at mars.
83. Haberle RM, McKay CP, Schaeffer J, Cabrol NA, Grin EA, Zent AP, Quinn R (2001) On the possibility of liquid water on present-day mars. *Journal of Geophysical Research-Planets* 106 (E10):23317-23326
84. Edwards HGM, Hargreaves MD (2008) Raman spectroscopy - the biomolecular detection of life in extreme environments. *Models, Mysteries and Magic of Molecules*:1-28
85. Edwards HGM, Mohsin MA, Sadooni FN, Hassan NFN, Munshi T (2006) Life in the sabkha: Raman spectroscopy of halotrophic extremophiles of relevance to planetary exploration. *Analytical and Bioanalytical Chemistry* 385 (1):46-56
86. Villar SEJ, Edwards HGM, Cockell CS (2005) Raman spectroscopy of endoliths from antarctic cold desert environments. *Analyst* 130 (2):156-162
87. Clark S (2002) Tough earth bug may be from mars. *New Scientist*.

88. Edwards HGM (2007) A novel extremophile strategy studied by raman spectroscopy. *Spectrochimica Acta Part a-Molecular and Biomolecular Spectroscopy* 68 (4):1126-1132
89. Jahnke L, Klein HP (1979) Oxygen as a factor in eukaryote evolution - some effects of low-levels of oxygen on *saccharomyces-cerevisiae*. *Origins of Life and Evolution of the Biosphere* 9 (4):329-334
90. Vitek P, Jehlicka J, Edwards HGM, Osterrothova K (2009) Identification of beta-carotene in an evaporitic matrix-evaluation of raman spectroscopic analysis for astrobiological research on mars. *Analytical and Bioanalytical Chemistry* 393 (8):1967-1975
91. McKay CP, Porco CC, Altheide T, Davis WL, Kral TA (2008) The possible origin and persistence of life on enceladus and detection of biomarkers in the plume. *Astrobiology* 8 (5):909-919
92. Edwards HGM, Vandenabeele P, Jorge-Villar SE, Carter EA, Perez FR, Hargreaves MD (2007) The rio tinto mars analogue site: An extremophilic raman spectroscopic study. *Spectrochimica Acta Part a-Molecular and Biomolecular Spectroscopy* 68 (4):1133-1137
93. Edwards HGM (2007) Raman spectroscopic approach to analytical astrobiology: The detection of key biomolecular markers in the search for life. *Origins of Life and Evolution of Biospheres* 37 (4-5):335-339
94. Villar SEJ, Edwards HGM (2006) Raman spectroscopy in astrobiology. *Analytical and Bioanalytical Chemistry* 384 (1):100-113
95. Peters KE, Walters CC, Moldowan JM (2005) *The biomarker guide*. 2nd ed. / K.E. Peters, C.C. Walters, J.M. Moldowan. edn. Cambridge University Press, Cambridge
96. Parnell J, Cullen D, Sims MR, Bowden S, Cockell CS, Court R, Ehrenfreund P, Gaubert F, Grant W, Parro V, Rohmer M, Sephton M, Stan-Lotter H, Steele A,

- Toporski J, Vago J (2007) Searching for life on mars: Selection of molecular targets for esa's aurora exomars mission. *Astrobiology* 7 (4):578-604
97. Aggeler R, Murray J, Marusich MF, Capaldi RA (2004) Focused proteomics: Monoclonal antibody-based isolation of the oxidative phosphorylation machinery and detection of phosphoproteins using a fluorescent phosphoprotein gel stain. *Electrophoresis* 25 (15):2520-2525
98. Saibil HR, Ranson NA (2002) The chaperonin folding machine. *Trends in Biochemical Sciences* 27 (12):627-632
99. Bowden SA, Parnell J (2007) Intracrystalline lipids within sulfates from the haughton impact structure - implications for survival of lipids on mars. *Icarus* 187 (2):422-429
100. Ourisson G, Albrecht P, Rohmer M (1982) Predictive microbial biochemistry - from molecular fossils to procaryotic membranes. *Trends in Biochemical Sciences* 7 (7):236-239
101. Edwards HGM, Moody CD, Villar SEJ, Wynn-Williams DD (2005) Raman spectroscopic detection of key biomarkers of cyanobacteria and lichen symbiosis in extreme antarctic habitats: Evaluation for mars lander missions. *Icarus* 174 (2):560-571
102. Izydorczyk K, Tarczynska M, Jurczak T, Mrowczynski J, Zalewski M (2005) Measurement of phycocyanin fluorescence as an online early warning system for cyanobacteria in reservoir intake water. *Environmental Toxicology* 20 (4):425-430
103. Albrecht P, Hebling Y, Schaeffer P, Behrens A, Adam P, Schmitt G, Schneckenburger P, Bernasconi SM (2006) Biomarker evidence for a major preservation pathway of sedimentary organic carbon. *Science* 312 (5780):1627-1631
104. Vitek P, Osterrothova K, Jehlicka J (2009) Beta-carotene-a possible biomarker in the martian evaporitic environment: Raman micro-spectroscopic study. *Planetary and Space Science* 57 (4):454-459

105. Grant WD (2004) Life at low water activity. *Philosophical Transactions of the Royal Society of London Series B-Biological Sciences* 359 (1448):1249-1266
106. Tegelaar EW, Deleeuw JW, Derenne S, Largeau C (1989) A reappraisal of kerogen formation. *Geochimica Et Cosmochimica Acta* 53 (11):3103-3106
107. Harwood JL, Russell NJ (1984) *Lipids in plants and microbes*. Allen & Unwin, London
108. Didyk BM, Simoneit BRT, Brassell SC, Eglinton G (1978) Organic geochemical indicators of paleo-environmental conditions of sedimentation. *Nature* 272 (5650):216-222
109. Price LC (1993) Thermal-stability of hydrocarbons in nature - limits, evidence, characteristics, and possible controls. *Geochimica Et Cosmochimica Acta* 57 (14):3261-3280
110. Brocks JJ, Logan GA, Buick R, Summons RE (1999) Archean molecular fossils and the early rise of eukaryotes. *Science* 285 (5430):1033-1036
111. Koopmans MP, Schouten S, Kohnen MEL, Damste JSS (1996) Restricted utility of aryl isoprenoids as indicators for photic zone anoxia. *Geochimica Et Cosmochimica Acta* 60 (23):4873-4876
112. Summons RE, Powell TG (1986) Chlorobiaceae in paleozoic seas revealed by biological markers, isotopes and geology. *Nature* 319 (6056):763-765
113. Ourisson G, Rohmer M (1992) Hopanoids .2. Biohopanoids - a novel class of bacterial lipids. *Accounts of Chemical Research* 25 (9):403-408
114. Parnell J (2004) Hopane biomarkers traced from bedrock to recent sediments and ice at the haughton impact structure, devon island: Implications for the search for biomarkers on mars. *Lunar and Planetary Science* 35

115. Peters KE, Moldowan JM (1991) Effects of source, thermal maturity, and biodegradation on the distribution and isomerization of homohopanes in petroleum. *Organic Geochemistry* 17 (1):47-61
116. Killops SD, Killops VJ (2005) Introduction to organic geochemistry. 2nd ed. edn. Blackwell, Oxford
117. Wolverton M (2004) The depths of space : The story of the pioneer planetary probes. Joseph Henry Press, Washington, D.C. ; [Great Britain]
118. Hamilton J (1998) Mariner missions to mars. ABDO & Daughters,
119. Calvin WM, King TVV, Clark RN (1994) Hydrous carbonates on mars - evidence from mariner 6/7 infrared spectrometer and ground-based telescopic spectra. *Journal of Geophysical Research-Planets* 99 (E7):14659-14675
120. Kieffer HH (1992) Mars. University of Arizona Press,
121. Toulmin P, Baird AK, Clark BC, Keil K, Rose HJ, Christian RP, Evans PH, Kelliher WC (1977) Geochemical and mineralogical interpretation of viking inorganic chemical results. *Transactions-American Geophysical Union* 58 (8):828-828
122. Hamilton VE, Wyatt MB, McSween HY, Christensen PR (2001) Analysis of terrestrial and martian volcanic compositions using thermal emission spectroscopy - 2. Application to martian surface spectra from the mars global surveyor thermal emission spectrometer. *Journal of Geophysical Research-Planets* 106 (E7):14733-14746
123. Pds geosciences node data and services: Mgs. <http://pds-geosciences.wustl.edu/missions/mgs/>. Accessed 23/07/11 2011
124. Burdick A (2005) Out of eden : An odyssey of ecological invasion. 1st ed. edn. Farrar, Straus and Giroux, New York, NY
125. Pelt MV (2006) Space invaders: How robotic spacecraft explore the solar system. Springer,

126. The esa-nasa exomars programme rover, 2018. <http://exploration.esa.int/science-e/www/object/index.cfm?fobjectid=45084>. Accessed 21/04/10 2010
127. Esa exomars scientific objectives.
http://www.esa.int/SPECIALS/ExoMars/SEM0VIAMS7F_0.html. Accessed 21/04/10 2010
128. The exomars instruments (2008). European Space Agency,
129. Vago J (2004) Pasteur newsletter 4.
130. Vago J (2006) Pasteur newsletter 5.
131. Esa- robotic exploration of mars: The exomars rover instrument suite.
<http://exploration.esa.int/science-e/www/object/index.cfm?fobjectid=45103&fbodylongid=2127>. Accessed 11/08/11 2011
132. Griffiths AD, Coates AJ, Jaumann R, Michaelis H, Paar G, Barnes D, Josset J (2006) Context for the esa exomars rover: The panoramic camera (pancam) instrument. *International Journal of Astrobiology* 5 (3):269–275
133. Esa- robotic exploration of mars: The exomars drill unit.
<http://exploration.esa.int/science-e/www/object/index.cfm?fobjectid=43611>. Accessed 11/08/11 2011
134. Delhez R, Marinangeli L, S. vdG (2005) Mars-xrd: The x-ray diffractometer for rock and soil analysis on mars in 2011. *Int Union of Crystallography Newsletter* 30:7-10
135. Popp J, Schmitt M (2004) Raman spectroscopy breaking terrestrial barriers! *Journal of Raman Spectroscopy* 35 (6):429-432
136. Pérez FR, Martínez-Frías J (2006) Raman spectroscopy goes to mars. *Spectroscopy Europe* 18 (18-21)

137. Ellery A, Wynn-Williams D (2003) Why raman spectroscopy on mars? A case of the right tool for the right job. *Astrobiology* 3 (3):565-579
138. Ellery A, Wynn-Williams D, Parnell J, Edwards HGM, Dickensheets D (2004) The role of raman spectroscopy as an astrobiological tool in the exploration of mars. *Journal of Raman Spectroscopy* 35 (6):441-457
139. Villar SEJ, Edwards HGM (2005) Near-infrared raman spectra of terrestrial minerals: Relevance for the remote analysis of martian spectral signatures. *Vibrational Spectroscopy* 39 (1):88-94
140. Jehlicka J, Edwards HGM, Vitek P (2009) Assessment of raman spectroscopy as a tool for the non-destructive identification of organic minerals and biomolecules for mars studies. *Planetary and Space Science* 57 (5-6):606-613
141. Kuptsov AH (1994) Applications of fourier-transform raman-spectroscopy in forensic-science. *Journal of Forensic Sciences* 39 (2):305-318
142. Pollack JB, Roush T, Witteborn F, Bregman J, Wooden D, Stoker C, Toon OB, Rank D, Dalton B, Freedman R (1990) Thermal emission-spectra of mars (5.4-10.5- μ m) - evidence for sulfates, carbonates, and hydrates. *Journal of Geophysical Research-Solid Earth and Planets* 95 (B9):14595-14627
143. Courreges-Lacoste GB, Ahlers B, Perez FR (2007) Combined raman spectrometer/laser-induced spectrometer for the next esa mission to breakdown mars. *Spectrochimica Acta Part a-Molecular and Biomolecular Spectroscopy* 68 (4):1023-1028
144. Edwards HGM, Hargreaves MD Raman spectroscopy - the biomolecular detection of life in extreme environments. In: Boeyens JCAOJF (ed) 5th International Indaba Workshop of the International-Union-of-Crystallography, Kruger Natl Pk, SOUTH AFRICA, Aug 20-25 2006. Springer, pp 1-+

145. Blanco A, D'Elia M, Licchelli D, Orofino V, Fonti S (2006) Studies of biominerals relevant to the search for life on mars. *Origins of Life and Evolution of the Biosphere* 36 (5-6):621-622
146. Simoneit BRT, Summons RE, Jahnke LL (1998) Biomarkers as tracers for life on early earth and mars. *Origins of Life and Evolution of the Biosphere* 28 (4-6):475-483
147. Moody CD, Villar SEJ, Edwards HGM, Hodgson DA, Doran PT, Bishop JL (2005) Biogeological raman spectroscopic studies of antarctic lacustrine sediments. *Spectrochimica Acta Part a-Molecular and Biomolecular Spectroscopy* 61 (10):2413-2417
148. McKay DS, Gibson EK, ThomasKeptra KL, Vali H, Romanek CS, Clemett SJ, Chillier XDF, Maechling CR, Zare RN (1996) Search for past life on mars: Possible relic biogenic activity in martian meteorite alh84001. *Science* 273 (5277):924-930
149. Allamandola LJ, Sandford SA, Wopenka B (1987) Interstellar polycyclic aromatic hydrocarbons and carbon in interplanetary dust particles and meteorites. *Science* 237 (4810):56-59
150. Clemett SJ, Dulay MT, Gillette JS, Chillier XDF, Mahajan TB, Zare RN (1998) Evidence for the extraterrestrial origin of polycyclic aromatic hydrocarbons in the martian meteorite alh84001. *Faraday Discussions* 109:417-436
151. Becker L, Glavin DP, Bada JL (1997) Polycyclic aromatic hydrocarbons (pahs) in antarctic martian meteorites, carbonaceous chondrites and polar ice. *Abstracts of Papers of the American Chemical Society* 213:240-GEOC
152. Somasundaran P (2006) *Encyclopedia of surface and colloid science*. CRC Press Inc,
153. McNaught AD, Wilkinson A (1997) *Compendium of chemical terminology : Iupac recommendations*. 2nd ed / compiled by Alan D. McNaught and Andrew Wilkinson. edn. Blackwell Science, Oxford

154. Sarma LP, Prasad PSR, Ravikumar N (1998) Raman spectroscopic study of phase transitions in natural gypsum. *Journal of Raman Spectroscopy* 29 (9):851-856
155. Liu Y, Wang A, Freeman JJ (2009) Raman, mir, and nir spectroscopic study of calcium sulfates: Gypsum, bassanite, and anhydrite. Paper presented at the 40th Lunar and Planetary Science Conference,
156. Berenblu.Bj, Dawson P, Wilkinso.Gr (1971) Raman spectrum of gypsum. *Spectrochimica Acta Part a-Molecular Spectroscopy A* 27 (9):1849-&
157. Bhagavantam S (1910) Effect of crystal orientation on the raman spectrum of calcite. *Proceedings Mathematical Sciences* 11 (1):62-71
158. Gunasekaran S, Anbalagan G, Pandi S (2006) Raman and infrared spectra of carbonates of calcite structure. *Journal of Raman Spectroscopy* 37 (9):892-899
159. Tabrizi MZ, Tayyari SF, Tayyari F, Behforouz M (2004) Fourier transform infrared and raman spectra, vibrational assignment and density functional theory calculations of naphthazarin. *Spectrochimica Acta Part a-Molecular and Biomolecular Spectroscopy* 60 (1-2):111-120
160. Sarkar A, Mahapatra S Synthesis of all crystalline phases of anhydrous calcium carbonate. *Crystal Growth & Design* 10 (5):2129-2135
161. Loste E, Park RJ, Warren J, Meldrum FC (2004) Precipitation of calcium carbonate in confinement. *Advanced Functional Materials* 14 (12):1211-1220
162. Klepetsanis PG, Koutsoukos PG (1989) Precipitation of calcium sulfate dihydrate at constant calcium activity. *Journal of Crystal Growth* 98 (3):480-486
163. Harris DC (2003) Quantitative chemical analysis. 6th ed. edn. W. H. Freeman, New York
164. Zumbusch A, Holtom GR, Xie XS (1999) Three-dimensional vibrational imaging by coherent anti-stokes raman scattering. *Physical Review Letters* 82 (20):4142-4145

165. Mahadevan-Jansen A, Lieber CA (2003) Automated method for subtraction of fluorescence from biological raman spectra. *Applied Spectroscopy* 57 (11):1363-1367
166. Shreve AP, Cherepy NJ, Mathies RA (1992) Effective rejection of fluorescence interference in raman-spectroscopy using a shifted excitation difference technique. *Applied Spectroscopy* 46 (4):707-711
167. Puppels GJ, Olminkhof JHF, Segersnolten GMJ, Otto C, Demul FFM, Greve J (1991) Laser irradiation and raman-spectroscopy of single living cells and chromosomes - sample degradation occurs with 514.5nm but not with 660nm laser-light. *Experimental Cell Research* 195 (2):361-367
168. De Gelder J, De Gussem K, Vandenabeele P, Moens L (2007) Reference database of raman spectra of biological molecules. *Journal of Raman Spectroscopy* 38 (9):1133-1147
169. Lyng FM, Faolain EO, Conroy J, Meade AD, Knief P, Duffy B, Hunter MB, Byrne JM, Kelehan P, Byrne HJ (2007) Vibrational spectroscopy for cervical cancer pathology, from biochemical analysis to diagnostic tool. *Experimental and Molecular Pathology* 82 (2):121-129
170. Urmos J, Sharma SK, Mackenzie FT (1991) Characterization of some biogenic carbonates with raman-spectroscopy. *American Mineralogist* 76 (3-4):641-646
171. Sasaki K, Tanaike O, Konno H (1998) Distinction of jarosite-group compounds by raman spectroscopy. *Canadian Mineralogist* 36:1225-1235
172. Warren JK (2006) *Evaporites : Sediments, resources and hydrocarbons*. Springer, Berlin
173. Edwards HGM, Villar SEJ, Pullan D, Hargreaves MD, Hofmann BA, Westall F (2007) Morphological biosignatures from relict fossilised sedimentary geological specimens: A raman spectroscopic study. *Journal of Raman Spectroscopy* 38 (10):1352-1361

174. Edwards HGM, Moody CD, Jorge Villar SE, Wynn-Williams DD (2005) Raman spectroscopic detection of key biomarkers of cyanobacteria and lichen symbiosis in extreme antarctic habitats: Evaluation for mars lander missions. *Icarus* 174:p. 560-571
175. Wynn-Williams DD, Edwards HGM (2000) Proximal analysis of regolith habitats and protective biomolecules in situ by laser raman spectroscopy: Overview of terrestrial antarctic habitats and mars analogs. *Icarus* 144 (2):486-503
176. Summons RE, Jahnke LL, Hope JM, Logan GA (1999) 2-methylhopanoids as biomarkers for cyanobacterial oxygenic photosynthesis. *Nature* 400 (6744):554-557
177. Peters KE, Walters CC, Moldowan JM (2005) *The biomarker guide*.
178. Alajtal AI, Edwards HGM, Scowen IJ (2010) Raman spectroscopic analysis of minerals and organic molecules of relevance to astrobiology. *Analytical and Bioanalytical Chemistry* 397 (1):215-221
179. Edwards HGM, Farwell DW, Grady MM, Wynn-Williams DD, Wright IP (1999) Comparative raman microscopy of a martian meteorite and antarctic lithic analogues. *Planetary and Space Science* 47 (3-4):353-362
180. Ourisson GaR, M. (1999) Bio-hopanoids: A novel class of bacterial lipids. *Acc Chem Res* 25:p. 403-408
181. Bloch KE (1983) Sterol structure and membrane-function. *Crc Critical Reviews in Biochemistry* 14 (1):47-92
182. Demel RA, Dekruyff B (1976) Function of sterols in membranes. *Biochimica Et Biophysica Acta* 457 (2):109-132
183. Vangraas G, Baas JMA, Vandegraaf B, Deleeuw JW (1982) Theoretical organic geochemistry .1. The thermodynamic stability of several cholestane isomers calculated by molecular mechanics. *Geochimica Et Cosmochimica Acta* 46 (11):2399-2402

184. Russell NC, Edwards HGM, Wynn-Williams DD (1998) Ft-raman spectroscopic analysis of endolithic microbial communities from beacon sandstone in victoria land, antarctica. *Antarctic Science* 10 (1):63-74
185. Huang WE, Griffiths RI, Thompson IP, Bailey MJ, Whiteley AS (2004) Raman microscopic analysis of single microbial cells. *Analytical Chemistry* 76 (15):4452-4458
186. Vitek P, Edwards HGM, Jehlicka J, Ascaso C, De los Rios A, Valea S, Jorge-Villar SE, Davila AF, Wierzchos J (2010) Microbial colonization of halite from the hyper-arid atacama desert studied by raman spectroscopy. *Philosophical Transactions of the Royal Society a-Mathematical Physical and Engineering Sciences* 368 (1922):3205-3221
187. [Anon] (2005) Raman spectroscopic detection of biogeological markers in terrestrial mars analogs: Instrumentation. *Astrobiology* 5 (2):284-284
188. [Anon] (2005) Abstract # 647-preservation of biosignatures in sulfates and iron oxides at rio tinto, spain: Implications for the astrobiological investigation of chemically analogous deposits at meridiani planum, mars. *Astrobiology* 5 (2):307-307
189. Bishop JL, Alpers CN, Coleman ML, Sobron P, Lane MD, Dyar MD, Schiffman P (2008) Sulfates on mars: Comparison with spectral properties of analog sites. *Geochimica Et Cosmochimica Acta* 72 (12):A85-A85
190. Edwards HGM, Garcia-Pichel F, Newton EM, Wynn-Williams DD (2000) Vibrational raman spectroscopic study of scytonemin, the uv-protective cyanobacterial pigment. *Spectrochimica Acta Part a-Molecular and Biomolecular Spectroscopy* 56 (1):193-200